Large Nonlinearities in Four-Wave Mixing in Photorefractive Crystals and Applications in Passive Optical Phase Conjugation

Thesis by

Mark Cronin-Golomb

In Partial Fulfillment of the Requirements

for the Degree of

Doctor of Philosophy

California Institute of Technology

Pasadena, California

1983

(Submitted May 26, 1983)

To Desmond Armstrong

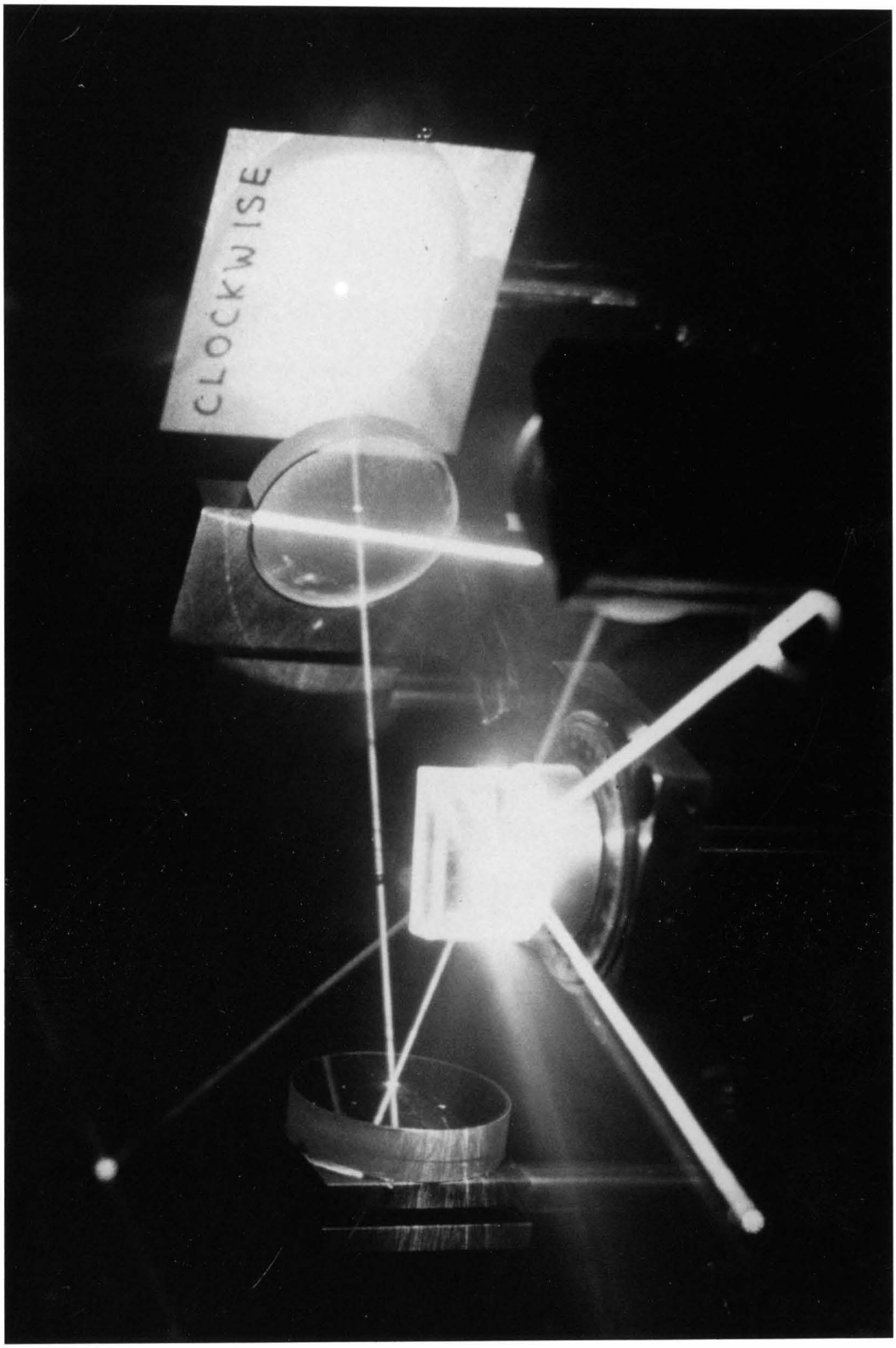

Unidirectional ring resonator using barium titanate pumped by a helium neon laser. (Chapter 3)

Acknowlegments

I am indebted first of all to my wife, Alice, for her understanding, her companionship, her emotional support, and her love. Without her I could not have done this.

To my parents, Lewis and Julie and my sisters Marcia and Jennifer whose constant encouragement and love (through even the terrible twos) finally enabled me to leave the nest and come across the sea from Australia to California.

To my advisor, Professor Amnon Yariv, who gave me his expert guidance and generous professional support. The atmosphere of his laboratory is one of true creativity.

To my colleagues: Jeffrey O. White, who taught me how to use an optics lab; Baruch Fischer, whose infectious enthusiasm and keen insights were a source to me of great inspiration; Joseph Nilsen who generously made his equipment available when ours was out of service, and who taught me how to use dye lasers; Sze-Keung Kwong, who has been with us for less than a year and is already beginning to make his mark. An open and enquiring mind such as his is bound to succeed. Thanks also go to Liew-Chuang Chiu, John S. Smith and Christoph S. Harder for their assistance in several phases of this work.

I would like to express appreciation to Jana Mercado, who prepared many of the published papers, sometimes through extensive revisions.

I dedicate this volume to Desmond Armstrong. His technical expertise and ready willingness to tackle even the most difficult projects have made this lab a delight to work in.

I am, of course, extremely thankful for the financial support of the California Institute of Technology, the Air Force Office of Scientific Research, the Army

Research Office, Durham N.C. and of the University of Sydney, which provided me with a Postgraduate Research Travelling Scholarship.

Finally, thanks go to the many friends I have made during the past four years in California, and especially to Mark and Lynn M. Finger.

Abstract

This thesis deals with some aspects of real-time holography, phase conjugation and four-wave mixing in photorefractive materials. These materials are particularly attractive because they can easily support real-time holograms of high diffraction efficiency. The effect which gives rise to these holograms is non-resonant and is operative in many crystals over the entire visible spectrum with low power (milliwatt) continuous wave laser beams. Two interwoven lines of research are pursued in this work.

Firstly, the phase shift between the light interference pattern and the refractive index grating, so characteristic of photorefractive holograms, and the magnitude of the diffraction efficiencies available in these crystals ($BaTiO_3$ and $Sr_{1-x}Ba_xNb_2O_6$) are such that a signal beam writing a hologram with a pumping beam will often experience gain. In a four-wave mixing situation, phase conjugate reflectivities well in excess of unity are possible.

We describe the demonstration of several optical oscillator structures which take advantage of this two- and four-wave mixing gain. These include a unidirectional ring resonator and the linear and ring passive phase conjugate mirrors. The linear mirror consists of a photorefractive crystal in a linear optical cavity. When the crystal is illuminated by a signal beam, oscillation builds up in the linear cavity, automatically providing a pair of counterpropagating beams which pump the crystal as a phase conjugate mirror for the signal beam. The beam coupling dynamics are such that once the oscillation has started it is possible to maintain operation even after removal of one of the linear cavity mirrors. This version of the linear mirror is known as the semilinear mirror. The ring mirror feeds the signal beam transmitted through the crystal back around an optical

ring cavity to the crystal again where it becomes one of the pumps. An oscillation beam builds up which serves both as the second pump and the phase conjugate beam. Phase conjugate reflectivities of up to thirty per cent are easily observed in these passive devices. Experiments are described which demonstrate phase conjugation in these devices. Another experiment shows the intracavity distortion correction capability of an argon ion laser with one of its end mirrors replaced by a linear passive phase conjugate mirror.

The second line of work in this thesis is theoretical. The mechanism of the photorefractive effect is discussed. A generalization of the standard rate equation model is described, and the predictions of the rate equation model and a competing theory, the hopping model, are compared.

A coupled wave theory of two- and four- wave mixing in photorefractive crystals is developed, showing the importance of the phase shift between the interference pattern and the refractive index grating. The well known effect of two-beam energy coupling is reviewed and applied to a unidirectional ring resonator. Four-wave mixing is solved in the undepleted pumps approximation which linearizes the theory. The effects of linear absorption are considered, and the identity of the behaviors of the reflection and transmission gratings is pointed out.

Fully nonlinear equations of four-wave mixing via a single grating are solved for the transmission grating and separately for the reflection grating. Bistability in the solutions is discussed, and the boundary conditions for regular phase conjugation, as well as for the linear and ring passive phase conjugate mirrors are fitted. Workable expressions for the reflectivities are presented. The dynamics predicted by these theories explains the observed natures of the passive phase conjugate mirrors including the striking abilities of the semilinear and

ring mirrors to function even at all. In addition, boundary conditions are fitted for the two interaction region passive phase conjugate mirror recently demonstrated by Feinberg.

Novel interpretations of photorefractive crystals as double phase conjugate mirrors and distortion correction elements in optical systems and circuits are introduced, and theoretically modelled. An application in ring lasers is suggested.

Finally, the relative merits of the ring, linear, semilinear and two interaction region passive phase conjugate mirrors are discussed with regard to threshold, reflectivity and ease of alignment.

Table of contents

Chapter 1 Introduction

Phase conjugation 1
The photorefractive effect 7
Outline of thesis 8
References for chapter 1 10

Chapter 2 The photorefractive effect

Introduction 13
The rate equation model 19
The hopping model 31
References for chapter 2 35

Chapter 3 Coupled wave equations and the undepleted pumps approximation

Introduction 38
The refractive index grating 38
The coupled wave equations 42
Two beam coupling and the unidirectional ring resonator 43
The transmission grating in the undepleted pumps approximation 47
The reflection grating in the undepleted pumps approximation 51
References for chapter 3 56

Chapter 4 Exact solution of the coupled wave equations with negligible linear absorption

Introduction 57
The transmission grating 57
The reflection grating 65
References for chapter 4 70

Chapter 5 Passive phase conjugate mirrors and optical aberration correction

Introduction	71
The linear and semilinear passive phase conjugate mirrors	71
A phase conjugate resonator laser using the linear or semilinear passive phase conjugate mirror	78
Intracavity distortion correction and double phase conjugation	90
The ring passive phase conjugate mirror	94
The two interaction region passive phase conjugate mirror	102
Threshold versus reflectivity versus ease of alignment	102
Conclusion	105
References for chapter 5	106

Chapter 1

Introduction

Phase Conjugation

When the laser was invented, it brought with it the easy availability of intense, coherent light. The field of optics was rejuvenated, for there were still many aspects of the interactions between light and matter that had previously gone unexplored for lack of suitable light sources. The new physics brought with it a wealth of applications, from the doubling of the frequency of beams of light to the processing of optical information.

As the field of optical information processing became more sophisticated, it became more and more important to reduce the errors introduced by imperfections in system components. Since much of the optical information in these systems lies encoded in the precise positioning of the waves of light, and the wavelength is typically about one millionth of a meter, these errors start creeping in even at extremely high machining tolerances. Unless there is provision for automatic correction of these errors, a high quality optical system will be bound to be very delicate. Fortunately, most of optics is invariant under time reversal. Consider a beam of light passing through a distorting piece of optics, such as a piece of etched glass , or a bad amplifier. If some way can be found to produce a copy of the distorted beam, identical in all respects to the original except that every photon in the beam has its sense of time reversed so that it retraces the path of the original beam *even back through the distortion* then it will emerge from the distortion as a perfect time reversed copy of the initial unaberrated beam. (Fig. 1.1). We will have achieved perfect reflection, and the effects of the bad optics will have been cancelled out.

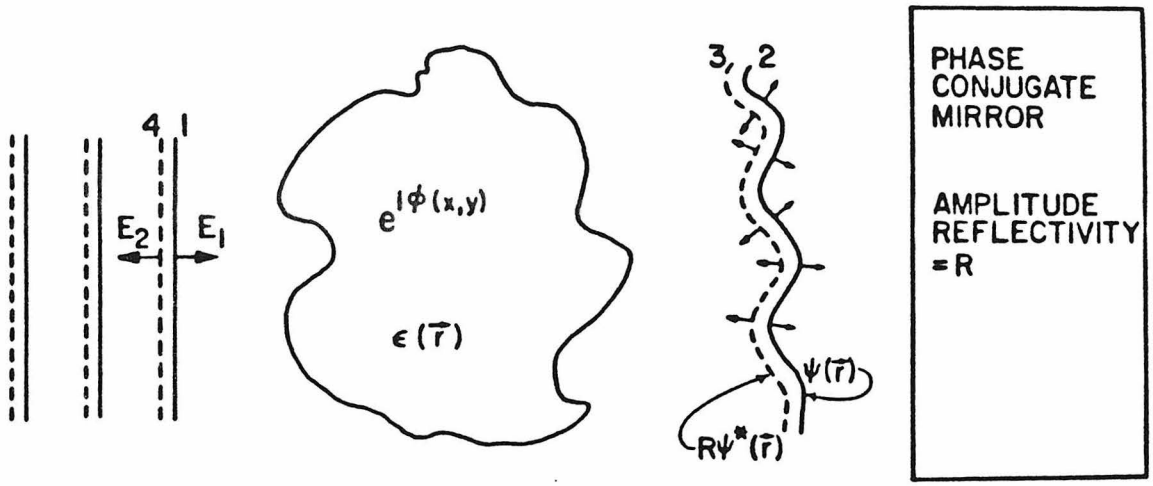

Figure 1.1 Typical geometry depicting the ability of time reversal to correct for a general spatially dependent phase aberration. A plane wave (1) incident from the left encounters a region of nonuniform refractive index, denoted by $\varphi(x,y)$. The resultant distorted wavefront (2) is now time reversed by a phase conjugate mirror resulting in (3) which after retroversing the same medium, emerges (4) having the initial planar wavefronts. The small arrows schematically indicate the (local) spatial plane wave propagation components of the given wavefront.

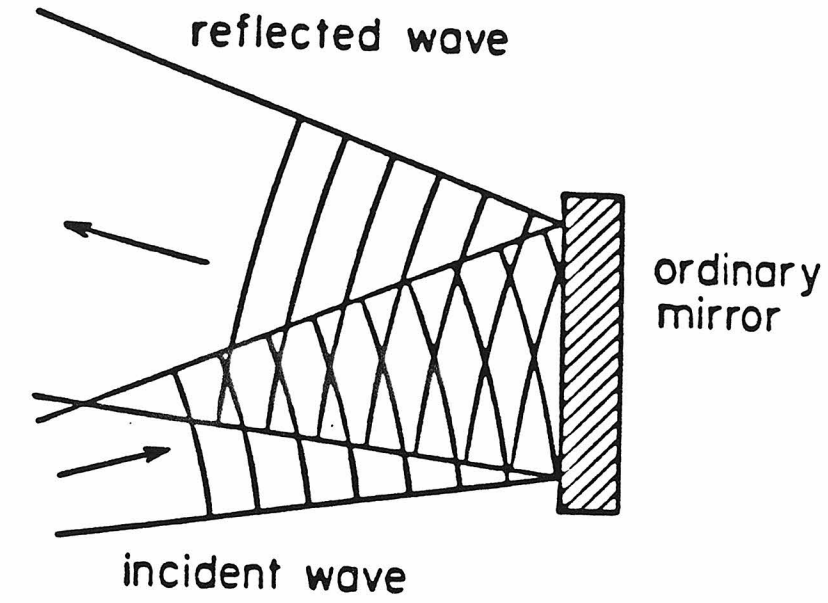

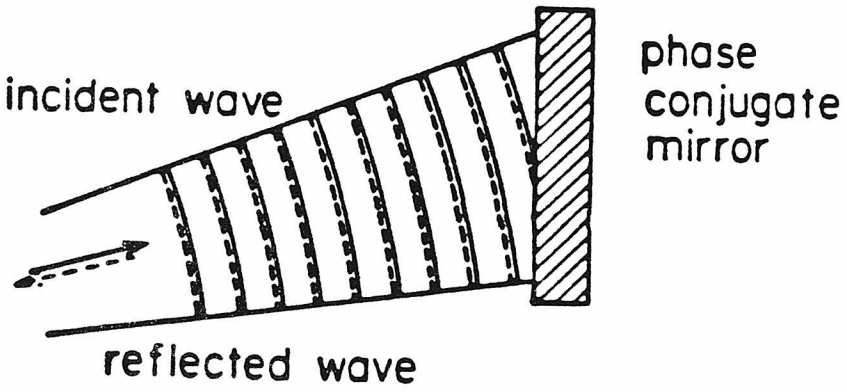

Figure 1.2 Comparison of a phase conjugate mirror to an ordinary mirror.

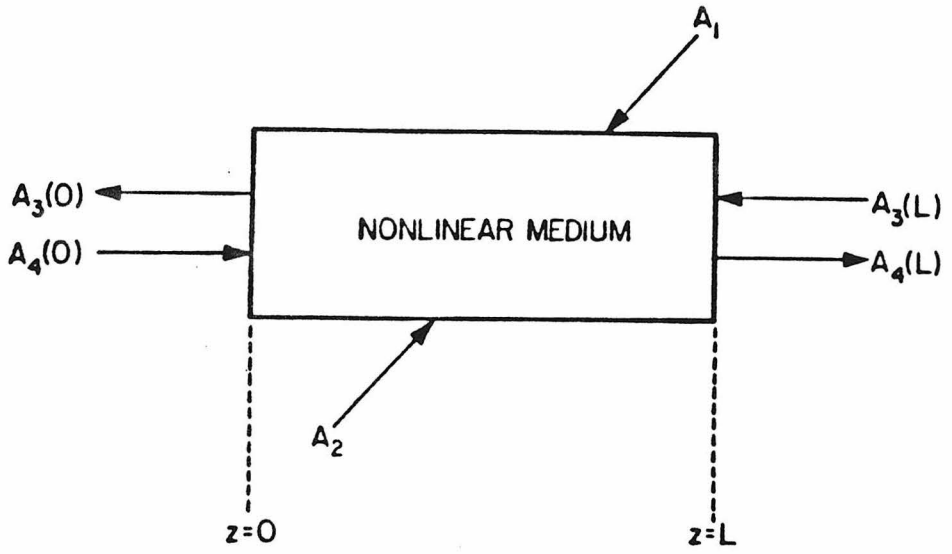

Figure 1.3 Geometry of four-wave mixing in a nonlinear or holographic medium. If $A_3(L)$ is zero, then $A_3(0)$ will be a time reversed copy of the probe, or signal beam $A_4(0)$

Phase conjugation is the name that has attached itself to this time reversal and the physical realization of a device which performs this operation is called a phase conjugate mirror, depicted in Fig. 1.2 next to its brother, the ordinary mirror. While an ordinary mirror reflects a diverging beam into another diverging beam, a phase conjugate mirror reflects a diverging beam back on itself into a converging beam.

The mathematical significance of phase conjugation may be seen by considering its effect on a given optical field

$$\mathbf{E}(\mathbf{r},t) = \tfrac{1}{2}A(\mathbf{r})e^{i(\mathbf{k}\cdot\mathbf{r}-\omega t)} + \tfrac{1}{2}A^*(\mathbf{r})e^{-i(\mathbf{k}\cdot\mathbf{r}-\omega t)} \tag{1.1}$$

The phase conjugate, or time reversal of this field is

$$\mathbf{E}_{PC}(\mathbf{r},t) = \tfrac{1}{2}A^*(\mathbf{r})e^{i(-\mathbf{k}\cdot\mathbf{r}-\omega t)} + \tfrac{1}{2}A(\mathbf{r})e^{-i(-\mathbf{k}\cdot\mathbf{r}-\omega t)} \tag{1.2}$$

so that the sign of the wavevector has changed sign and the amplitude A has been replaced by its complex conjugate. Another reason for the name comes from the field of holography. When a hologram is illuminated by a plane wave travelling opposite to the original reference wave the diffracted wave forms what is known as the conjugate image, as it has been called since well before the invention of phase conjugation. In fact, one of the most common methods for performing phase conjugation is based in this very same principle, using holographic recording materials which need not be taken out of the the optical apparatus to be developed. The hologram is written in real time, while the object wave is still present together with the reference wave and the time reversed readout wave. This technique is known as four-wave mixing (Fig 1.3). The reference wave and the readout wave now enjoy equivalent status and new names: pumps, for both read and both write the hologram pumping energy into the phase conjugate beam, and often the object beam. There are now a large number of different holographic gratings that can be written, both in space and

time, and the relative strengths of these gratings depends on the various nonlinear susceptibilities of the material in question. All four waves are mixed by the holographic gratings they write, and complex recursive dynamics arise in which the four mixing beams affect the diffraction grating, which in its turn affects the propagation of the four mixing beams. Furthermore, there can be no real distinction between the pumping pair and the object/conjugate pair, since the pumps are phase conjugates of each other too. In the latter chapters of this thesis situations will be encountered where the traditional roles of these pairs are reversed. When the four-wave mixing induced by the grating becomes strong enough to couple significant fractions of the beams into each other, then the nonlinearities inherent in the recursion cause many intricate physical phenomena. These too, will be dealt with in this thesis.

There are several other ways apart from four-wave mixing to implement phase conjugation such as three- and six-wave mixing, and stimulated Brillouin and Raman scattering. There are many materials which have been used in real time holography and four-wave mixing such as dyes, semiconductors and atomic vapors. And there are a multitude of applications: the study of the physics of the coupling phenomena, thermal and acoustic effects, excitons, plasmas and atomic population dynamics; nonlinear and Doppler free spectroscopy; narrow bandpass filtering; photolithography; image transmission through optical fibers and atmosphere, laser fusion; pulse compression; optical computing; gravitational wave detection through two photon coherent states. For a review of phase conjugation and these applications, the reader is referred to several comprehensive articles in the literature[1-4].

The photorefractive effect

Through the recent years' boom in nonlinear optical phase conjugation, photorefractive (PR) materials such as $LiNbO_3$, $Bi_{12}Si_{20}O_3$ (BSO), $BaTiO_3$ and $Sr_{1-x}Ba_xNb_2O_6$ (SBN) have been assuming ever increasing prominence due to their unique capability for displaying strong nonlinear effects with milliwatt beams over the entire visible spectrum and beyond.

In the late sixties it was noticed that certain frequency doubling crystals were subject to "optical damage" characterized by degraded phase matching due to light induced changes in refractive index[5–7]. These index variations persisted in the dark, sometimes for many months, and could be erased by flooding the crystal with uniform illumination. That the effect could actually be put to use was noticed by those interested in real time volume holography who thought to use PR materials as very dense optical memories ($\approx 10^{11}$ bits /cm^3) and for real time optical information processing[8–25]. Concurrent theoretical developments involved both investigation of the physical mechanism whereby light intensity was converted to refractive index variations, and the optical nonlinearities involved in the beam coupling due to the self-developing hologram[26–38]. While no true third order constitutive nonlinearity was involved, the diffraction of two beams into each other by the very grating they wrote resulted in strong third order interactions. The physics of the PR effect is such that the index grating is often $\pi/2$ out of phase in space with the interference pattern and one beam is coherently amplified at the expense of the other. The implications for coherent optical processing are clear.

In the mid-seventies the field of phase conjugate optics began to prosper because of potential applications in aberration correction. The main problem to be faced was and still is the development of fast media with large nonlinearities.

While phase conjugation by four-wave mixing is often thought of in terms of nonlinear optical susceptibilities, the formal analogy with real time holography[39] has made it clear that PR materials could be used effectively in phase conjugation. As a result, a whole new branch in phase conjugate optics has been developed[40–48]. High reflectivity phase conjugation with low power lasers has become an easy task. Resonators using PR phase conjugate mirrors have been built[44], and many new nonlinear optical devices have been demonstrated including ring oscillators and passive phase conjugate mirrors (PPCM's)[45–48].

Among the PR materials that we have used so far, we find $BaTiO_3$[36] and SBN[49] most suited to experiments where large coupling strengths are required since they have very large electrooptic coefficients. The main disadvantage of these materials is their slow response times, typically about $10/I$ sec. where I is the total intensity of the interacting beams in mW/mm^2. One main research direction in the future is going to be optimization of this time; much work has already been done with $LiNbO_3$, where the use of reduced iron impurities seems to be effective[50].

Outline of thesis

This thesis describes some more recent developments in the use of PR materials in phase conjugation. Chapter 2 details the coupling mechanism for two and four-wave mixing in PR materials, and two models of the process are developed and compared. Chapter 3 discusses two-beam coupling and describes an experimental demonstration of a unidirectional ring resonator based on this effect. The four coupled wave equations of four-wave mixing phase conjugation are introduced and their solutions in the undepleted pumps and single grating approximations are given. The effects on phase conjugation of the spatial phase shift between the index grating and the light interference pattern are discussed.

In Chapter 4 solutions are obtained in which no use is made of the undepleted pumps approximation. The multistability that results from considering the full nonlinear nature of the problem is described. In Chapter 5 application of the theory to the new PPCM's is explained and the results of experimental demonstrations of these devices are shown. Novel interpretations of PR crystals as distortion correcting elements and as double phase conjugate mirrors in optical systems and circuits are introduced.

References for Chapter 1

1. A. Yariv, IEEE Journ. Quant. Electron. **QE-14**, 650 (1978)
2. Special issue on optical phase conjugation, Opt. Electron. **21**, no. 2
3. "Optical phase conjugation", (Ed. R.A. Fisher, New York, Academic Press, 1983)
4. C.R. Giuliano, Phys. Today **34**, 27 (1981) April 1981
5. A. Ashkin, G.D. Boyd, J.M. Dziedzic, R.G. Smith, A.A. Ballman, J.J. Levinstein and K. Nassau, Appl. Phys. Lett. **9**, 72 (1966)
6. F.S. Chen, J. Appl. Phys. **38**, 3418 (1967)
7. F.S. Chen, J. Appl. Phys. **40**, 3389 (1969)
8. F.S. Chen, J.T. LaMacchia and D.B. Fraser, Appl. Phys. Lett. **13**, 223 (1968)
9. R.L. Townsend and J.T. LaMacchia, J. Appl. Phys. **41**, 5188 (1970)
10. J.B. Thaxter and M. Kestigian, Appl. Opt. **13**, 913 (1974)
11. A.M. Glass, D. von der Linde and T.J. Negran, Appl. Phys. Lett. **25**, 233 (1974)
12. J.P. Huignard, J.P. Herriau and F. Micheron, Rev. de Phys. Appl. **10**, 417 (1975)
13. D. von der Linde and A.M. Glass, Appl. Phys **8**, 85 (1975)
14. J.P. Huignard and F. Micheron, Appl. Phys. Lett. **29**, 591 (1976)
15. K. Megumi, H. Kozuka, M. Kobayashi and Y Furuhita, Appl. Phys. Lett. **30**, 631 (1977)
16. R. Orlowski, E Kratzig and H. Kurz, Opt. Commun. **20**, 171 (1977)
17. J.P. Huignard and J.P. Herriau, Appl. Opt. **16**, 1807 (1977)

18. M. Peltier and F. Micheron, J. Appl. Phys. **48**, 3683 (1977)

19. J.P. Huignard, J.P. Herriau and T. Valentin, Appl. Opt. **16**, 2796 (1977)

20. H. Kurz, Philips Tech. Rev. **37**, 109 (1977)

21. J.P. Herriau, J.P. Huignard and P. Aubourg, Appl. Opt. **17**, 1851 (1978)

22. M.P. Petrov, S.I. Stepanov and A.A. Kamshilin, Opt. and Laser Tech. June 1979, 149 (1979)

23. R. Orlowski, L.A. Boatner and E. Kratzig, Opt. Commun. **35**, 45 (1980)

24. J.O. White and A. Yariv, Appl. Phys. Lett. **37**, 5 (1980)

25. J.P. Huignard and A. Marrakchi, Opt. Commun. **38**, 249 (1981)

26. J.J. Amodei, RCA Rev. **32**, 185 (1971)

27. Y. Ninomaya, J. Opt. Soc. Am. **63**, 1124 (1973)

28. L. Young, W.K.Y. Wong, M.L.W. Thewalt and W.D. Cornish, Appl. Phys. Lett. **24**, 264 (1974)

29. D.M. Kim, R.R. Shah, T.A. Rabson and F.K. Tittel, Appl. Phys. Lett. **28**, 338 (1975)

30. D.W. Vahey, J. Appl. Phys. **46**, 3510 (1975)

31. S.F. Su and T.K. Gaylord, J. Appl. Phys. **46**, 5208 (1975)

32. R. Magnusson and T.K. Gaylord, J. Appl. Phys. **47**, 190 (1976)

33. M.G. Moraham and L. Young, J. Appl. Phys. **48**, 3230 (1977)

34. B.I. Sturman, Sov. Phys. Tech. Phys. **23**, 589 (1978)

35. N.V. Kukhtarev, V.B. Markov, S.G. Odulov, M.S. Soskin and V.L. Vinetskii, Ferroelectrics **22**, 949 (1979)

36. J. Feinberg, D. Heiman, A.R Tanguay,Jr. and R.W. Hellwarth, J. Appl. Phys. **51**, 1297 (1980)

37. J. Feinberg, Opt. Lett. **5**, 330 (1980)

38. S.I. Stepanov, V.V. Kulikov and M.P. Petrov, Opt. Commun. **44**, 19 (1982)

39. A. Yariv, Opt. Commun. **25**, 23 (1978)

40. J.P. Huignard, J.P. Herriau, P. Aubourg and E. Spitz, Opt. Lett. **4**, 21 (1979)

41. J.P. Huignard, J.P. Herriau and G. Rivet, Opt. Lett. **5**, 102 (1980)

42. N.V. Kukhtarev, Sov. J. Quant. Electron. **11**, 878 (1981)

43. P.N. Gunter, Opt. Lett. **7**, 10 (1982)

44. J. Feinberg, Opt. Lett. **5**, 519 (1980)

45. J.O. White, M. Cronin-Golomb, B. Fischer and A. Yariv, Appl. Phys. Lett. **40**, 450 (1982)

46. M. Cronin-Golomb, B. Fischer, J. Nilsen, J.O. White and A. Yariv, Appl. Phys. Lett. **41**, 219 (1982)

47. M. Cronin-Golomb, B. Fischer, J.O. White and A. Yariv, Appl. Phys. Lett. **41**, 689 (1982)

48. M. Cronin-Golomb, B. Fischer, J.O. White and A. Yariv, to be published, Appl. Phys. Lett, June 1 (1983)

49. B. Fischer, M. Cronin-Golomb, J.O. White, A. Yariv and R. Neurgaonkar, Appl. Phys. Lett. **40**, 863 (1982)

50. For a review see: P. Gunter, to be published, Rev. Mod. Phys.

Chapter 2

The Photorefractive Effect

Introduction

The mechanism of the photorefractive (PR) effect is still today a subject of ongoing debate, not so much because of any fundamental problem in physics, but because there are so many different contributions that can be taken into consideration, and the relative importance of these effects is different in different materials. The basic phenomenon involves the holographic recording of a light interference pattern (Fig 2.1). Charge carriers inside the crystal redistribute themselves because of the spatially varying light intensity, whereupon the electric field associated with the space charge operates through the electrooptic effect to produce a refractive index grating. Many attempts, with varying degrees of sophistication, have been made to formulate theoretical models of the effect[1-15], and recently, there has been considerable success in fitting experimental results to the predictions of these theories. There is a large literature (see for example Refs. 16-26) concerning the photorefractive sensitivity of many crystals under many different experimental conditions. It deals mainly with two classes of crystal:

i) Oxygen octahedra ferroelectrics such as barium titanate ($BaTiO_3$), barium sodium niobate ($Ba_2NaNb_5O_{15}$), strontium barium niobate ($Sr_{1-x}Ba_xNb_2O_6$) and potassium niobate ($KNbO_3$), (see Fig. 2.2 for typical band structure). Many of these crystals have the perovskite structure (Fig. 2.3)

ii) Sillenites such as bismuth silicon oxide ($Bi_{12}SiO_{20}$, BSO) and bismuth germanium oxide ($Bi_{12}GeO_{20}$, BGO) (see Fig. 2.4 for typical band structure).

Experiments have been done to improve the sensitivity of the crystals by

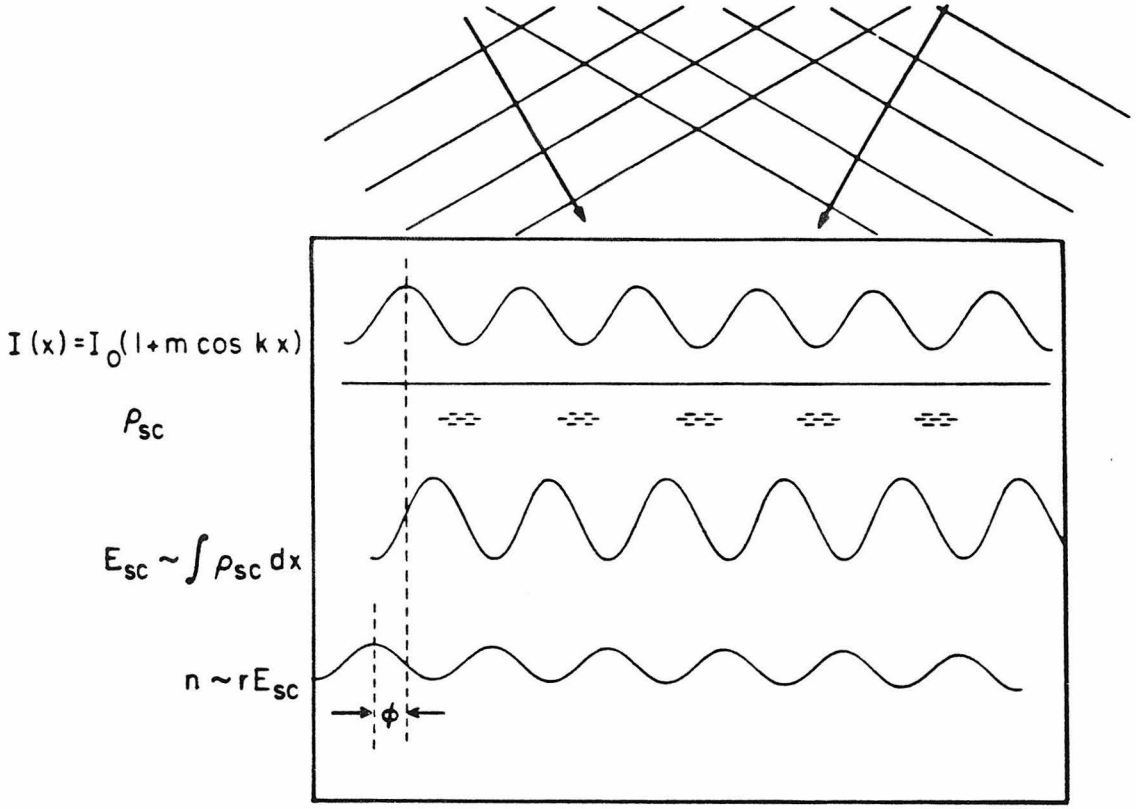

Figure 2.1 The photorefractive mechanism. Two laser beams intersect, forming an interference pattern. Charge is excited where the intensity is large and migrates to regions of low intensity. The electric field associated with the resultant space charge operates through the electrooptic coefficients to produce a refractive index grating.

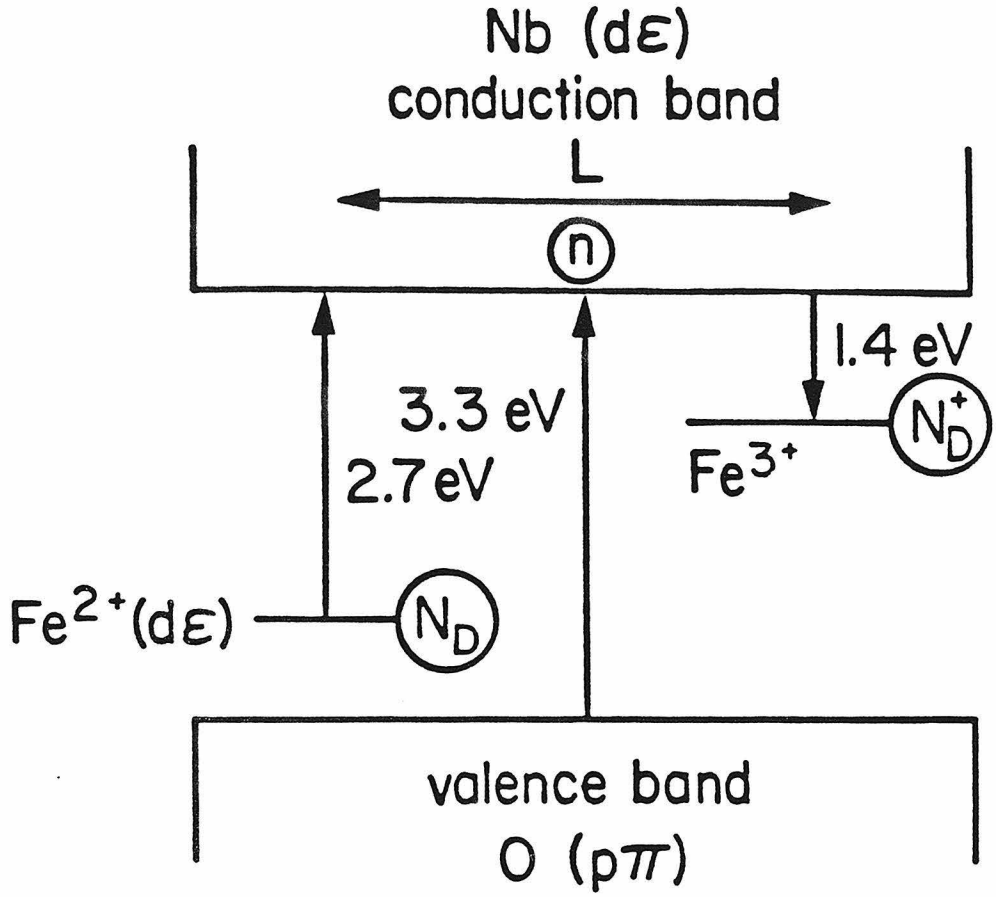

Figure 2.2 Oxygen pπ valence band, niobium dε conduction band and Fe^{2+} donor and Fe^{3+} acceptor levels of the oxygen octahedra ferroelectric $KNbO_3$:Fe (after Ref. 38)

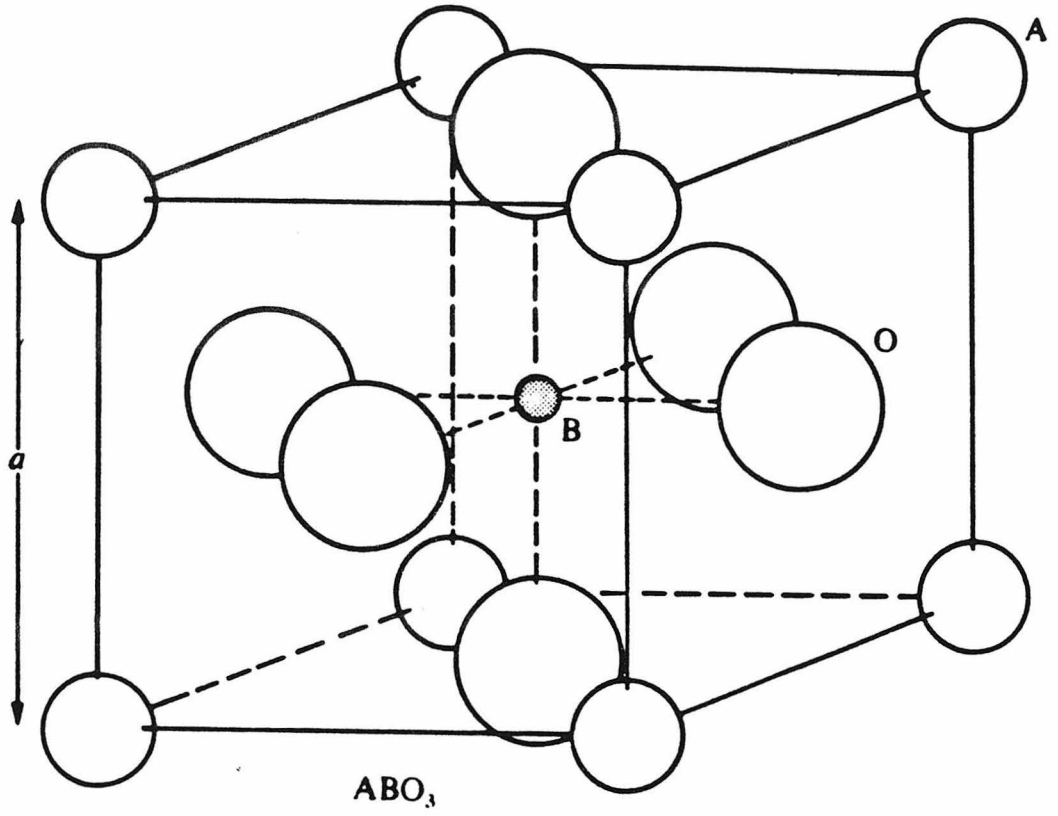

Figure 2.3 The cubic ABO_3 perovskite structure (after Ref. 39)

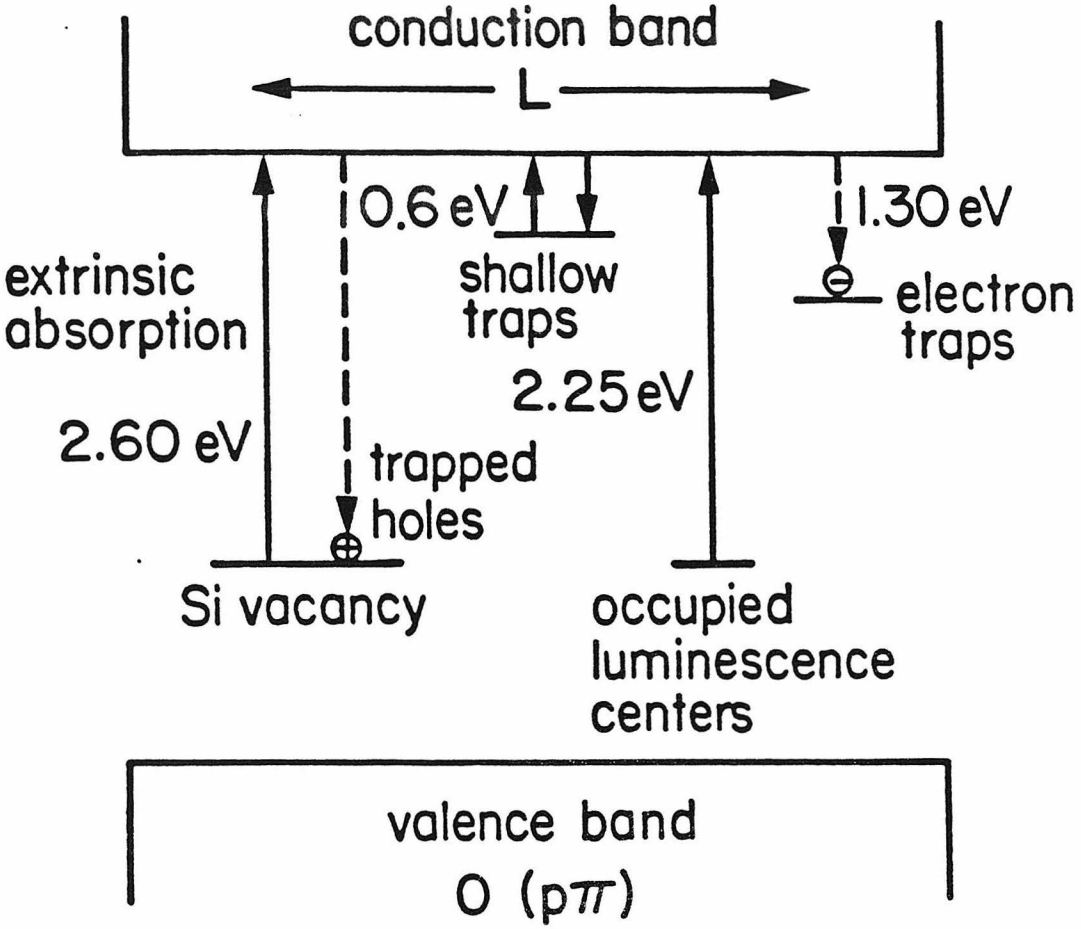

Figure 2.4 Energy band diagram of $Bi_{12}SiO_{20}$ (after Ref. 23)

introducing various dopants including chromium[27], nickel[27], copper[27], manganese[27], rhodium[28], uranium[29], cobalt[27], cesium[30], and iron[27]. The transition metals are effective because they can give up and capture d electrons. They enter the ABO_3 lattice substitutionally in either the A or B sites, both of which are surrounded by an octahedral array of oxygen atoms. The difference in valencies can be compensated by oxygen vacancies. Iron performs particularly well as a dopant, and has been responsible for photorefractive effects even in nominally "pure" samples[31]. By varying the reduction / oxidation state of the iron impurities, one can adjust the relative populations of charge carrier donors and traps[32] (Fe^{2+} and Fe^{3+} respectively for electron charge carriers).

Most models of the dynamics of the charge migration have involved rate equations, with the most complete, albeit linearized model having been formulated by Kukhtarev in 1977, taking into consideration the effects of externally applied electric fields and the recursive effects of the space charge electric field on the space charge itself[10]. His theory also included the photovoltaic effect[11], in which the asymmetry of the crystal caused photoionized charge carriers to be ejected into the conduction band preferentially in a particular direction relative to the optic axis of the crystal thus giving rise to a photocurrent. The steady state predictions of this theory have been impressively borne out in experiments with BSO by Huignard et. al.[33]. In this case, the photovoltaic effect was absent, as in the experiments of Feinberg et. al[13] who used barium titanate. Feinberg and coworkers, however, used a different theory to analyse their results. This theory, the hopping model, involved a simple physical picture of charge carriers hopping from site to site, with the probability to hop dependent on the local light intensity and electric field. The hopping model too, gave impressive agreement with theory.

In the following paragraphs we will treat the rate equation model, starting from a viewpoint somewhat more general than that used by Kukhtarev. The hopping model will then be examined, to see the basic differences and similarities with the rate equation model.

The rate equation model

We consider the writing of a holographic diffraction grating by two beams intersecting in a slice of PR material sufficiently thin that effects due to diffraction from one writing beam to another may be ignored; these will be treated in depth in subsequent chapters. Suppose the intensity interference pattern, possibly in motion in the x direction, is given by

$$I(x) = I_0 + I_1 e^{i(kx+\Omega t)} + I_1^* e^{-i(kx+\Omega t)} \qquad (2.1)$$

Apart from this illumination, we also make provision in the theory for the presence of a uniform electric field E_0 superimposed on the space charge field which develops. This uniform field may be either externally applied or may be intrinsically due to the photovoltaic effect when applicable. It is assumed to be directed along the wavevector of the grating.

Charge is excited by the periodic intensity distribution into a conduction band, where it migrates under the influence of diffusion and drift in the internal electric field. A periodic space charge is thus set up which in turn, modulates the refractive index via the electrooptic effect. Since the bandgap of common PR materials is in the ultraviolet and the holographic recording takes place in the visible, the charge cannot be excited directly from the valence band to the conduction band, and this is just as well, because otherwise, the crystals would not be sufficiently transparent for the writing of thick holograms. Let us suppose that electrons are excited into the conduction band from a variety of different

kinds of impurity or defect site. With each site is associated a label j which may be discrete or continuous. For each type of site j we define the following quantities:

N^j = number density of sites of type j

q^j = charge of vacant site of type j in units of electronic charge e

$p^j(x,t)$ = local number density of vacant sites of type j

α^j = absorption coefficient for excitation of electrons out of sites of type j

σ^j = recombination coefficient for sites of type j with electrons in the conduction band. The number of electrons available for distribution among these sites can be found from considerations of charge neutrality:

$$n_{tot} = \sum_j N^j q^j \tag{2.2}$$

Suppose we write a hologram, and then turn the writing beams off. A short time later all the electrons in the conduction band have, by drift and diffusion, been able to recombine with sites. If there are as many electrons as sites, the distribution of electrons is going to be as uniform as the distribution of sites. The whole crystal is going to be everywhere neutral, and we have no space charge field, no hologram. So to explain the observed persistence of holograms in the dark, we need to have more sites than electrons. That is

$$0 < \sum_j N^j q^j = n_{tot} < \sum_j N^j \tag{2.3}$$

Since q^j is integral, we need at least two kinds of site. In the simplest case, we have absorption centers ($q^j = 1$) and traps ($q^j = 0$).

Now we are in a position to write down the standard rate equations governing the formation of the space charge field E(x,t)

$$\frac{\partial p^j}{\partial t} = \alpha^j (N^j - p^j) I(x) - \sigma^j p^j n \tag{2.4a}$$

$$\frac{\partial n}{\partial t} = \frac{\partial}{\partial t}\sum_j p^j + \frac{1}{e}\frac{\partial J}{\partial x} \tag{2.4b}$$

$$\frac{\partial E}{\partial x} = [\sum_j p^j q^j + \sum_j (N^j - p^j)(q^j - 1) - n]e/\varepsilon \tag{2.4c}$$

$$J = \mu enE + k_B T \mu \frac{\partial n}{\partial x} \tag{2.4d}$$

where n(x,t) is the number density of electrons in the conduction band, μ is their mobility and J is the electric current they comprise, k_B is Boltzmann's constant, T is the temperature and ε is the electric permittivity. The first equation describes ionization and deionization of sites of type j. The second is an equation expressing charge conservation. The third is Poisson's equation and the fourth describes the current in terms of drift and diffusion.

Let N be the total number density of sites, p be the local number density of vacant sites, α be an average absorption coefficient, σ be an average recombination coefficient, p_d be the spatially averaged number density of sites in the dark.

$$N = \sum_j N^j \tag{2.5a}$$

$$p(x,t) = \sum_j p^j(x,t) \tag{2.5b}$$

$$\alpha(x,t) = [\sum_j \alpha^j (N^j - p^j)]/[\sum_j (N^j - p^j)] \tag{2.5c}$$

$$\sigma(x,t) = \sum_j \sigma^j p^j / \sum_j p^j \tag{2.5d}$$

$$p_d = \sum_j N^j (1 - q^j) \tag{2.5e}$$

In terms of these new variables the rate equations become

$$\frac{\partial p}{\partial t} = \alpha(N - p)I(x) - \sigma pn \tag{2.6a}$$

$$\frac{\partial n}{\partial t} = \frac{\partial p}{\partial t} + \frac{1}{e}\frac{\partial J}{\partial x}$$

(2.6b)

$$\frac{\partial E}{\partial x} = (p - n - p_d)e/\varepsilon \tag{2.6c}$$

$$J = \mu enE + k_B T \mu \frac{\partial n}{\partial x} \tag{2.6d}$$

And here we have a nonlinear model, similar in spirit to the one formulated in 1977 by Kukhtarev. In the next section, we will make approximations which linearize the theory and make it soluble.

We make the following assumptions and approximations

i) For simplicity it is assumed that there are only two types of site: traps ($q^j = 0$) and absorption centres ($q^j = 1$).

ii) The uniform electric field E_0 is directed along the wavevector of the grating. If there is a photovoltaic field present, the wavevector is assumed to lie along the optic axis of the crystal, if it is uniaxial.

iii) The coefficients α and σ are constant in space and time. Looking at the equations for α and σ (2.5c,2.5d) we see that if for every nonzero p^j, α^j and σ^j are independent of j then the above assumption is valid. In the case of two types of site we see that this condition holds if the traps are always full - $p^{trap} = 0$ or the characteristics of traps and absorption centers are sufficiently similar that $\alpha^{trap} = \alpha^{absorption\ center}$ and $\sigma^{trap} = \sigma^{absorption\ center}$.

iv) We assume that the electric field E, ionized site density p and electron density n can be approximated by their first Fourier components

$$E = E_0 + E_1 e^{ikx} + E_1^* e^{-ikx} \tag{2.7a}$$

$$p = p_0 + p_1 e^{ikx} + p_1^* e^{-ikx} \tag{2.7b}$$

$$n = n_0 + n_1 e^{ikx} + n_1^* e^{-ikx} \tag{2.7c}$$

In fact it has been shown experimentally that the higher harmonics are impor-

tant when the modulation index approaches unity[34], so that our theory is limited to cases where the modulation index of the interference pattern is significantly less than one.

v) The zero order electron density n_0 is constant in time. With this assumption, the equations become linear, and may be solved by elementary techniques. We note that in the experimental situation of interest, the initial condition is one of uniform charge distribution , with no illumination. The light is turned on at time $t=0$ and the hologram proceeds to develop. We are interested in finding solutions to the problem both as a function of time and in the steady state. If we can be content with solving the problem for times long compared to the risetime of the photocurrent (proportional to n_0) then we can take it as being constant in time. In order to apply this linearization, we need to check in each case that the risetime of the photocurrent is small compared to the risetime of the space charge field. Our experiments with BSO, for example show that this is indeed the case.

vi) For simplicity, we also assume that a) the total density N of sites is much greater than the density p_d of sites ionized in the dark which in turn is b) much greater than the zero order density n_0 of electrons in the conduction band and c) n_1 is zero on the scale of p_1. The first assumption is experimentally verified in BSO for example by studies of the energy band structure[23,35]. N is found to be of the order of $10^{19}/cm^3$ and p_d, equal to the number density of traps is found to be of the order of $10^{16}/cm^3$. The second assumption is verified by measurements of the photoconductivity[23], photoelectron mobility[23] and quantum efficiency[35] which show n_0 to be of the order of $5\times10^{12}/cm^3$ for $I_0 = 100mW/cm^2$. The third assumption is justified by looking at the space charge density required to produce the diffraction efficiencies of several percent observed in BSO, given its electrooptic coefficients. The active space charge field cannot be directly due

to the photoionized charge carriers; these serve mainly to mediate a redistribution of charge among the much more populous absorption centers and traps. Several of the earlier theories, such as the one of Kim et. al.[5] made no explicit mention of this much larger scale charge redistribution, and hence their predictions were quite different and not as well supported by experimental evidence as the present theory. Also, we can neglect $\partial n_1/\partial t$ in comparison with $\partial p_1/\partial t$, for it can only be otherwise if n_1 oscillates rapidly. The effects of such oscillation will cancel out over times characteristic of the rate of change of the ionized site density p.

Using the Fourier expansion with the other approximations we obtain, first from (2.6c)

$$p_0 = n_0 + p_d \approx p_d \tag{2.8}$$

and then from (2.6a)

$$\frac{\partial p_0}{\partial t} = \alpha N I_0 - \sigma p_d n_0 \approx 0 \tag{2.9}$$

The simplified equations relevant to the calculation of the space charge are

$$\frac{\partial p}{\partial t} = \alpha N I - \sigma p n \tag{2.10a}$$

$$\frac{\partial p}{\partial t} = -\frac{1}{e}\frac{\partial J}{\partial x} \tag{2.10b}$$

$$\frac{\partial E}{\partial x} = \frac{(p - p_d)e}{\varepsilon} \tag{2.10c}$$

$$J = \mu e n E + k_B T \mu \frac{\partial n}{\partial x} \tag{2.10d}$$

We use the Fourier expansion again, substitute (2.10d) into (2.10b) and eliminate n and E using (2.10a) and (2.10c) respectively, define the characteristic fields for drift, diffusion and space charge respectively $E_\mu = \frac{\sigma p_d}{\mu k}$, $E_d = \frac{k_B T k}{e}$, and

$E_p = \frac{ep_d}{\varepsilon k}$, and finally arrive at the following equation for the space charge field p_1

$$[E_0 + i(E_d + E_\mu)]\, t_0 \frac{dp_1}{dt} = -p_1[E_0 + i(E_d + E_p)] + \frac{I_1}{I_0} p_d e^{i\Omega t}(E_0 + iE_d) \qquad (2.11)$$

where the characteristic time t_0 is given by

$$t_0 = p_d/(\alpha N I_0) \qquad (2.13)$$

For a grating with one micron period in BSO at room temperature the characteristic fields derived from Refs. 32 and 22 are $E_\mu \approx 0.1$kV/cm, $E_d \approx 1.6$kV/cm and $E_p \approx 10$kV/cm. The solution for p_1 is given by

$$\frac{p_1}{p_d} = \frac{I_1/I_0(E_0 + iE_d)(e^{i\Omega t} - e^{-t/\tau})}{[E_0 - \Omega\, t_0(E_d + E_\mu)] + i(E_d + E_p + \Omega\, t_0 E_0)} \qquad (2.14)$$

where τ is the complex time constant

$$\tau = t_0 \frac{E_0 + i(E_d + E_\mu)}{E_0 + i(E_d + E_p)} \qquad (2.15)$$

The space charge field is obtainable directly from this by means of Poisson's equation through which an additional phase shift of $\pi/2$ is introduced between the light interference pattern and the refractive index grating. In 1977 Kukhtarev et. al. published the steady state behaviour of a similar theory. The results, not surprisingly, were the same as the ones presented here, and have described very well the experimental results of Huignard et. al.[33]. who measured phase conjugate reflectivities of holograms in BSO as a function of grating wavenumber k and uniform electric field E_0 (see Fig. 2.5). It can be seen that the external application of an electric field causes significant enhancement in the reflectivity, and hence in the space charge field, in accordance with (2.14). An increase in temperature would increase the diffusion field, and also enhance the space charge field. These effects are due to the fact that the space charge

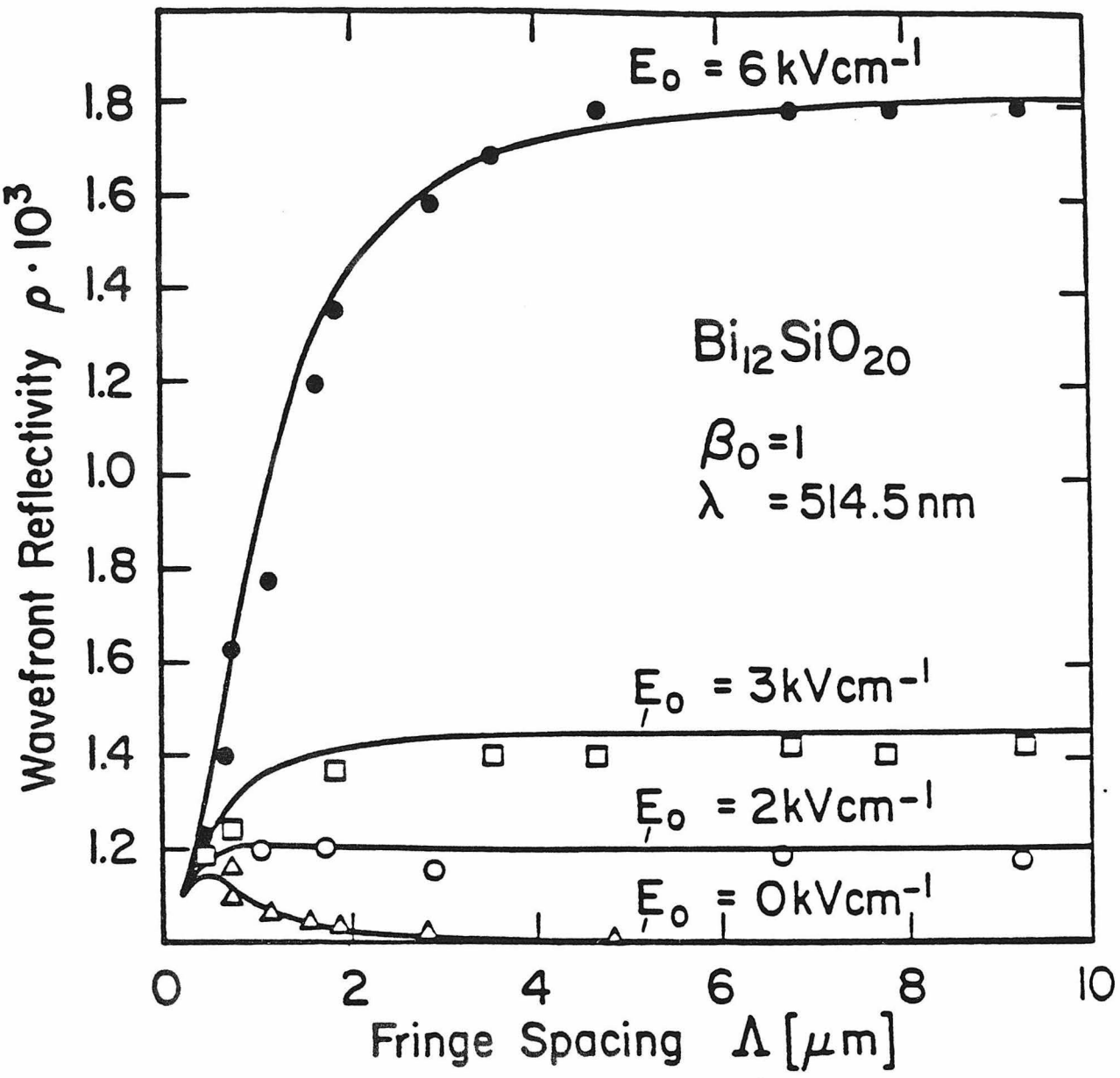

Figure 2.5 Phase conjugate wavefront reflectivity versus fringe spacing for different values of applied field E_0 (after Ref. 33). Theory (solid lines) and experiment (points).

tends to smooth itself out via the self-repulsion represented by E_p. An applied field E_0 as well as the diffusion field E_d on the other hand, tend to make the charge carriers assume the same distribution as the intensity. If these helpful fields are made large compared to the damaging space charge field, an improvement will result. It would not be effective to simply reduce E_p by reducing the number of traps, because of the appearance of the density of traps p_d in the denominator in the left hand side of (2.14). It has been observed experimentally that in agreement with theory steady state diffraction efficiency is independent of the spatially averaged light intensity I_0 in $KNbO_3$, except for intensities less than about one watt per square centimeter (Fig. 2.6). For very weak beams, we expect that leakage currents due to thermal populations of charge carriers drain the space charge fields as they grow, thus diminishing the steady state diffraction efficiency. The theory also indicates that the risetime should be inversely proportional to the spatially averaged charge carrier intensity n_0 and hence the total writing intensity I_0. With the same exception of very low intensities, this has also been verified in $KNbO_3$. (Fig. 2.7) and through our experience with the photorefractive devices descibed in the following chapters.

The effect of moving the interference fringes at constant speed was included in the theoretical analysis for two reasons. In the first case to search for resonances[36] in diffraction efficiency, and in the second case to examine the possiblility of adjusting the phase shift ψ[37]. The physical picture is one of fringes of the space charge field chasing the illumination fringes across the crystal. The phase difference between this pair of fringes depends on how well the space charge is able to keep up with the illumination travelling at velocity Ω/k. At the same time the crystal itself is suffering a force with frequency Ω, and when this frequency is the same as that given by the complex part of the transient time constant τ, the response resonates.

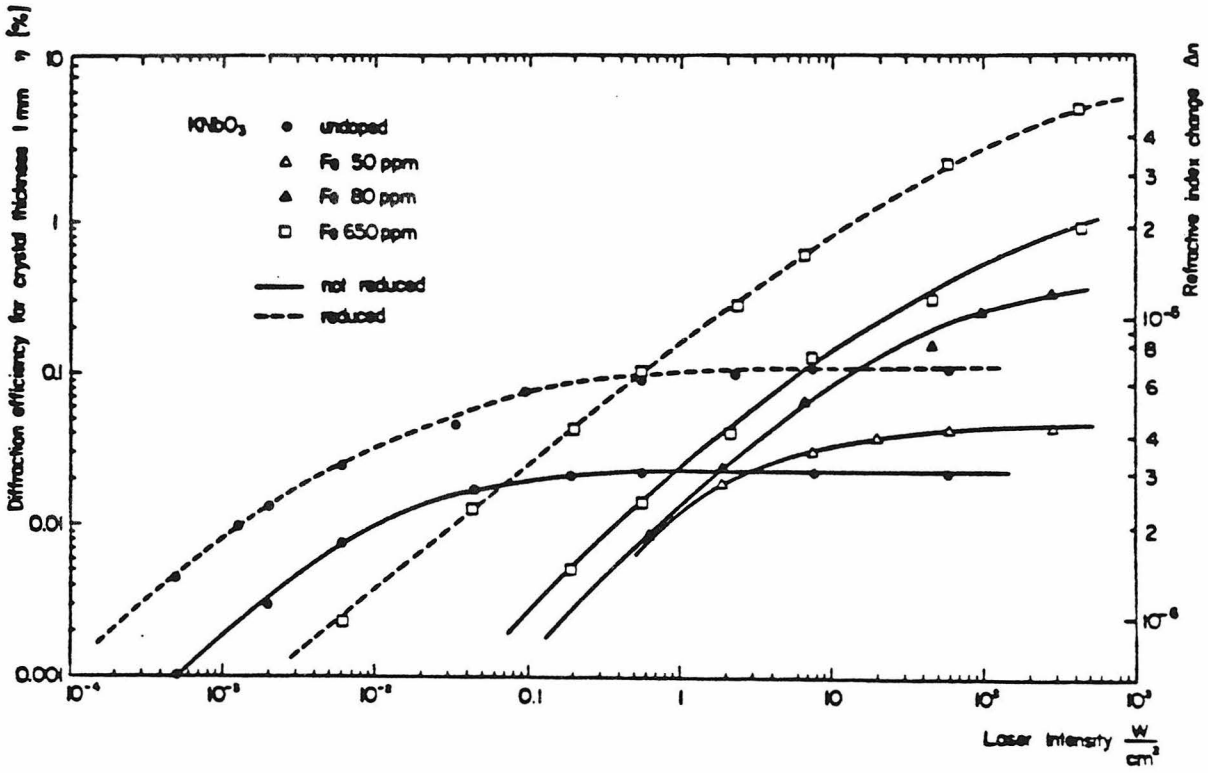

Figure 2.6 Steady state diffraction efficiency and refractive index modulation amplitude versus laser intensity in $KNbO_3$:Fe at 488.0 nm (after Ref. 38)

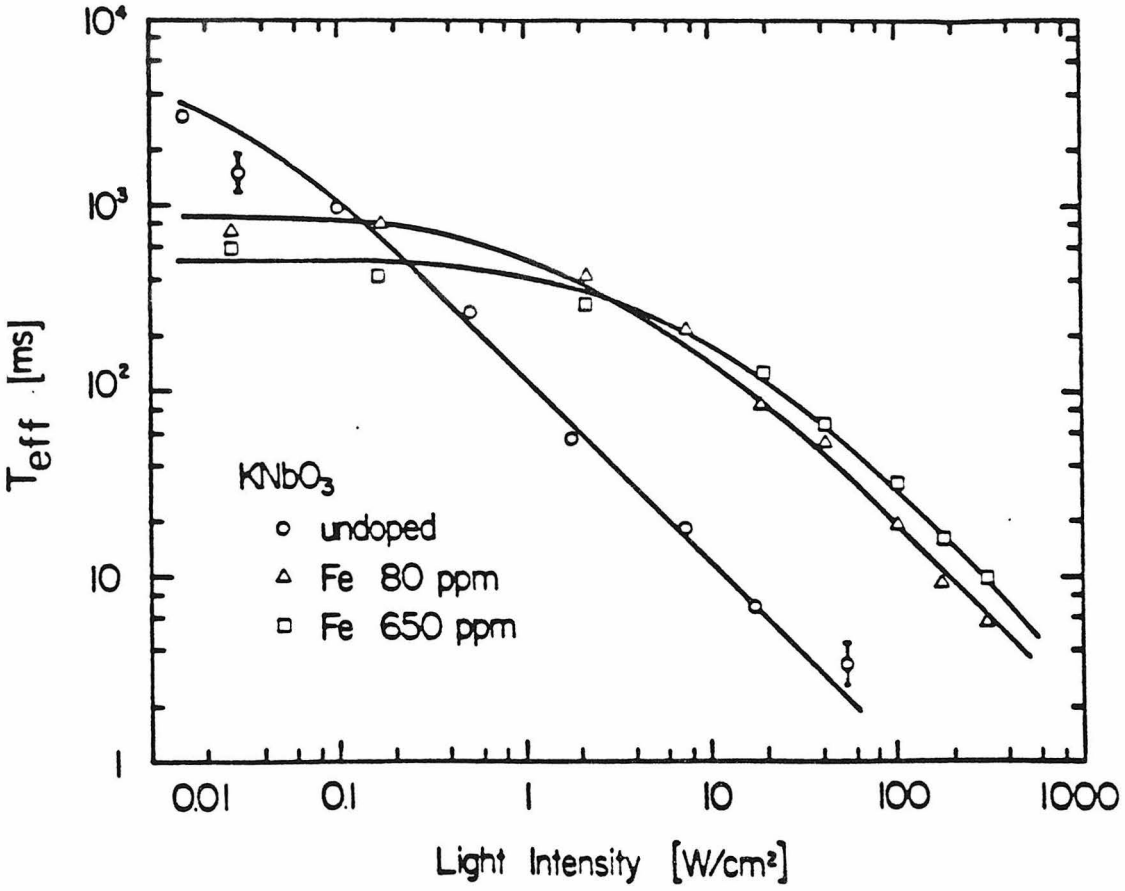

Figure 2.7 Intensity dependence of the diffraction efficiency risetime T_{ef} for $KNbO_3$:Fe (after Ref. 38)

$$\Omega_{res} = \frac{E_0(E_p - E_\mu)/t_0}{(E_d + E_\mu)^2 + E_0^2} \qquad (2.15a)$$

We should note that at zero applied field, the resonance is at $\Omega = 0$.

That the resonant oscillation frequency is the same as the natural oscillation frequency of the space charge is probably a general principle, not limited by the validity of our particular model. To find out in any real case the optimum fringe speed, one need only record a hologram with stationary fringe illumination and note the frequency of oscillations observed in the diffraction efficiency as it proceeds to steady state. It should be realized that the sign of Ω is very important. It is not sufficient simply to sweep the fringes back and forth: they must be made to travel in the proper direction across the face of the crystal. This could be accomplished in practice by applying a sawtooth modulation to one of the writing beams.

One area where the theory does not agree with experiment, however, is in the observation of these predicted transient frequencies. In our experimental experience with BSO, the magnitude of these transients has never been as large as might be expected on the basis of the theory. Indeed it is debatable whether or not they exist at all. The growth of diffraction efficiency seems to be simply exponential.

One important application of photorefractive holography is the coherent amplification of information carrying beams of light. According to the coupled mode theory of two beam coupling which will be discussed in chapter 3, the energy coupling between the two writing beams is maximized when the phase shift ψ is $\pi/2$. This is why it might be important to be able to adjust this phase as was done in a vibration analysis experiment by Huignard and Marrakchi[37] It is $\pi/2$ when

$$\Omega = \frac{E_0 E_p / t_0}{E_0^2 + E_d E_\mu + E_d^2} \qquad (2.15b)$$

The hopping model

In this model, put forward by Feinberg and coworkers in 1980[13], there are a certain number of charges in the crystal which can occupy a large number of sites in any of a large number of permutations. In darkness, each charge stays fixed at a site, but when charge is exposed to an optical intensity I, it tends to "hop" to an adjacent site with a probability per second that is proportional to I. In terms of the probability W_n that a migrant charge occupies the nth site at position x_n, they expressed their theory mathematically by

$$\frac{dW_n}{dt} = -\sum_m D_{mn}[W_n I_n \exp(\tfrac{1}{2}\beta\varphi_{nm}) - W_m I_m \exp(\tfrac{1}{2}\beta\varphi_{mn})] \qquad (2.16)$$

where the sum is over the neighbouring sites m and the intensity at site n in I_n. The rate constant $D_{mn}\exp(\tfrac{1}{2}\beta\varphi_{mn})$ measures the tendency towards light-induced hopping from site m to site n. It is written in terms of the parameters $D_{mn} = D_{nm}$ and of the static potential difference φ_{nm} between the sites m and n. Here, β is $q/(k_B T)$ with q the charge of the carrier. This factor ensures that the relative site occupancy in steady state under weak uniform illumination will obey statistical mechanics, viz., that $W_m/W_n = \exp(\beta\varphi_{nm})$. Specific sources of the potential are internal fields due to charge migration, externally applied fields and intrinsic chemical potentials. When a hologram is written by a pair of intersecting beams of light it is the final distribution of the hopping charge that acts through the electrooptic effect to produce the refractive index grating. Through considerations of the sign of the electrooptic coefficients and the direction of coupling in two beam amplification experiments, it was determined that in the particular sample of barium titanate used by Feinberg et. al. the sign of the charge carriers was positive[13].

In the rate equation model, on the other hand, it is the distribution of empty sites that gives rise to the principal contribution to the holographic space charge. Variations in this distribution are mediated by the much less populous carriers (assumed above to be electrons) excited to the conduction band by the light interference pattern. We can interpret the rate equation model as a hopping model, by realizing that an empty site has positive charge, much as a hole in a semiconductor is positively charged. The hopping charge carrier of the hopping model corresponds to the empty, or ionized site of the rate equation model where hopping is accomplished by transfer of electrons. It turns out that under the approximations used in each case, the steady state results of the two theories are the same up to minor differences in the phase of the index grating with respect to the light interference pattern. The temporal behaviors of the two models are different, however, because of the difference in hopping dynamics; the first thing to notice is that the charge carrier mobility which appears in the time constant of the rate equation model is absent in the hopping model.

The total number of charge carriers in the hopping model corresponds to the number of sites ionized in the dark in the rate equation model. Where W appears in the hopping model, we can replace it by p/N of the rate equation. We now proceed to a solution of the hopping model with the approximations used in the original treatment by Feinberg et. al. It is assumed that

i) The direction of any uniform electric field and the grating wavevector are assumed to be parallel or antiparallel to the optic axis of a uniaxial crystal.

ii) The sites are equally rather than randomly spaced by the distance s along the wavevector.

iii) $ks << 1$, that is, there are many sites in the space of one grating period.

iv) The hopping constant D_{mn} is zero except for nearest neighbours where it takes the value D.

v) Typically, $s \approx 10^{-6}$ cm and β corresponds to room temperature ($\approx 1/40$ eV) so that if internal electric fields are below 50 kV/cm, $\frac{1}{2}\beta\varphi_{mn}$ is much less than unity. This is borne out by experimental experience in our experiments with BSO and $BaTiO_3$.

With these assumptions, and replacing finite differences by derivatives, we find that the hopping model reduces to the following equation

$$\frac{\partial W}{\partial t} = -Ds^2 \frac{\partial}{\partial x}(\beta W I E - \frac{\partial}{\partial x} W I) \tag{2.17}$$

which looks very much like the charge conservation equation (2.10b) of the rate equation model. With this in mind it becomes more understandable that the results of the theories are so similar. Time differences arise because when the conduction band electron density in (2.10d) is replaced by an expression in terms of p using (2.10a) extra time derivatives are introduced into the right hand side. If additionally

vi) the various quantities are approximable, as for the rate equation model by their first Fourier expansions,

and we replace W by p/N we find that in terms of the characteristic fields the equation becomes

$$iE_d t_0 \frac{dp_1}{dt} = p_1[E_0 - i(E_p + E_d)] + \frac{I_1}{I_0} p_d e^{i\Omega t}[E_0 - iE_d] \tag{2.18}$$

where the characteristic time t_0 is now given by

$$t_0 = 1/(Ds^2 I_0) \tag{2.19}$$

The solution is given by

$$\frac{p_1}{p_d} = \frac{-I_1/I_0(E_0 - iE_d)(e^{i\Omega t} - e^{-t/\tau})}{[E_0 + \Omega t_0 E_d)] - i(E_d + E_p)} \tag{2.20}$$

where τ is the complex time constant

$$\tau = t_0 \frac{-iE_d}{E_0 - i(E_d + E_p)} \tag{2.21}$$

Since the steady state, stationary fringe behaviours of the two models are so similar, it is worthwhile to examine the differences in some detail. The rate equation model under these conditions gives

$$\frac{p_1}{p_d} = \frac{I_1/I_0(E_0 + iE_d)}{E_0 + i(E_d + E_p)} \tag{2.22}$$

while the hopping model gives

$$\frac{p_1}{p_d} = \frac{-I_1/I_0(E_0 - iE_d)}{E_0 - i(E_d + E_p)} \tag{2.23}$$

Firstly, we notice that the magnitudes of these distributions are in fact the same. Secondly, in the absence of uniform electric field, the hopping charge density is π out of phase with the light interference pattern because the light drives the charge carriers out of the regions of high intensity. On the other hand, in the rate equation model the excess space charge is left behind in the region of high intensity when the charge carriers leave. Thus the space charge is in phase with the interference pattern. And finally, the effect of a uniform electric field is the same in each case; the grating moves in the direction of the electric field, because while the sign of the mobile charge carriers is opposite in each case, they also travel in different directions under the influence of the field.

References for Chapter 2

1. J.J. Amodei, RCA Rev. **32**, 185 (1971)
2. Y. Ninomaya, J. Opt. Soc. Am. **63**, 1124 (1973)
3. L. Young, W.K.Y. Wong, M.L.W. Thewalt and W.D. Cornish, Appl. Phys. Lett. **24**, 264 (1974)
4. D.W. Vahey, J. Appl. Phys. **46**, 3510 (1975)
5. D.M. Kim, R.R. Shah, T.A. Rabson and F.K. Tittel, Appl. Phys. Lett. **28**, 338 (1975)
6. S.F. Su and T.K. Gaylord, J. Appl. Phys. **46**, 5208 (1975)
7. R. Magnusson and T.K. Gaylord, J. Appl. Phys. **47**, 190 (1976)
8. M.G. Moraham and L. Young, J. Appl. Phys. **48**, 3230 (1977)
9. B.I. Sturman, Sov. Phys. Tech. Phys. **23**, 589 (1978)
10. N.V. Kukhtarev, V.B. Markov, S.G. Odulov, M.S. Soskin and V.L. Vinetskii, Ferroelectrics **22**, 949 (1979)
11. A.M. Glass, D. von der Linde and T.J. Negran, Appl. Phys. Lett. **25**, 233 (1974)
12. M.G. Moharam, T.K. Gaylord, R. Magnusson and L. Young, J. Appl. Phys. **50**, 5642 (1979)
13. J. Feinberg, D. Heiman, A.R Tanguay,Jr. and R.W. Hellwarth, J. Appl. Phys. **51**, 1297 (1980)
14. J. Feinberg, Opt. Lett. **5**, 330 (1980)
15. S.I. Stepanov, V.V. Kulikov and M.P. Petrov, Opt. Commun. **44**, 19 (1982)
16. R.L. Townsend and J.T. La Macchia, J. Appl. Phys. **41**, 5188 (1970)

17. P. Gunter, U. Fluckiger, J.P. Huignard and F. Micheron, Ferroelectrics **13**, 297 (1976)

18. F.S. Chen, J. Appl. Phys. **38**, 3148 (1967)

19. R. Orlowski, L.A. Boatner and E. Kratzig, Opt. Commun. **35**, 45 (1980)

20. J.J. Amodei, D.L. Staebler and A.W. Stephens, Appl. Phys. Lett. **18**, 507 (1971)

21. J.B. Thaxter, Appl. Phys. Lett., **15**, 210 (1969)

22. L.H. Lin, Proc. IEEE **57**, 252 (1969)

23. M. Peltier and F. Micheron, J. Appl. Phys. **48**, 3683 (1977)

24. V.M. Fridkin, B.N. Popov and K.A. Verkhovskaya, Appl. Phys. **16**, 313 (1978)

25. A. Ashkin, B. Tell, and J.M. Dziedzic, IEEE J. Quant. Electron. **QE-3**, 400 (1967)

26. T.Nakamura, V. Fridkin, R. Magomadov, M Takashige and K. Verkhovskaya, J. Phys. Soc. Jap. **48**, 1588 (1980)

27. W.Philips, J.J. Amodei and D.L. Staebler, RCA Rev. **33**, 94 (1972)

28. A. Ishida, O. Mikami, S. Miyazawa and M. Sumi, Appl. Phys. Lett. **21**, 193 (1972)

29. E. Okamoto, H. Ikeo and K Muto, Appl. Opt. **14**, 2453 (1975)

30. K. Megumi, H. Kozuka, M. Kobayashi and Y. Furuhata, Appl. Phys. Lett. **30**, 631 (1977)

31. G.E. Peterson, A.M. Glass and T.J. Negran, Appl. Phys. Lett. **19**, 130 (1971)

32. R. Orlowski and E. Kratzig, Solid State Commun. **27**, 1351 (1978)

33. J.P. Huignard, J.P. Herriau and G. Rivet, Opt. Lett. **5**, 102 (1980)

34. M.P. Petrov, S.V. Miridonov, S.I. Stepanov and V.V. Kulikov, Opt. Commun. **31**, 301 (1979)

35. S.L. Hou, R.B. Lauer and R.E. Aldrich, J. Appl. Phys. **44**, 2652 (1973)

36. S.I. Stepanov, V.V. Kulikov and M.P. Petrov, Opt. Commun. **44**, 19 (1982)

37. J.P. Huignard and A. Marrakchi, Opt. Commun. **38**, 249 (1981)

38. P. Gunter, to be published, Rev. Mod. Phys.

39. M.E. Lines, A.M. Glass, 'Principles and Applications of Ferroelectrics and Related Materials", (Clarendon Press, Oxford, 1977)

Chapter 3

Coupled Wave Equations and the Undepleted Pumps Approximation

Introduction

Microscopic theories of the photorefractive effect generally involve photoionization of charge carriers from impurity levels. These carriers are subject to drift and diffusion in the spatially varying intensity of the recording beams and the electric field associated with the resultant space charge operates through the electrooptic effect to modulate the index of refraction. This effect is nonlocal, with one manifestation being that the index grating is not in phase with the interference pattern. For this reason, phase conjugation by degenerate four-wave mixing in PR crystals is different in kind than phase conjugation in other media and we cannot characterize the medium response by a simple constitutive third order nonlinear constant $\chi^{(3)}$. The derivation of the coupled wave equations with the associated effective third order nonlinearities is as follows.

The refractive index grating

The basic interaction geometry is illustrated in Fig. 3.1. Four waves of equal frequency ω and, for simplicity, of the same polarization are propagating through the PR medium. Let the electric field amplitude associated with the jth beam be

$$\mathbf{E}_j(\mathbf{r},t) = A_j(\mathbf{r})\exp[i(\mathbf{k}_j\cdot\mathbf{r}-\omega t)] + \text{c.c.} \tag{3.1}$$

We solve the problem in steady state so that the A_j may be taken to be time independent. The propagation directions come in two oppositely directed pairs,

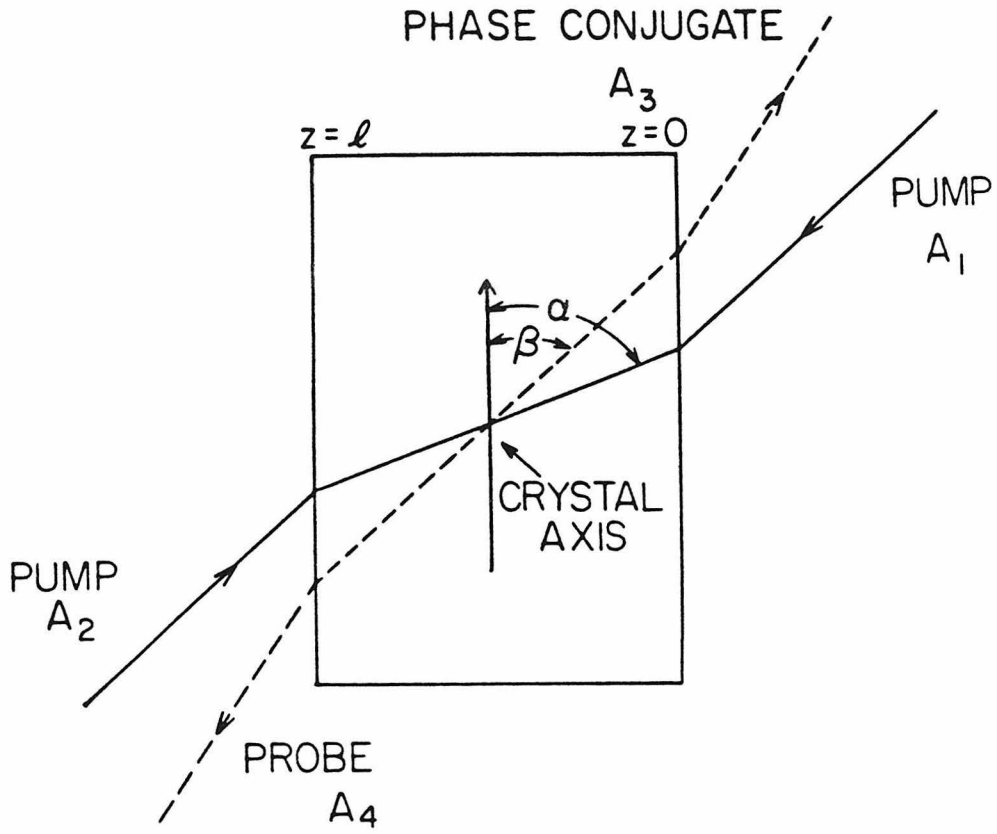

Figure 3.1 Four-wave mixing arrangement appropriate to phase conjugation showing the pump beams (solid) and probe and phase conjugate beams (dashed), as well as the relative orientation of the c-axis of the crystal.

$\mathbf{k}_1 = -\mathbf{k}_2$ and $\mathbf{k}_3 = -\mathbf{k}_4$, whereas the relative direction of $\mathbf{k}_1$ and $\mathbf{k}_4$ is arbitrary.

It is the fringes in the time independent part of the light intensity that generate the hologram, whose fringes have the same periodicity as the light interference pattern. In general, the holographic fringes of refractive index will have a spatial phase shift with respect to the interference pattern, so we can write the fundamental components of the intensity induced grating as

$$n = n_0 + \frac{n_I e^{i\varphi_I}}{2}\frac{(A_1^* A_4 + A_2 A_3^*)}{I_0}\exp(i\mathbf{k}_I\cdot\mathbf{r}) + c.c.$$

$$+ \frac{n_{II} e^{i\varphi_{II}}}{2}\frac{(A_1 A_3^* + A_2^* A_4)}{I_0}\exp(i\mathbf{k}_{II}\cdot\mathbf{r}) + c.c.$$

$$+ \frac{n_{III} e^{i\varphi_{III}}}{2}\frac{(A_1 A_2^*)}{I_0}\exp(i\mathbf{k}_{III}\cdot\mathbf{r}) + c.c.$$

$$+ \frac{n_{IV} e^{i\varphi_{IV}}}{2}\frac{(A_3^* A_4)}{I_0}\exp(i\mathbf{k}_{IV}\cdot\mathbf{r}) + c.c. \qquad (3.2)$$

where

$$I_0 = \sum_{j=1}^{4} I_j \qquad (3.3)$$

with I_j the intensity $|A_j|^2$ of beam j. Through this normalization by I_0 we anticipate that the coupling strengths in the PR effect are approximately independent of total intensity, in direct contrast with four-wave mixing via nonlinear polarizabilities. The phases φ_I, φ_{II}, φ_{III} and φ_{IV} are real and n_I, n_{II}, n_{III} and n_{IV} represent the amplitudes of the various gratings. Their real and imaginary parts represent the dispersive and absorptive components of the grating respectively. $\mathbf{k}_I = \mathbf{k}_4 - \mathbf{k}_1 = \mathbf{k}_2 - \mathbf{k}_3$, $\mathbf{k}_{II} = \mathbf{k}_1 - \mathbf{k}_3 = \mathbf{k}_4 - \mathbf{k}_2$, $\mathbf{k}_{III} = 2\mathbf{k}_1$ and $\mathbf{k}_{IV} = 2\mathbf{k}_4$. The complex constant $n_I e^{i\varphi_I}$, as an example, characterizes the spatial hologram written by the intensity interference pattern of beams 1 and 4 and also that of beams 2 and 3. These two pairs of waves are characterized by the same constant because $\mathbf{k}_4 - \mathbf{k}_1$

$= \mathbf{k}_2 - \mathbf{k}_3$.

The expressions for these various constants are obtained by solving the specific physical process responsible for the hologram formation. Expressions for n_I and φ_I, for example, derived from the rate equation model described in Chapter 2 are

$$n_I = \frac{r_{eff} n_o^3 E_p}{2} \left[\frac{E_0^2 + E_d^2}{E_0^2 + (E_d + E_p)^2} \right]^{1/2} \tag{3.4}$$

$$\tan \varphi_I = \frac{E_d(E_d + E_p) + E_0^2}{E_0 E_p} \tag{3.5}$$

where n_o is the ordinary refractive index, r_{eff} is the relevant electrooptic coefficient, E_0 is a superimposed spatially uniform electric field, either applied or intrinsic (due, e.g. to the photovoltaic effect[1]) directed along $\mathbf{k}_I$, and E_d and E_p are electric fields characteristic of diffusion and maximum space charge respectively. $E_d = k_B T k_I / e$ and $E_p = e p_d / (\varepsilon k_I)$, where p_d is the density of traps in the material, k_B is Boltzmann's constant, T is the temperature, e is the electron charge, ε is the permittivity of the material and $k_I = |\mathbf{k}_I|$. The electrooptic coefficient is given by

$$r_{eff} = \varepsilon_{ii}(r_{ijk}\mathbf{k}_{Ik})\varepsilon_{jj}/(k_I n_o^3 n_\lambda) \tag{3.6a}$$

Where n_λ is n_e or n_o depending on whether the mixing beams are of extraordinary or ordinary polarization. For crystals of the point group 4mm such as SBN and $BaTiO_3$ the nonzero electrooptic coefficients and their conventional contracted notations are $r_{zzz} \equiv r_{33}$, $r_{xxz} = r_{yyz} \equiv r_{13}$, and $r_{yzy} = r_{xzx} \equiv r_{42}$. Equation (3.6a) reduces to

$$r_{eff} = r_{13} \sin[(\alpha + \beta)/2] \tag{3.6b}$$

for mixing beams of ordinary polarization and

$$r_{eff} = \{n_e^4 r_{33}\sin\alpha\sin\beta + 2n_e^2 n_o^2 r_{42}\cos^2[(\alpha+\beta)/2] \qquad (3.6c)$$

$$+ n_o^4 r_{13}\cos\alpha\cos\beta\}\sin[(\alpha+\beta)/2]/(n_e n_o^3)$$

for mixing beams of extraordinary polarization where α and β are the angles of the pump beams and the probe and phase conjugate beams with respect to the optic axis of the crystal as shown in Fig. 3.1. The r_{ij} are the electrooptic coefficients and n_o and n_e are the ordinary and extraordinary refractive indices respectively.

In $BaTiO_3$ the large electrooptic coefficient[2] is r_{42}. To observe the largest effects it is necessary to use extraordinary polarization and to orient the crystal so that the grating wavevector is not parallel to any of the crystal axes. In SBN on the other hand, it is r_{33} that is large[3] ($\approx 10^{-9}$m/V). While it is still necessary to use extraordinary polarization, the grating wavevector can here be parallel to the optic axis of the crystal.

Notice that according to (3.4) n_I is real; the dispersive part of the grating is dominant, and from now on, the n_j will be assumed real.

The coupled wave equations

By using (3.2) in the scalar wave equation

$$\nabla^2 E + k^2 E = 0 \qquad (3.7)$$

and the standard slowly varying field approximation[2]

$$\left|\frac{d^2 A_j}{dz^2}\right| << k\left|\frac{dA_j}{dz}\right| \qquad (3.8)$$

we can derive four coupled wave equations with z the coordinate along the crystal normal (Fig 3.1), ϑ_1 and ϑ_2 the angles of pump 1 and probe 4 with respect to the crystal normal and α the linear absorption:

$$\frac{2c}{\omega}\cos\vartheta_1\frac{dA_1}{dz}=-\frac{in_I e^{-i\varphi_I}}{I_0}(A_1A_4^*+A_2^*A_3)A_4-\frac{in_{II}e^{i\varphi_{II}}}{I_0}(A_1A_3^*+A_2^*A_4)A_3$$

$$-\frac{in_{III}e^{i\varphi_{III}}}{I_0}(A_1A_2^*)A_2-\frac{2c}{\omega}\cos\vartheta_1\alpha A_1 \qquad (3.9a)$$

$$\frac{2c}{\omega}\cos\vartheta_1\frac{dA_2}{dz}=\frac{in_I e^{i\varphi_I}}{I_0}(A_1^*A_4+A_2A_3^*)A_3+\frac{in_{II}e^{-i\varphi_{II}}}{I_0}(A_1^*A_3+A_2A_4^*)A_4$$

$$+\frac{in_{III}e^{-i\varphi_{III}}}{I_0}(A_1^*A_2)A_1+\frac{2c}{\omega}\cos\vartheta_1\alpha A_2 \qquad (3.9b)$$

$$\frac{2c}{\omega}\cos\vartheta_2\frac{dA_3}{dz}=\frac{in_I e^{-i\varphi_I}}{I_0}(A_1A_4^*+A_2^*A_3)A_2+\frac{in_{II}e^{-i\varphi_{II}}}{I_0}(A_1^*A_3+A_2A_4^*)A_1$$

$$+\frac{in_{IV}e^{-i\varphi_{IV}}}{I_0}(A_3A_4^*)A_4+\frac{2c}{\omega}\cos\vartheta_2\alpha A_3 \qquad (3.9c)$$

$$\frac{2c}{\omega}\cos\vartheta_2\frac{dA_4}{dz}=-\frac{in_I e^{i\varphi_I}}{I_0}(A_1^*A_4+A_2A_3^*)A_1-\frac{in_{II}e^{i\varphi_{II}}}{I_0}(A_1A_3^*+A_2^*A_4)A_2$$

$$-\frac{in_{IV}e^{i\varphi_{IV}}}{I_0}(A_3^*A_4)A_3-\frac{2c}{\omega}\cos\vartheta_2\alpha A_4 \qquad (3.9d)$$

Two beam coupling and the unidirectional ring resonator

When A_3 and A_2 are taken to be zero in the above equations, we recover the well-known theory of holographic two beam coupling[4–6]. There too, the spatial phase difference φ_I between the light interference pattern and the index grating plays an important role. Its sign determines the direction of energy transfer from one beam to the other. It introduces an asymmetry that allows one beam to be amplified by constructive interference with radiation scattered by the grating, while the other beam is attenuated by destructive interference with diffracted radiation. This asymmetry is available because we are using the linear electrooptic effect, which is not invariant under space inversion and can only arise in noncentrosymmetric media. Explicitly, the coupled wave equations for

two beam coupling, derived from (3.9) are (see 3.16 for γ)

$$\frac{dA_1}{dz} = -\frac{\gamma}{I_0}A_1|A_4|^2 - \alpha A_1 \tag{3.10a}$$

$$\frac{dA_4}{dz} = +\frac{\gamma^*}{I_0}A_4|A_1|^2 - \alpha A_4 \tag{3.10b}$$

which can be rewritten

$$\frac{dI_1}{dz} = -\Gamma\frac{I_1I_4}{I_0} - 2\alpha I_1 \tag{3.11a}$$

$$\frac{dI_4}{dz} = \Gamma\frac{I_1I_4}{I_0} - 2\alpha I_4 \tag{3.11b}$$

$$\frac{d\psi}{dz} = \Gamma'\frac{(I_1 - I_4)}{I_0} \tag{3.11c}$$

where $\Gamma = 2\mathrm{Re}\,\gamma$ represents the component of the grating in quadrature and $\Gamma' = \mathrm{Im}\,\gamma$ represents the component of the grating in phase with the interference pattern. ψ, defined as the phase of A_1 minus the phase of A_4, is the absolute phase of the interference pattern. Any in-phase component of the grating will cause this phase to vary with z so that the planes of the interference pattern, and hence the grating, will be bent. Such in-phase components are common in many other real time holographic media, including centrosymmetric ones. The asymmetry in the bent holograms cannot then be due to material asymmetry. Indeed, inspection of (3.11c) indicates that the asymmetry is in the relative intensities of the interacting beams. The in-quadrature component of the grating causes energy transfer from beam 1 to beam 4 (if Γ is positive), regardless of the relative intensities of the beams. This asymmetry, as discussed above, is in fact a property of the holographic medium. The solutions of (3.11) are[4-6]

$$I_1(z) = \frac{I_0(0)e^{-\alpha z}}{1 + (I_4(0)/I_1(0))e^{\Gamma z}} \tag{3.12a}$$

$$I_4(z) = \frac{I_0(0)e^{-\alpha z}}{1 + (I_1(0)/I_4(0))e^{-\Gamma z}} \tag{3.12b}$$

$$\psi = \frac{\Gamma'}{\Gamma}\ln\left[\frac{(1 + I_4(0)/I_1(0))^2 e^{\Gamma z}}{(1 + (I_4(0)/I_1(0))e^{\Gamma z})^2}\right] \tag{3.12c}$$

Suppose we were to build a ring resonator containing a PR crystal pumped by beam 1 (Fig. 3.2). Then, if the amplification of beam 4 due to two beam coupling from beam 1 were sufficient to overcome cavity losses and absorption in the crystal, we could expect an oscillation beam to build up in the ring. And, as pictured in the frontispiece, this is exactly what happens[7]. A $BaTiO_3$ crystal measuring 7×4.5×4mm was used, oriented so that the angle α (Fig. 3.1) was 168° and the angle β was 160°. It was placed in an oil filled cuvette, so as to provide some degree of index matching; the refractive indices of $BaTiO_3$ are about 2.5. In the photograph, this cuvette appears swamped in the red helium neon laser light, entering from bottom right. The diffuse light which seems to spray from the left hand side of the cuvette is due to the fanning effect[8], which is probably extreme holographic two beam amplification of stray scattered light. The mirror in the top right is in fact a beam splitter, so that some of the oscillation beam is transmitted to the screen. The gain exceeds the losses in the clockwise direction only, and the oscillation beam runs only in that direction. In ring dye lasers, for example, a great deal of effort is devoted to enforcing unidirectional oscillation to eliminate spatial holeburning.

An expression for the intensity of the oscillating beam in this device is now easily obtainable by fitting boundary conditions:

$$I_4(0) = (1 - L)I_4(l) \tag{3.13}$$

where L represents the cavity's fractional linear intensity loss per round trip.

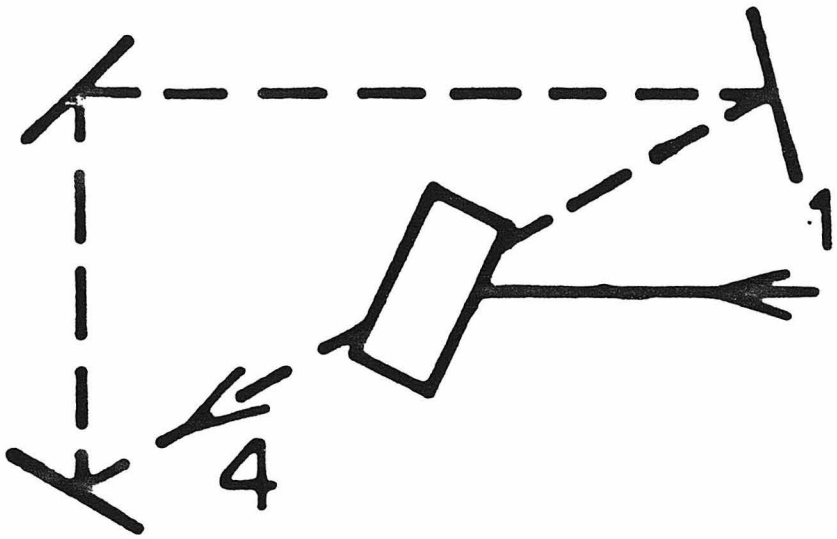

Figure 3.2 Unidirectional ring resonator. Power is transferred from pumping beam 1 to oscillation beam 4 by holographic two beam coupling.

The ratio of oscillating energy to pumping energy is

$$\frac{I_4(0)}{I_1(0)} = \frac{1 - e^{-(\Gamma - \alpha)L}}{L} - 1 \tag{3.14}$$

We note that $I_4(0)/I_1(0)$ is infinite for $L = 0$ and becomes zero, i.e., there is no oscillation at $L = 1 - e^{-(\Gamma - \alpha)L}$.

The asymmetries dealt with in this section carry over to phase conjugation where they give rise to many striking effects. In the next section, for example, we will show that they lead to an asymmetry between the roles of the counterpropagating pumping beams 1 and 2.

The transmission grating in the undepleted pumps approximation

The problem may be simplified by making two assumptions. First, we consider a holographic system whose spatial frequency response is such that of all the gratings present in the system, only one gives rise to strong beam coupling. This predominance of one grating is enforced in most practical situations by a choice of the directions, polarization and coherence relationships of the four beams relative to the crystal axes and to the application in some cases of an electric field that enhances certain gratings. Here, we consider the case of the transmission grating, where only n_I is nonzero. In addition we make the assumption $\vartheta_1 = \vartheta_2$, for later convenience in Chapter 4, when we solve the four coupled wave equations in the undepleted pumps approximation with negligible linear absorption.

The equations reduce to

$$\frac{dA_1}{dz} = -\frac{\gamma}{I_0}(A_1A_4^* + A_2^*A_3)A_4 - \alpha A_1 \tag{3.15a}$$

$$\frac{dA_2^*}{dz} = -\frac{\gamma}{I_0}(A_1A_4^* + A_2^*A_3)A_3^* + \alpha A_2^* \tag{3.15b}$$

$$\frac{dA_3}{dz} = \frac{\gamma}{I_0}(A_1A_4^* + A_2^*A_3)A_2 + \alpha A_3 \tag{3.15c}$$

$$\frac{dA_4^*}{dz} = \frac{\gamma}{I_0}(A_1A_4^* + A_2^*A_3)A_1^* - \alpha A_4^* \tag{3.15d}$$

where we have defined the coupling constant γ by

$$\gamma = \frac{i\omega n_1 e^{-i\varphi_1}}{2c\cos\vartheta_2} \tag{3.16}$$

Secondly, in this chapter, we make use of the undepleted pumps approximation, in which $I_1, I_2 >> I_3, I_4$. In this case, the nonlinear terms in (3.16a,b) are of the order of A_4^2 or A_3A_4, and can be neglected. With these approximations and boundary conditions appropriate for phase conjugation, ($A_3(l) = 0$ and $A_4^*(0)$ known), the solution of (3.16) is

$$A_1(z) = A_1(0)e^{-\alpha z} \tag{3.17a}$$

$$A_2(z) = A_2(l)e^{\alpha(z-l)} \tag{3.17b}$$

$$A_3(z) = -\frac{A_2(l)A_4^*(0)e^{\alpha(z-l)+\gamma z}}{A_1^*(0)}\frac{J(z)}{J(0)-1} \tag{3.17c}$$

$$A_4^*(z) = -A_4^*(0)e^{-\alpha z+\gamma z}\left[\frac{J(z)-e^{-\gamma z}}{J(0)-1}\right] \tag{3.17d}$$

where

$$J(z) = \int_{\gamma z}^{\gamma l}\frac{\exp(-x)dx}{1 + r\,e^{-2\hat{\alpha}\gamma l}\exp(4\hat{\alpha}x)} \tag{3.18}$$

with r the ***pump ratio*** I_2/I_1 and $\hat{\alpha}$ the normalized linear absorption α/γ. The

phase conjugate reflectivity is thus

$$\rho \equiv \frac{A_3(0)}{A_4^*(0)} = -\frac{A_2(l)}{A_1^*(0)}\frac{J(0)\,e^{-\alpha l}}{J(0)-1} \tag{3.19}$$

In Fig. 3.3 we plot the phase conjugate intensity reflectivity $R = |\rho|^2$ as a function of pump ratio for $\gamma l = \pm 3$ and for various values of the normalized linear absorption $\hat{\alpha}$. We see that the effect of increasing linear absorption is primarily to decrease the reflectivity, with the greater decrease being for negative γl. We observe too that the reflectivity for zero absorption is unchanged under the transformation $r \to 1/r$ and $\gamma \to -\gamma$. This means that probe beams travelling in opposite directions to each other will experience the same reflectivity from a given PR phase conjugate mirror. This is of considerable practical importance in the design of various optical resonator devices based on four-wave mixing in PR crystals.

The integration for the function J can be explicitly performed when $\hat{\alpha}$ is zero. In syntax error file etv0.tbl, between lines 1505 and 1505 that case, the solutions given in (3.18) reduce

$$A_1(z) = A_1(0) \tag{3.20a}$$

$$A_2(z) = A_2(l) \tag{3.20b}$$

$$A_3(z) = \frac{A_2(l)A_4^*(0)}{A_1^*(0)}\left[\frac{e^{\gamma(z-l)}-1}{e^{-\gamma l}+r}\right] \tag{3.20c}$$

$$A_4^*(z) = A_4^*(0)\left[\frac{e^{\gamma(z-l)}+r}{e^{-\gamma l}+r}\right] \tag{3.20d}$$

so that the reflectivity is simply

$$\rho = -\left[\frac{A_1A_2}{A_1^*A_2^*}\right]^{1/2}\frac{\sinh(\frac{1}{2}\gamma l)}{\cosh(\frac{1}{2}\gamma l + \frac{1}{2}\ln r)} \tag{3.21}$$

When the phase shift is zero, the magnitude of the coupling strength crystal

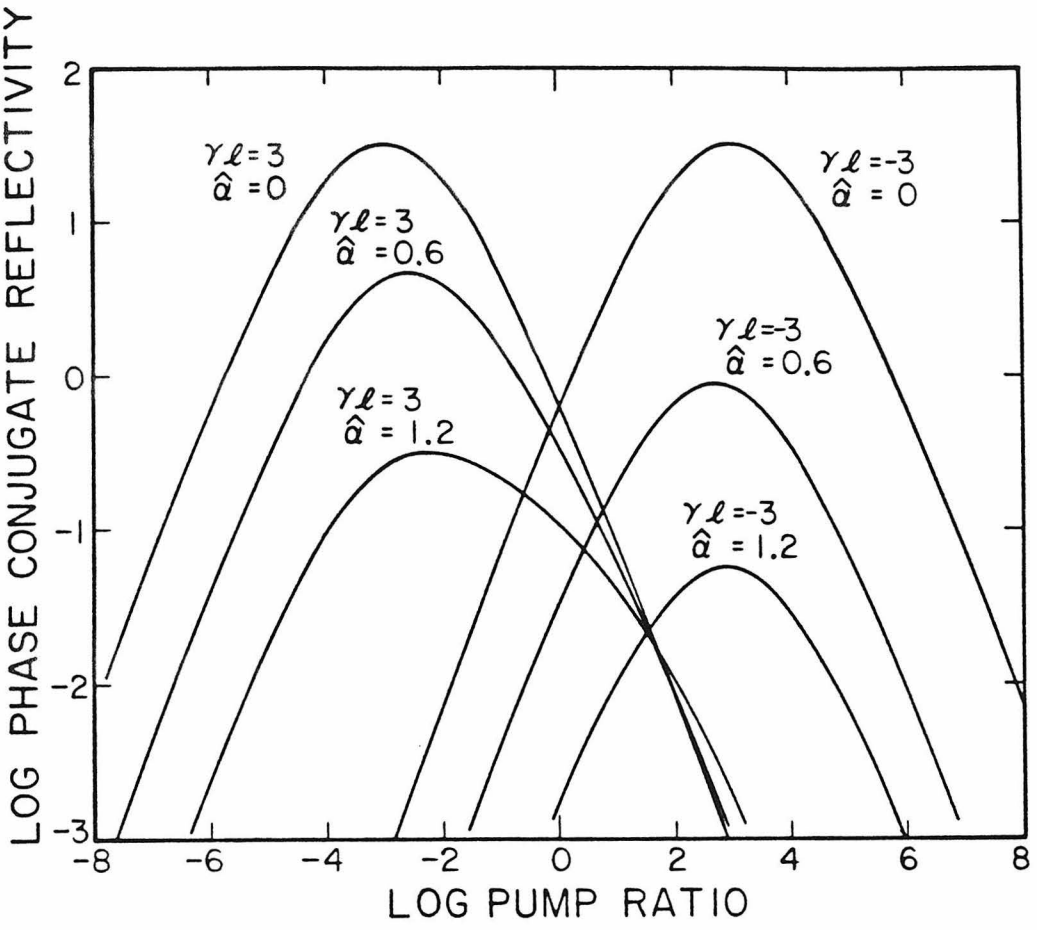

Figure 3.3 Phase conjugate intensity reflectivity in the undepleted pumps approximation as a function of pump ratio $I_2(l)/I_1(0)$ for coupling constant $\gamma l = \pm 3$ and for various values of the linear absorption normalized to γ: $\hat{\alpha} = \alpha/\gamma$.

length product is π and the pumping beams are of equal intensity the reflectivity becomes infinite, corresponding to the self oscillation effect[10]: we have finite output for zero input. Figure 3.4 is a graph of the reflectivity for various phase shifts. In each case the magnitude of the coupling strength length product is the same. The most important feature we observe here is that with the nonzero phase shifts common in PR four wave mixing the intensities of the pumping beams should be unequal for optimum reflectivity. This is in direct contrast with the situation familiar in four-wave mixing in media with a local response where the intensities of the pumping beams should be equal. Also, with the ninety degree phase shift common in our crystals, we find that self oscillation is not possible. However, by detuning the probe beam from the pump beams, the holographic phase shift is changed since the slowly responding grating lags behind the moving interference fringes. Recently, Lam pointed out that this departure from ninety degree phase shift can cause self oscillation[11]. This is shown here in the graph for phase shift $\pi/6$. We should also mention that the phase can be adjusted by applying an electric field; in that case, self oscillation should again become possible.

The reflection grating in the undepleted pumps approximation

The results above were derived with reference to the case n_I nonzero, where experimental conditions were such that the inteference of beams 1 and 4, and beams 2 and 3 induced a transmission grating. If instead, because of changes in the relative coherence of the interacting beams or because of different crystal orientation, it is the interference between beams 1 and 3 and beams 2 and 4 that is effective in hologram writing, then a reflection grating will result. This is described in the coupled wave equations (3.9) by taking n_{II} nonzero, all other coupling constants being negligible. The applicable coupled wave equations

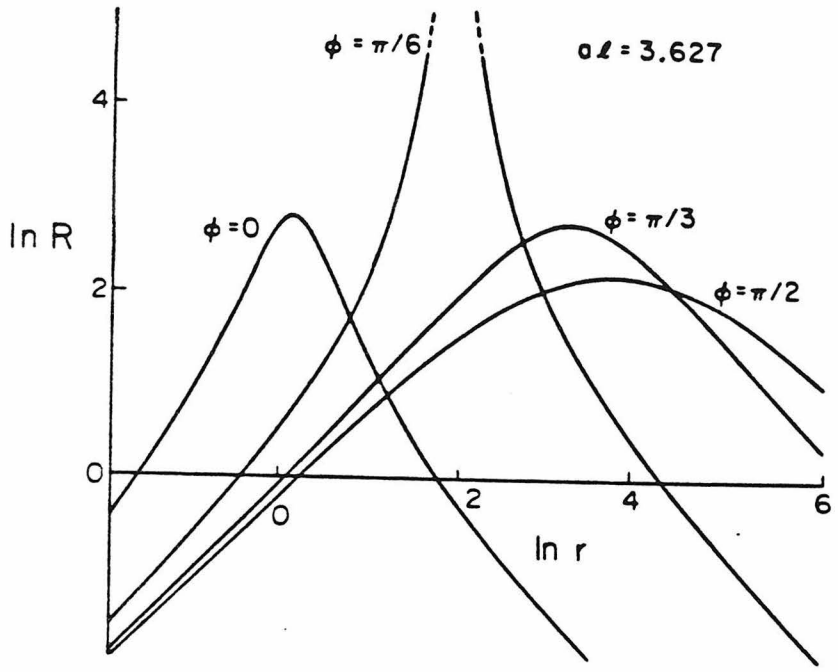

Figure 3.4 Phase conjugate reflectivity in the undepleted pumps approximation for coupling strength $\gamma l = -3.627$ and peaking from left to right, $\varphi = 0, \pi/6, \pi/3$ and $\pi/2$. Mirrorless self oscillation occurs here for $\varphi = \pi/6$ and $r = 6.13$.

reduce to

$$\frac{dA_1}{dz} = \frac{\gamma}{I_0}(A_1A_3^* + A_2^*A_4)A_3 - \alpha A_1 \tag{3.22a}$$

$$\frac{dA_2^*}{dz} = \frac{\gamma}{I_0}(A_1A_3^* + A_2^*A_4)A_4^* + \alpha A_2^* \tag{3.22b}$$

$$\frac{dA_3^*}{dz} = \frac{\gamma}{I_0}(A_1A_3^* + A_2^*A_4)A_1^* + \alpha A_3^* \tag{3.22c}$$

$$\frac{dA_4}{dz} = \frac{\gamma}{I_0}(A_1A_3^* + A_2^*A_4)A_2 - \alpha A_4 \tag{3.22d}$$

where the coupling constant γ is now given by

$$\gamma = \frac{-i\omega n_{II} e^{i\varphi_{II}}}{2c\cos\vartheta_2} \tag{3.23}$$

So that we may compare the results for the transmission and reflection gratings more closely, we rename the beams without changing the physics: $A_1 \rightarrow A_3 \rightarrow A_2 \rightarrow A_4 \rightarrow A_1$ (Fig. 3.5). It will now be easier to look for basic differences and similarities.

$$\frac{dA_1}{dz} = \frac{\gamma}{I_0}(A_1A_4^* + A_2^*A_3)A_4 - \alpha A_1 \tag{3.24a}$$

$$\frac{dA_2^*}{dz} = \frac{\gamma}{I_0}(A_1A_4^* + A_2^*A_3)A_3^* + \alpha A_2^* \tag{3.24b}$$

$$\frac{dA_3}{dz} = \frac{\gamma}{I_0}(A_1A_4^* + A_2^*A_3)A_2 + \alpha A_3 \tag{3.24c}$$

$$\frac{dA_4^*}{dz} = \frac{\gamma}{I_0}(A_1A_4^* + A_2^*A_3)A_1^* - \alpha A_4^* \tag{3.24d}$$

The close similarity between the coupled wave equations for the reflection and transmission gratings is readily apparent. The only difference between them is the sign of the nonlinear terms in the pump equations (3.15a,b) and (3.22a,b). It follows immediately that the results for the transmission grating and the

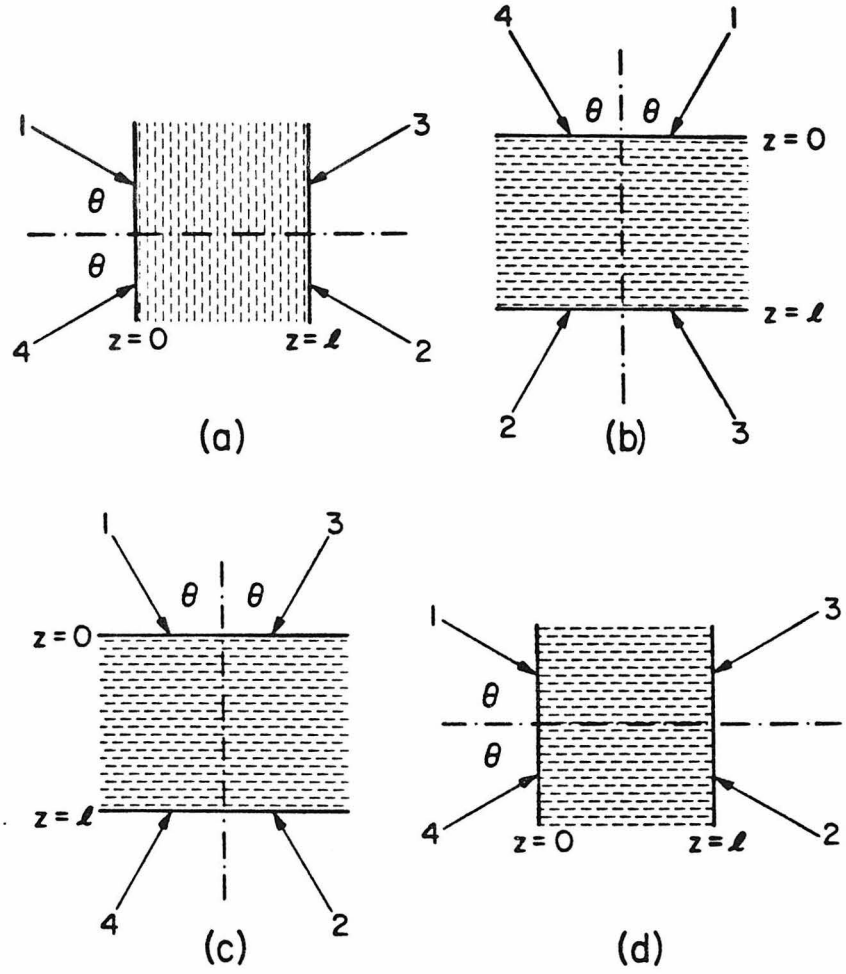

Figure 3.5 A transformation to facilitate comparision between transmission and reflection gratings.
a) The reflection grating.
b) The reflection grating rotated 90°.
c) The rotated reflection grating with renamed beams is now directly comparable to the transmission grating
d) The transmission grating

reflection grating are the same in the undepleted pumps approximation. As we show in the next chapter, however, the inclusion of pump depletion introduces important differences in the behaviours of the two types of grating.

References for Chapter 3

1. A.M. Glass, D. von der Linde and T.J. Negran, Appl. Phys. Lett. **25**, 233 (1974)
2. A. Yariv, "Quantum Electronics", (Wiley, New York, 1975)
3. B. Fischer, M. Cronin-Golomb, J.O. White, A. Yariv and R. Neurgaonkar, Appl. Phys. Lett. **40**, 863 (1982)
4. D.W. Vahey, J. Appl. Phys. **46**, 3510 (1975)
5. M.G. Moraham and L. Young, J. Appl. Phys. **48**, 3230 (1977)
6. N.V. Kukhtarev, V.B. Markov, S.G. Odulov, M.S. Soskin and V.L. Vinetskii, Ferroelectrics **22**, 949 (1979)
7. J.O. White, M. Cronin-Golomb, B. Fischer and A. Yariv, Appl. Phys. Lett. **40**, 450 (1982)
8. V.V. Voronov, I.R. Dorosh, Yu. S. Kuz'minov and N.V. Tkachenko, Sov. J. Quant. Electron. **10**, 1346 (1980)
9. B. Fischer, M. Cronin-Golomb, J.O. White and A.Yariv, Opt. Lett. **5**, 519 (1981)
10. A. Yariv and D.M. Pepper, Opt. Lett. **1**, 16 (1977)
11. J.F. Lam, Appl. Phys. Lett. **42**, 155 (1983)

Chapter 4

Exact Solution of the Coupled Wave Equations with Negligible Linear Absorption

Introduction

Four wave mixing coupled wave equations with pump depletion were first solved in 1979 by Marburger and Lam who used a Lagrangian method[1,2]. Subsequently, graphs of phase conjugate reflectivity much like those shown in Fig. 4.1 below were produced[3]. This solution, however, could not accommodate the photorefractive phase shifts between interference pattern and index grating. It was also only strictly valid for collinear pump and probe. In that case, extra polarization terms arose in the coupled wave equations which spoilt the phase conjugate nature of the reflected signal. Since then, Kessel and Musin have presented a solution for a very general class of nonlinear parametric processes including four-wave mixing[4]. This solution does not require the finding of conservation laws for the decoupling of the equations. However, it is still only valid for local nonlinear susceptibilities. In the paragraphs below, we find solutions for a system with nonlocal susceptibilities, the photorefractive crystal. It should be pointed out that all of these analyses derive the intensities and not the phases of the various beams so that the effects of strong nonlinearities on the phases of the output beams are not yet understood, and are the subject of current theoretical efforts. These effects will be important in considerations of the faithfulness of phase conjugation and the performance of resonators employing phase conjugate mirrors.

The transmission grating

We develop here the exact solution of (3.15) for four-wave mixing in PR media by the transmission grating with negligible linear absorption[5]. The first step is to write down a set of conservation laws.

$$A_1A_2 + A_3A_4 = c_1 \equiv c \tag{4.1a}$$

$$A_1A_3^* - A_2^*A_4 = c_2 \tag{4.1b}$$

$$I_1 + I_4 = d_1 \tag{4.1c}$$

$$I_2 + I_3 = d_2 \tag{4.1d}$$

where $c_1 \equiv c$, c_2, d_1, and d_2 are constants of integration. These relations may be checked easily using the coupled wave equations.

With the help of these conservation laws, (3.15a) and (3.15b) with zero absorption can be decoupled from (3.15c) and (3.15d)

$$\frac{dA_1}{dz} = -\frac{\gamma}{I_0}[A_1d_1 - A_1(I_1 + I_2) + A_2^*c] \tag{4.2a}$$

$$\frac{dA_2^*}{dz} = -\frac{\gamma}{I_0}[A_1c^* - A_2^*(I_1 + I_2) + A_2^*d_2] \tag{4.2b}$$

$$\frac{dA_3}{dz} = \frac{\gamma}{I_0}[A_3d_2 - A_3(I_3 + I_4) + A_4^*c] \tag{4.2c}$$

$$\frac{dA_4^*}{dz} = \frac{\gamma}{I_0}[A_3c^* - A_4^*(I_3 + I_4) + A_4^*d_1] \tag{4.2d}$$

By eliminating the term in $I_1 + I_2$ between (4.2a) and (4.2b), and the term in $I_3 + I_4$ between (4.2c) and (4.2d) we find the following expressions for $A_{12} \equiv A_1/A_2^*$ and $A_{34} \equiv A_3/A_4^*$

$$\frac{dA_{12}}{dz} = -\frac{\gamma}{I_0}[c + (d_1 - d_2)A_{12} - c^*A_{12}^2] \tag{4.3a}$$

$$\frac{dA_{34}}{dz} = \frac{\gamma}{I_0}[c + (d_2 - d_1)A_{34} - c^* A_{34}^2] \tag{4.3b}$$

Noting that I_0 is constant because of the conservation laws, we see that these equations are immediately integrable:

$$A_{12} = -\left[\frac{S_- De^{-\mu z} - S_+ D^{-1} e^{\mu z}}{2c^*(De^{-\mu z} - D^{-1}e^{\mu z})}\right] \tag{4.4a}$$

$$A_{34} = \left[\frac{S_- Ee^{-\mu z} - S_+ E^{-1} e^{\mu z}}{2c^*(Ee^{-\mu z} - E^{-1}e^{\mu z})}\right] \tag{4.4b}$$

where we define the following quantities

$$\Delta \equiv d_2 - d_1 \tag{4.5}$$

$$Q \equiv (\Delta^2 + 4|c|^2)^{1/2} \tag{4.6}$$

$$S_\pm \equiv \Delta \pm Q \tag{4.7}$$

$$\mu = \gamma Q/(2I_0) \tag{4.8}$$

and D and E are constants of integration.

We will first describe the application of this theory to the derivation of the reflectivity of a phase conjugate mirror with externally provided pumps. In this case, the amplitudes of all beams at their respective entrance faces are known.

We observe first of all that the power flux $\Delta = I_2(l) - I_1(0) - I_4(0)$ is known so we need only solve for D, E and c to finally obtain the phase conjugate reflectivity. The starting equations are the values of (4.4) at the boundaries z = 0 and z = l. The conservation law (4.1a) is also used to express the unknown field quantities $A_1(l)$ and $A_2^*(0)$ in terms of c, $A_3(0)$ and known fields

$$A_{12}(l) = -\left[\frac{S_- De^{-\mu l} - S_+ D^{-1} e^{\mu l}}{2c^*(De^{-\mu l} - D^{-1}e^{\mu l})}\right] = \frac{c}{I_2(l)} \tag{4.9a}$$

$$A_{12}(0) = -\left[\frac{S_- D - S_+ D^{-1}}{2c^*(D - D^{-1})}\right] = \frac{I_1(0)}{c^* - \rho^* I_4(0)} \tag{4.9b}$$

$$A_{34}(l) = \left[\frac{S_- E e^{-\mu l} - S_+ E^{-1} e^{\mu l}}{2c^*(E e^{-\mu l} - E^{-1} e^{\mu l})}\right] = 0 \tag{4.9c}$$

$$A_{34}(0) = \left[\frac{S_- E - S_+ E^{-1}}{2c^*(E - E^{-1})}\right] = \rho \tag{4.9d}$$

The procedure used to solve the equations is

a) Solve for E in terms of $|c|^2$ using (4.9c)

$$E = \left[\frac{S_+}{S_-}\right]^{1/2} = \left[\frac{\Delta + (\Delta^2 + 4|c|^2)^{1/2}}{\Delta - (\Delta^2 + 4|c|^2)^{1/2}}\right]^{1/2} e^{\mu l} \tag{4.10}$$

b) Solve for ρ in terms of $|c|^2$ using (4.9d) and (4.10)

$$\rho = \frac{-2cT}{\Delta T + (\Delta^2 + 4|c|^2)^{1/2}} \tag{4.11}$$

where $T = \tanh \mu l$

c) Solve for D in terms of $|c|^2$ using (4.9a)

$$D = \left[\frac{\Delta^2 + (\Delta^2 + 4|c|^2)^{1/2} - 2\Delta|c|^2 I_2(l)}{\Delta^2 - (\Delta^2 + 4|c|^2)^{1/2} - 2\Delta|c|^2 I_2(l)}\right]^{1/2} e^{\mu l} \tag{4.12}$$

d) Solve for $|c|^2$ using (4.9b), (4.11) and (4.12). We find that $|c|^2$ is given by the roots of the following equation

$$(|c|^2 - I_1(0)I_2(l))\,|\Delta T + (\Delta^2 + 4|c|^2)^{1/2}| + 4|c|^2|T|^2 I_4(0)I_2(l)$$

$$+ 2|c|^2 I_4(0)(\Delta^2 + 4|c|^2)^{1/2}(T + T^*) = 0 \tag{4.13}$$

e) The phase conjugate reflectivity is then given by the squared modulus of (4.11)

When considering reflectivity as a function of the various input beam intensities, it is convenient to define the *probe ratio*, q:

$$q \equiv \frac{I_4(0)}{I_1(0) + I_2(l)} \tag{4.14}$$

so that only two parameters are required to describe the input beams: the probe ratio q and the pump ratio $r = I_2(l)/I_1(0)$. In terms of these parameters we have

$$I_1(0) = \frac{I_0}{(r+1)(q+1)} \tag{4.15a}$$

$$I_2(l) = \frac{rI_0}{(r+1)(q+1)} \tag{4.15b}$$

$$I_4(0) = \frac{qI_0}{(q+1)} \tag{4.15c}$$

In Fig. 4.1, for example, we plot the reflectivity of a phase conjugate mirror as a function of the coupling strength $|\gamma l|$ for the case where the phase shift between the grating and the interference fringes is 5°. The intensities of the two pumping beams are equal ($r = 1$) and the probe intensity is twenty per cent of the total pumping intensity ($q = 0.2$). The top of the graph corresponds to the reflectivity that would result if all the power of beam 2 were transferred to beam 3. This is the maximum reflectivity consistent with the conservation laws (4.1). The peaks in the curve correspond to the poles in the reflectivity of a phase conjugate mirror with no pump depletion ($R = |\tanh(\frac{\gamma l}{2})|^2$ for no phase shift between the grating and interference fringes). We have set the phase shift slightly nonzero to demonstrate the resultant damping of the oscillatory behaviour. The peaks bend toward the right, probably since pump depletion causes high reflectivities to demand higher coupling strengths than are required for the same behaviour in the undepleted phase conjugate mirror. The bending of the peaks can even be sufficient for bistability, as can be seen in the first two peaks of Fig 4.1.

In Fig. 4.2, we show a contour plot of phase conjugate reflectivity for $\gamma l = -3$,

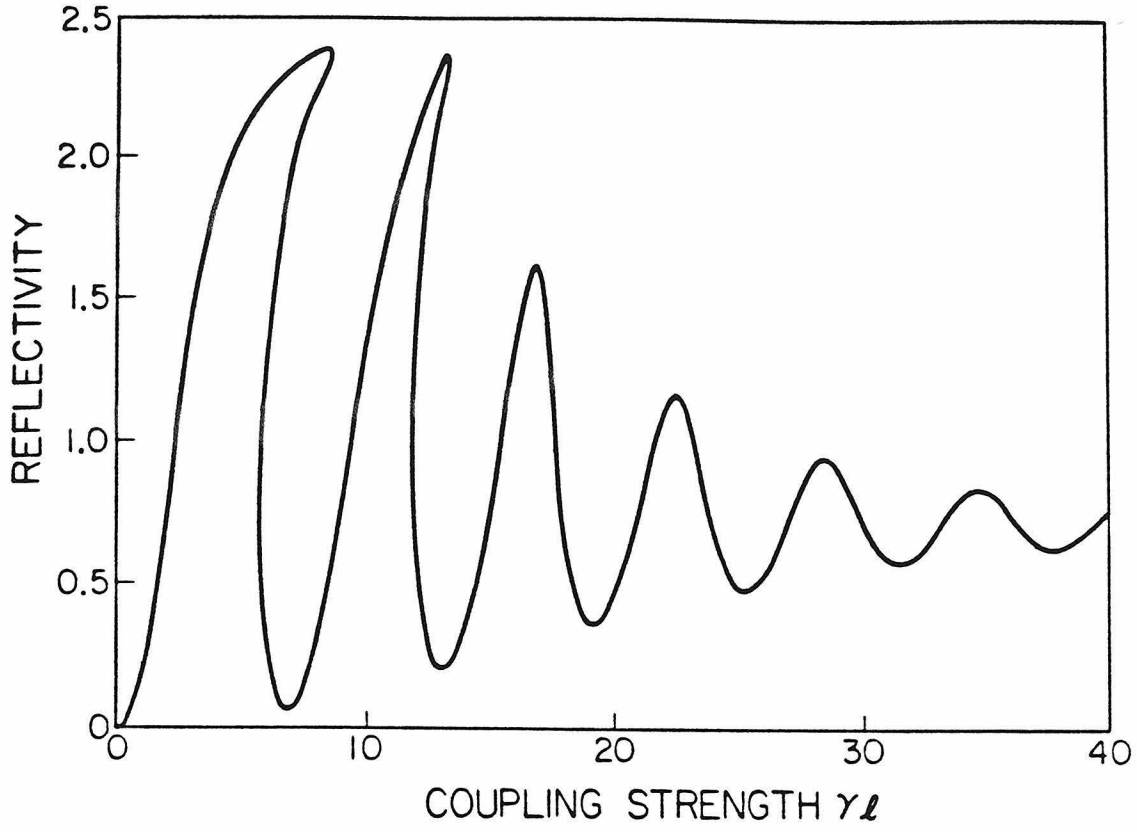

Figure 4.1 Reflectivity of a PR phase conjugate mirror versus coupling strength magnitude $|\gamma l|$. The incident pump beams are of equal intensity (r = 1), the intensity of the incident probe beam is 20% of the total incident pumping intensity and the phase shift between the index grating and the interference fringes is 5°. The four-wave mixing is via the transmission grating.

as a function of both pump and probe ratios. The first point to notice is the region of multistability, a direct result of the non-uniqueness of the solution of (4.13) for a certain range of parameters. Secondly, we observe that the reflectivity can remain finite as the pump ratio tends to infinity. This possibility for phase conjugation in the absence of pumping beam 2 has important consequences for the passive phase conjugate mirrors described below.

The basic physical difference between the two solution surfaces of Fig. 4.2 lies in the relative phases of the two terms $A_1A_4^*$ and $A_2^*A_3$ in the interference factor $(A_1A_4^* + A_2^*A_3)$ which appears in the coupled wave equations (3.15). When the phase conjugate mirror is operating on the main surface, the one which extends over the entire q-r plane, the phase conjugate beam is generated so that the interference pattern formed between itself and beam 2 is in phase with the interference pattern formed between the forward going beams 1 and 4. On the secondary surface, these two terms are π out of phase with each other, so that both the grating strength and the reflectivity are diminished.

It is often convenient to be able to examine the intensities of the various beams as a function of location z in the crystal. For example, in the next chapter of this thesis, we will consider several devices whose boundary conditions are given by the ratios of intensities of pumping beams. These ratios appear in functions whose zeros must be found to reach a solution. Occasionally, since the ratio of two negative numbers is positive, these functions will indicate solutions with negative intensities which nevertheless satisfy the boundary conditions. It is important in checking for these spurious solutions to have expressions for beam intensities as a function of z. These may be derived by using the amplitude ratio functions A_{12} and A_{34} in the conservation laws (4.1).

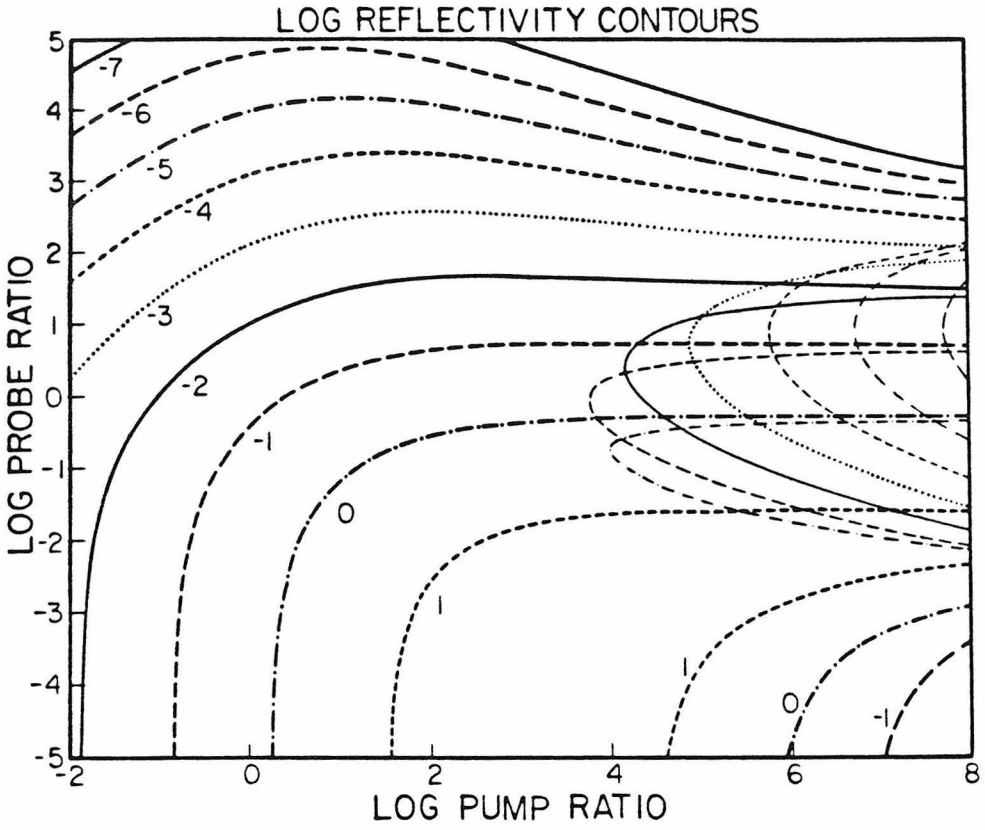

Figure 4.2 Contour plot of phase conjugate reflectivity for $\gamma l = -3$ as a function of both pump and probe ratios. The transmission grating is operative.

$$I_1(z) = I_{12}(z)\left[\frac{d_2 - I_{34}(z)d_1}{1 - I_{12}(z)I_{34}(z)}\right] \tag{4.16a}$$

$$I_2(z) = \left[\frac{d_2 - I_{34}(z)d_1}{1 - I_{12}(z)I_{34}(z)}\right] \tag{4.16b}$$

$$I_3(z) = I_{34}(z)\left[\frac{d_1 - I_{12}(z)d_2}{1 - I_{12}(z)I_{34}(z)}\right] \tag{4.16c}$$

$$I_4(z) = \left[\frac{d_1 - I_{12}(z)d_2}{1 - I_{12}(z)I_{34}(z)}\right] \tag{4.16d}$$

where $I_{ij} = I_i/I_j$.

The reflection grating

Our procedure for the solution of the coupled wave equations 3.24 for the reflection grating differs significantly from that for the transmission grating, mainly because the spatially averaged intensity I_0 is no longer conserved. We have so far only been able to demonstrate complete solutions for $\pi/2$ and zero phase shift φ between index and interference patterns.

The first step is to observe that there is a simple solution for the interference term $g \equiv (A_1A_4^* + A_2^*A_3)$. Using (3.24) for negligible absorption we can immediately write

$$\frac{dg}{dz} = \gamma g \tag{4.17}$$

so that

$$g = g_0 e^{\gamma z} \tag{4.18}$$

This result can be used to simplify the coupled wave equations (3.24) to

$$\frac{dA_1}{dz} = \frac{\gamma g_0 e^{\gamma z}}{I_0} A_4 \tag{4.19a}$$

$$\frac{dA_2^*}{dz} = \frac{\gamma g_0 e^{\gamma z}}{I_0} A_3^* \tag{4.19b}$$

$$\frac{dA_3}{dz} = \frac{\gamma g_0 e^{\gamma z}}{I_0} A_2 \tag{4.19c}$$

$$\frac{dA_4^*}{dz} = \frac{\gamma g_0 e^{\gamma z}}{I_0} A_1^* \tag{4.19d}$$

From these equations, we find that I_0 is given by

$$I_0 = (4|g_0|^2 e^{(\gamma+\gamma^*)z} + K)^{1/2} \tag{4.20}$$

where K is a constant of integration. (4.19) can then be completely decoupled by combining (4.19b) with (4.19c) and (4.19a) with (4.19d) to give

$$\frac{d^2A_1}{dz^2} - \gamma\frac{dA_1}{dz} - |g_0\gamma|^2 A_1 e^{(\gamma+\gamma^*)z} = 0 \tag{4.21a}$$

$$\frac{d^2A_2^*}{dz^2} - \gamma\frac{dA_2^*}{dz} - |g_0\gamma|^2 A_2^* e^{(\gamma+\gamma^*)z} = 0 \tag{4.21b}$$

$$\frac{d^2A_3}{dz^2} - \gamma\frac{dA_3}{dz} - |g_0\gamma|^2 A_3 e^{(\gamma+\gamma^*)z} = 0 \tag{4.21c}$$

$$\frac{d^2A_4^*}{dz^2} - \gamma\frac{dA_4^*}{dz} - |g_0\gamma|^2 A_4^* e^{(\gamma+\gamma^*)z} = 0 \tag{4.21d}$$

For $\gamma + \gamma^* = 0$, corresponding to zero spatial phase shift, these equations have constant coefficients and can be solved by elementary techniques. Otherwise, there is no clear way to integrate them. Fortunately, for the phase shift of greatest interest to us in the PR effect, $\varphi = \pi/2$, there is an alternative way to proceed to a solution. We make a change of variable from z to u defined by

$$\frac{\gamma g_0 e^{\gamma z}}{I_0} dz = du \tag{4.22}$$

which gives

$$u = \frac{1}{2|g_0|}\ln\left[\frac{2|g_0|e^{\gamma z} + (4|g_0|^2 e^{(\gamma+\gamma^*)z} + K)^{1/2}}{2|g_0| + (4|g_0|^2 + K)^{1/2}}\right] \tag{4.23}$$

Then (4.19) becomes

$$\frac{dA_1}{du} = g_0 A_4 \tag{4.24a}$$

$$\frac{dA_2^*}{du} = g_0 A_3^* \tag{4.24b}$$

$$\frac{dA_3}{du} = g_0 A_2 \tag{4.24c}$$

$$\frac{dA_4^*}{du} = g_0 A_1^* \tag{4.24d}$$

Only if the phase shift $\varphi = \pi/2$ so that the coupling constant γ is real will we be able to work easily with the complex conjugates of the equations belonging to (4.24) to proceed by standard methods to the solution with $A_3(0) = 0$, $A_1(0)$, $A_2(l)$ and $A_4(l)$ known:

$A_1(u) =$ (4.25a)

$$\frac{g_0^{1/2}\left[\left(\frac{A_4(l)}{g_0^{*1/2}} + \frac{A_1(0)}{g_0^{1/2}}e^{-|g_0|u(l)}\right)e^{|g_0|u} + \left(\frac{A_1(0)}{g_0^{1/2}}e^{|g_0|u(l)} - \frac{A_4(l)}{g_0^{*1/2}}\right)e^{-|g_0|u}\right]}{e^{|g_0|u(l)} + e^{-|g_0|u(l)}}$$

$$A_2(u) = A_2(l)\frac{\left[e^{|g_0|u} + e^{-|g_0|u}\right]}{e^{|g_0|u(l)} + e^{-|g_0|u(l)}} \tag{4.25b}$$

$$A_3(u) = \left(\frac{g_0}{g_0^*}\right)^{1/2} A_2(l)\frac{\left[e^{|g_0|u} - e^{-|g_0|u}\right]}{e^{|g_0|u(l)} + e^{-|g_0|u(l)}} \tag{4.25c}$$

$A_4(u) =$ (4.25d)

$$\frac{g_0^{*1/2}\left[\left(\frac{A_4(l)}{g_0^{*1/2}} + \frac{A_1(0)}{g_0^{1/2}}e^{-|g_0|u(l)}\right)e^{|g_0|u} - \left(\frac{A_1(0)}{g_0^{1/2}}e^{|g_0|u(l)} - \frac{A_4(l)}{g_0^{*1/2}}\right)e^{-|g_0|u}\right]}{e^{|g_0|u(l)} + e^{-|g_0|u(l)}}$$

The phase conjugate reflectivity is thus given by

$$R = \frac{I_2(l)}{I_4(l)}\tanh^2(|g_0|u(l)) \tag{4.26}$$

To evaluate this expression we may use the following procedure:

a) Use the solution (4.25) in the expression (4.18) for g to find an equation relating $e^{\gamma z}$ to $e^{|g_0|u}$.

b) Use the change of variable formula (4.23) to obtain another equation similar to that found in a) above.

c) Using the expressions found in a) and b) to find a single equation in $e^{|g_0|u}$ and $e^{-|g_0|u}$, equate coefficients of the various exponential terms to find the following equation whose roots give $A = K/(4|g_0|^2)$

$$\frac{\left|\pm I_4(l)^{1/2} + I_1(0)^{1/2}e^{-|g_0|u(l)}\right|^2 + I_2(l)}{\left|\pm I_4(l)^{1/2} - I_1(0)^{1/2}e^{|g_0|u(l)}\right|^2 + I_2(l)} = \frac{(1 + (1+A)^{1/2})^2}{A} \tag{4.27}$$

Only the upper sign yields solutions, since the right-hand side is greater than one, and the left-hand side is less than one for the lower sign.

d) The constant A may then be used in (4.23) to find $|g_0|u(l)$ and hence the reflectivity R from (4.26).

Fig. 4.3 is a contour plot of phase conjugate reflectivity for the reflection grating as a function of pump and probe ratios, for γl = -3. It is directly comparable to Fig. 4.2, the contour plot for the transmission grating. We see that in the case of the reflection grating, the reflectivity is not multivalued. Also, in contrast to the case of the transmission grating, it does not remain finite in the limit of infinite pump ratio.

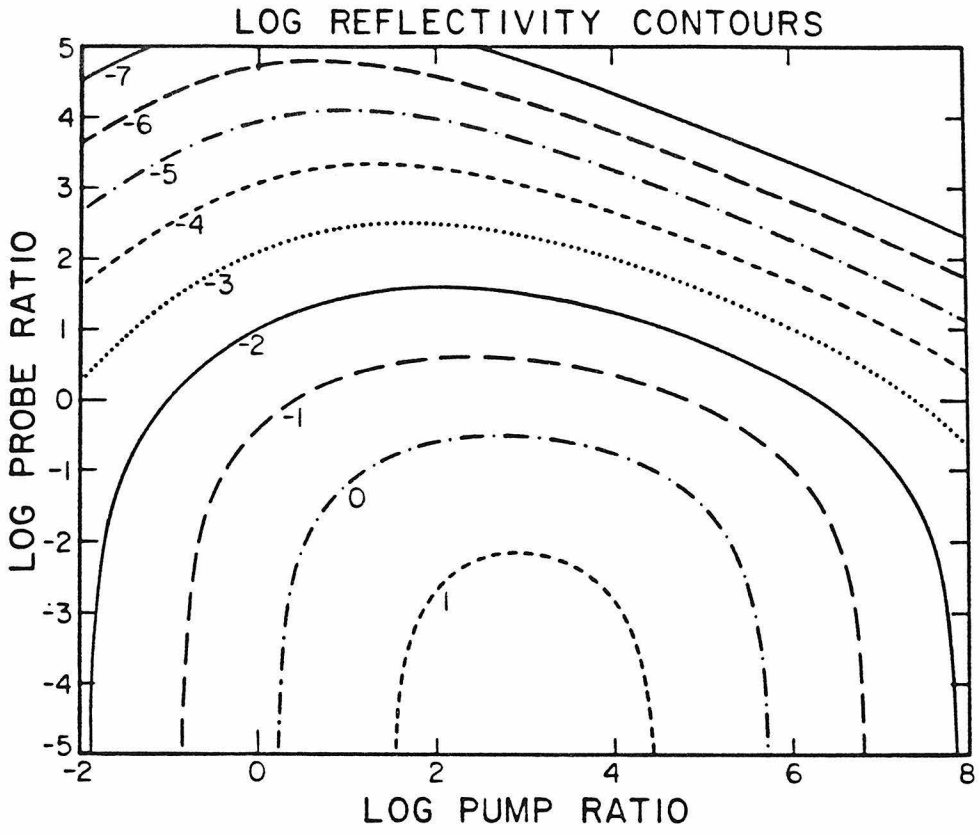

Figure 4.3 Contour plot of phase conjugate reflectivity for $\gamma l = -3$ as a function of both pump and probe ratios. The reflection grating is operative.

References for Chapter 4

1. J.H. Marburger and J.F. Lam, Appl. Phys. Lett. **34**, 389 (1979)

2. J.H. Marburger and J.F. Lam, Appl. Phys. Lett. **35**, 249 (1979)

3. H.G. Winful and J.H. Marburger, Appl. Phys. Lett. **36**, 613 (1980)

4. A.R. Kessel and V.M. Musin, Opt. Commun. **44**, 133 (1982)

5. M. Cronin-Golomb, B. Fischer, J.O. White and A. Yariv, Opt. Lett. **7**, 313 (1982)

Chapter 5

Passive Phase Conjugate Mirrors and Optical Aberration Correction

Introduction

Certain PR materials such as $BaTiO_3$ and SBN are endowed with electrooptic coefficients so large ($\approx 1000 pV\,m^{-1}$) that values of γ of the order of $10^3 m^{-1}$ are easily obtainable with milliwatt input beams. Not only does this make it possible to build phase conjugate mirrors with large reflectivities but also, it enables the construction of phase conjugate resonators[1-8]. (PCR's), as well as other useful resonator devices such as passive phase conjugate mirrors (PPCM's) and unidirectional ring resonators. The main advantage of the PPCM is that it obviates the high quality externally provided pumping beams needed for conventional four-wave mixing phase conjugate mirrors. In this chapter we describe the theory and recent experimental demonstrations of several PPCM's. Novel interpretations of a photorefractive crystal as an error correcting optical element and as a double phase conjugate mirror will also be introduced.

The linear and semilinear passive phase conjugate mirrors

The first passive PR phase conjugate mirror was the linear mirror[9-11], a device consisting of an appropriately oriented PR crystal lying in a cavity bounded by two ordinary mirrors. (Fig. 5.1a). It has been used in imaging experiments and as the end mirror of an argon ion laser. It has also proved to be amenable to analysis by the nonlinear PR four-wave mixing theory described in the preceding paragraphs. The theory has been useful in developing an understanding of

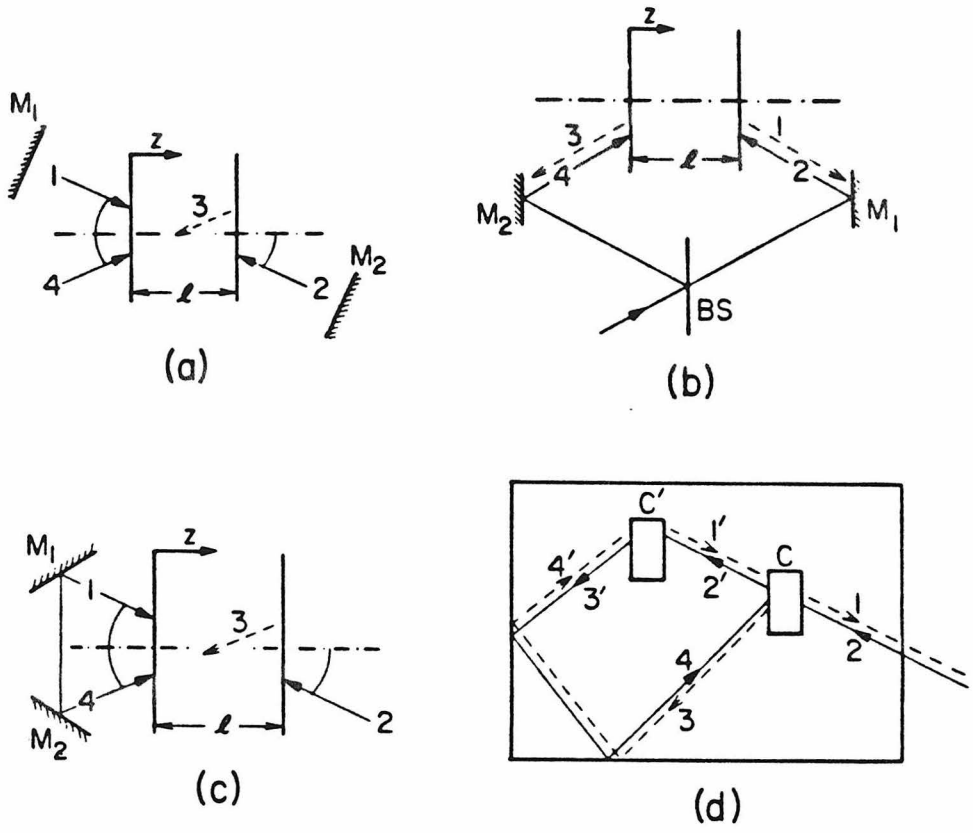

Figure 5.1 a) Geometry of the linear passive phase conjugate mirror. The probe is beam 4 and its phase conjugate is beam 3. The two pumping beams, 1 and 2 oscillate in the cavity bounded by mirrors M_1 and M_2.

b) Geometry of a four wave mixing oscillator which can produce output beams which are not phase conjugates of the input beams. (See text.) Beams 2 and 4 are provided from an external source and beams 1 and 3 build up via four wave mixing.

c) Geometry of the ring passive phase conjugate mirror. Consistent with the convention that the intensity of beam 3 should be zero at its entrance face, the probe is designated as beam 2. Pump beam 4 is provided by reflection of the probe beam by mirrors M_1 and M_2. The second pump, beam 3 and the phase conjugate beam 1 are self- induced by the nonlinear medium.

d) Geometry of the two-interaction-region mirror. It consists of a ring mirror (using interaction region C) with a double phase conjugate mirror (using interaction region C') in its feedback loop. Both interaction regions are inside a single crystal whose boundary (large rectangle) gives rise to feedback by total internal reflection.

the more unusual features of the device. For example, we can understand the fact that under certain circumstances, it is possible to maintain operation when one of the external cavity mirrors is removed.

The physical basis for buildup of oscillation in the linear PPCM is the phenomenon of light amplification by two beam coupling described in Chapter 3. The c-axis of the crystal is oriented so that light in beam 1 is amplified by two beam coupling from input beam 4 and is fed back by successive reflections from mirrors M_2 and M_1. Oscillation continues to build up until steady state is reached for beams 1 and 2 which are now pumping the crystal as a phase conjugate mirror for input beam 4. We show here how to derive the reflectivity of the device (i.e. the intensity of beam 3 divided by the intensity of beam 4) in the slowly varying field, negligible linear absorption and single grating approximations. Because the pumping beams are derived from and fed by the signal beam itself, the commonly used undepleted pumps approximation is inappropriate. Thus we use the analysis of Chapter 4 where we derived the reflectivity of a PR phase conjugate mirror without assuming undepleted pumps, but assuming knowledge of their input intensities. From now on except where otherwise noted, the theory for the transmission grating is used and all intensities are normalized by the conserved quantity I_0. When discussing the reflection grating, this normalization is not used.

Because the boundary conditions in the linear PPCM are not the input intensities $I_1(0)$ and $I_2(l)$, but rather the reflectivities of mirrors M_1 and M_2, some further development of the theory is required. We make use of the functions A_{12} and A_{34} to fit these new boundary conditions (See (4.4),(4.10),(4.12)), assuming that the mirrors are placed so that the $M_1 - M_2$ cavity is in resonance. The effects of departure from cavity resonance is a topic of current theoretical and experimental research.

$$M_1 = I_{12}(0) = \frac{|c|^2}{I_2(l)^2}\left|\frac{T + (\Delta^2 + 4|c|^2)^{1/2}}{\Delta T + (\Delta^2 + 4|c|^2)^{1/2} + 2|c|^2 T/I_2(l)}\right|^2 \tag{5.1a}$$

$$M_2 = 1/I_{12}(l) = I_2(l)^2/|c|^2 \tag{5.1b}$$

Since

$$I_2(l) = (\Delta+1)/2 \tag{5.2a}$$

and

$$|c|^2 = (\Delta+1)^2/(4M_2) \tag{5.2b}$$

we see that (5.1) is really a function of the single variable Δ, together with the known quantities γl, M_1 and M_2. Similarly the reflectivity R may be rewritten as a function of these same variables. We have

$$M_1M_2 = I_{12}(0)/I_{12}(l) = \left|\frac{T + [\Delta^2 + (\Delta+1)^2/M_2]^{1/2}}{\Delta T + [\Delta^2 + (\Delta+1)^2/M_2]^{1/2} + (1+\Delta)T/M_2}\right|^2 \tag{5.3}$$

where

$$T = \tanh\left(\frac{\gamma l}{2}[\Delta^2 + (\Delta+1)^2/M_2]^{1/2}\right) \tag{5.4}$$

$$R = I_{34}(0) = \frac{(1+\Delta)^2|T|^2}{M_2|\Delta T + [\Delta^2 + (\Delta+1)^2/M_2]^{1/2}|^2} \tag{5.5}$$

Thus the reflectivity of the PPCM may be found by solving (5.3) for Δ and then using the resultant value(s) in (5.5) for R. We note that (5.3) may have multiple roots.

We show in Fig. 5.2 a contour plot of the reflectivity R as a function of M_1 and M_2 for a particular value of the coupling strength $\gamma l = -3$ (i.e. with the $\pi/2$ phase shift typical of photorefractive materials). We see that towards the left of this plot the reflectivity can be multivalued, and also that when M_2 is high the reflectivity remains high even when M_1 is small. We shall show that there is a threshold coupling strength above which it is possible to obtain finite

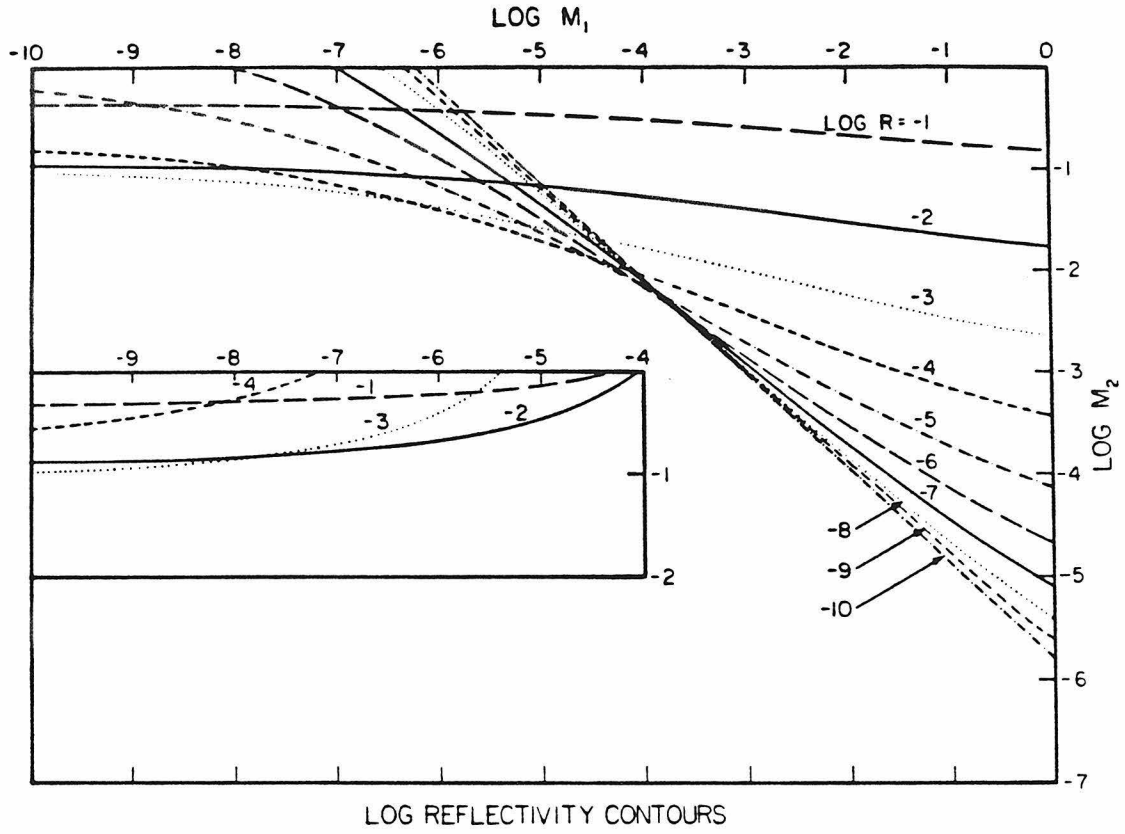

Figure 5.2 Contour plots of the reflectivity of the passive phase conjugate mirror. Equality of contour levels in the region where the function is multivalued is indicated by equality of line form (dashes, dots, etc.) The coupling strength $\gamma l = -3$. For the sake of clarity some of the contours at low M_1 and high M_2 have been redrawn in an inset.

reflectivities even in the absence of mirror M_1.

But first, we consider the threshold coupling strength for the buildup of oscillation from zero oscillation intensity in the M_1-M_2 crystal cavity. This corresponds to taking $I_1(0) = I_2(l) = 0$, that is, $\Delta = -1$. From (5.3) the threshold may be obtained as

$$M_1 M_2 = \exp((\gamma + \gamma^*) l) \tag{5.6}$$

This fits in well with the heuristic explanation of oscillation buildup given earlier; the gain in the crystal simply has to be sufficient to overcome the losses due to the mirrors M_1 and M_2. Since the threshold depends only on the real part of the coupling strength, it follows that a nonlinear medium with no phase shift between the index grating and the interference pattern will not support operation beginning from zero oscillation strength. This is because of the absence in these materials of unidirectional two beam coupling.

In addition, we see that no buildup of operation from zero oscillation strength is possible in the absence of mirror M_1 even when γl does have a real part. However, by providing a seed beam in the M_2 - crystal cavity, so that the initial probe ratio is not infinite, it *is* possible in some cases to maintain oscillation in the absence of mirror M_1. We call this device the *semilinear mirror*. It will not start itself by gain in four-wave mixing, but once initiated, it keeps going. Kwong has recently shown that the semilinear mirror can, in fact, start itself by seeding from the fanning effect (Ref. 10) in which light scattered from the incident beam experiences such large gain that it leaves the crystal as a broad, easily visible fan of light. Such behaviour could have been anticipated from Fig. 4.2 which indicated that finite reflectivities were available at infinite pump ratio which is exactly the situation confronting us here. It can also be shown that semilinear operation is not possible with the use of four-wave mixing

via the reflection grating. A semilinear mirror using the reflection grating would have the interference term g $(A_1A_4^* + A_2^*A_3)$ equal to zero either at the plane $z = l$ or at the plane $z = 0$, because we must have either $A_4(l)$ and $A_2(l)$ or $A_1(0)$ and $A_3(0)$ zero. Since $g = g_0e^{\gamma z}$ (4.18) if g is zero at one plane, it must be zero everywhere, so that no coupling is possible.

The theory of the transmission grating with $M_1 = 0$ implies (see (5.3)) that

$$\tanh(-\frac{\gamma l}{2}[\Delta^2 + (\Delta + 1)^2/M_2]^{1/2}) = [\Delta^2 + (\Delta + 1)^2/M_2]^{1/2} \tag{5.7}$$

so that Δ may found from the solution of the quadratic equation

$$\Delta^2 + \frac{(\Delta + 1)^2}{M_2} = a^2 \tag{5.8}$$

where a is simply related to the coupling constant γl by

$$\tanh(-\frac{\gamma l}{2}a) = a \tag{5.9}$$

The reflectivity can therefore be written in closed form as

$$R = \left[\frac{M_2^{1/2} \pm (a^2(1+M_2)-1)^{1/2}}{M_2+2 \mp M_2^{1/2}(a^2(1+M_2)-1)^{1/2}}\right]^2 \tag{5.10}$$

so that the device is at threshold with reflectivity $R = R_t$

$$R_t = \frac{M_2}{(M_2+2)^2} \tag{5.11}$$

when a^2 equals a_t^2

$$a_t^2 = \frac{1}{(1+M_2)} \tag{5.12}$$

In terms of γ this threshold is given by

$$\gamma l_t = (1 + M_2)^{1/2} \ln\left[\frac{(1 + M_2)^{1/2} - 1}{(1 + M_2)^{1/2} + 1}\right] \tag{5.13}$$

It is possible to show that of the two possible values of above-threshold

reflectivity (5.10) only the one associated with the upper sign is stable. This mode of operation, without M_1 has been observed in our laboratory and, as we describe below, has been used in the PPCM as an end mirror for an argon ion laser.

Having examined the theory of this device, we now turn to results of two experimental verifications of the phase conjugating nature of the linear PPCM. The first is a demonstration of the phase conjugate imaging property of the PPCM. The second is an experiment showing intracavity distortion correction in an argon ion laser operated with one of its end mirrors replaced by linear and semilinear PPCM's.

In the first experiment (Fig. 5.3) the expanded and spatially filtered output of a dye laser illuminated a transparency T (Fig. 5.4a) The beam passed through lens L_2 and converged on the linear mirror, consisting of a single poled crystal of barium titanate lying in the M_1–M_2 resonator cavity. The reflected beam was picked off by a beam splitter BS and photographed at the location where a phase conjugate image would be expected. The result is shown in Fig. 5.4b. The phase conjugating behaviour of the linear mirror is quite evident. Intensity patterns of the oscillation beams in the M_1–M_2 cavity are shown in Figs. 5.4c,d. These were photographs of the intensities at mirrors M_1 and M_2 respectively. The information in the probe beam has been filtered out, leaving speckle-like patterns due to optical inhomogeneities in the crystal.

A phase conjugate resonator laser using the linear or semilinear passive phase conjugate mirrors

The use of phase conjugate mirrors as the end mirrors for lasers and other resonant cavities has been a topic of considerable practical interest, especially

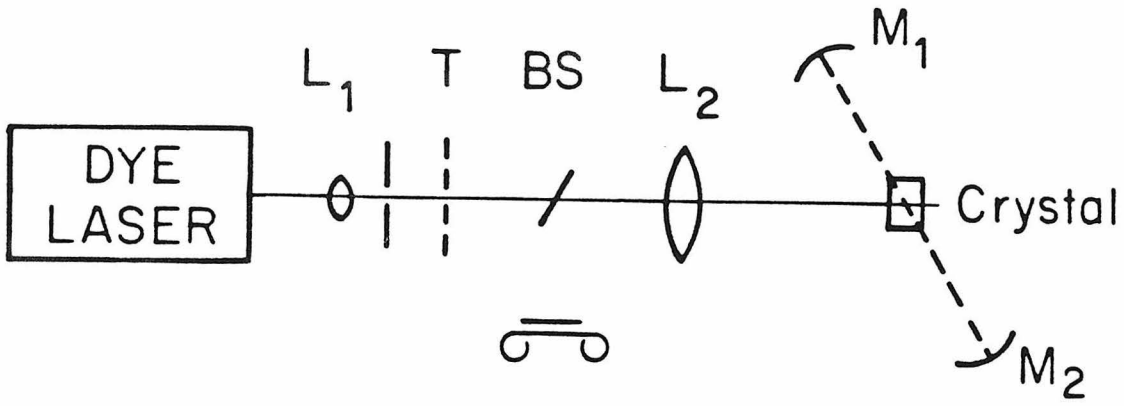

Figure 5.3 The experimental arrangement used to demonstrate phase conjugation in the linear mirror. The dye laser used was a Spectra Physics 380 ring laser with Rhodamine 6G at 579.2nm in single longitudinal mode. Using a cartesian coordinate system with the abscissa coincident with the beam direction, the locations of the elements measured in centimeters were: 20x beam expander L_1 (-64,0), transparency T (-55,0), beam splitter for observing phase conjugate reflection BS (-38,0), 14cm focal length lens L_2 (-20,0), barium titanate crystal (0,0), 50cm radius concave mirror M_1, (-28,11), 50cm radius concave mirror M_2 (30,-13). The c-axis of the crystal pointed in the direction of the vector (0.94,0.35). This crystal measured 7×4.5×4 mm and was poled into a single domain so that the c-axis was parallel to the 4 mm side.

Figure 5.4 Results of the linear mirror phase conjugation experiment.
a) The transparency T.
b) The phase conjugate beam picked off by beam splitter BS.
c) The intensity pattern of the oscillation beam on mirror M_1.
d) The intensity pattern of the oscillation beam on mirror M_2.

(a) 1mm

(b) 1mm

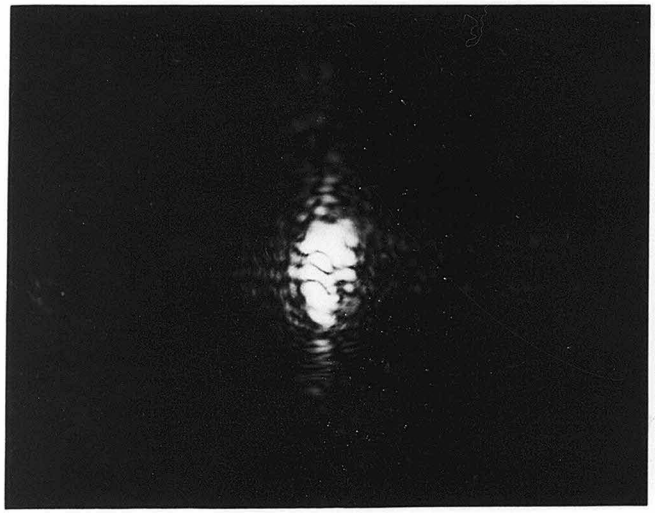

(c) 2mm

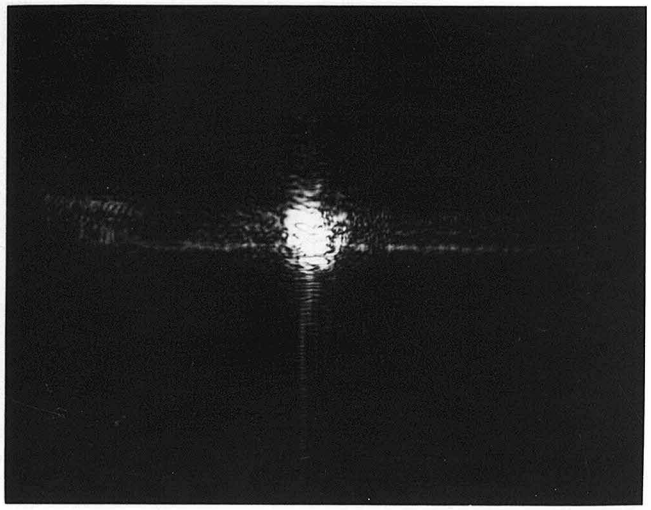

(d) 2mm

in the field of high energy lasers where aberrations in the gain medium are a significant problem. There are several advantages to be had in designing a laser with a phase conjugate end mirror. These stem from differences between the nature of the modes in resonators bounded by two ordinary mirrors and in phase conjugate resonators (PCR's).

Consider first the longitudinal modes of a PCR (Fig. 5.5). If the pumping beams both have radian frequency ω and the incident beam is of frequency $\omega - \delta$, then, by conservation of energy in the four photon interaction, the reflected beam must be of frequency $\omega + \delta$. Thus a phase conjugate mirror "flips" the frequency of the incident beam about the frequency of the pumps. The detuning δ cannot be too great, otherwise phase matching problems or limitations on the speed of response of the mixing medium will severely reduce the reflectivity. It will take two round trips for given beam in a PCR to revert to its original frequency. By that time, it will have accumulated an additional phase of

$$2[k(-\delta) - k(\delta)]l = -4\delta l/c \tag{5.14}$$

which at resonance, must be an integer multiple of 2π. Thus the oscillation spectrum of a PCR consists of modes spaced by $c/4l$ centered around the pumping frequency. Contrast this to the behaviour of an ordinary resonator where the longitudinal (or axial) modes are spaced by $c/2l$ and are not centered around any particular frequency. The "half-axial" modes of a PCR were first observed by Lind and Steel in 1981 who used sodium vapor at the D line in their phase conjugate mirror[7]. The slow response time of the PR effect unfortunately makes it impractical to observe these half-axial modes in our experiments.

The transverse modes of a paraxial cylindrically symmetric optical cavity may be found in terms of Hermite-Gaussian beams[12] (Fig. 5.6)

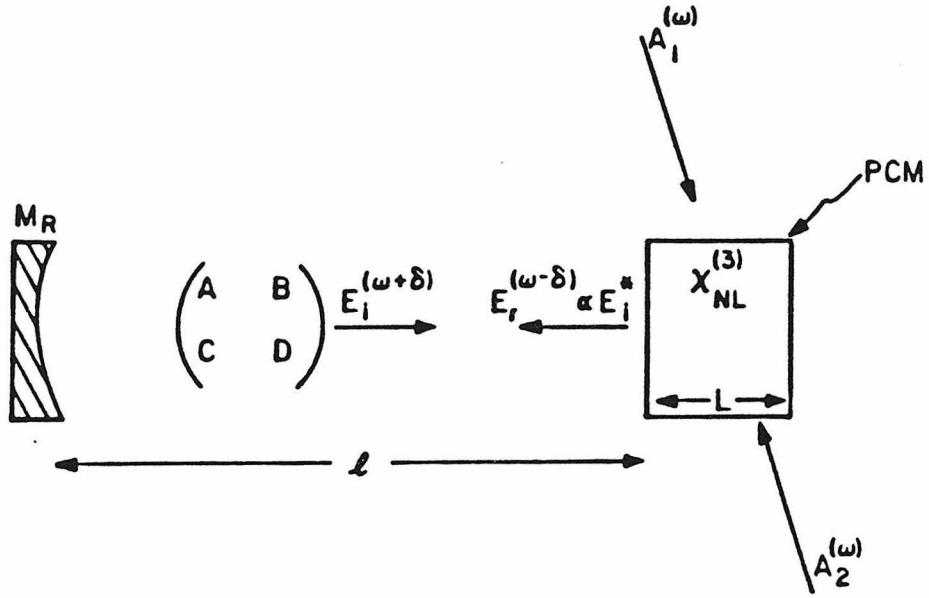

Figure 5.5 The phase conjugate resonator (PCR). An ordinary mirror with radius of curvature R and a phase conjugate mirror enclose the general optical elements described collectively by an equivalent ABCD matrix.

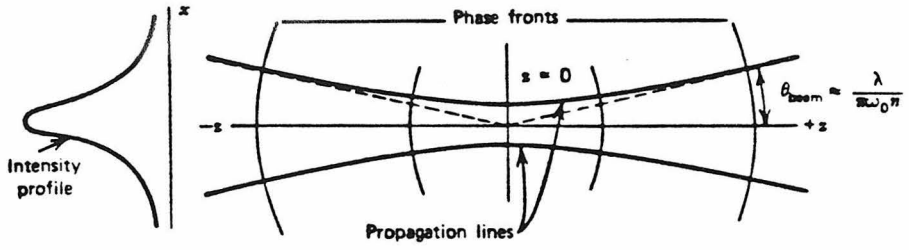

Figure 5.6 Propagating Gaussian beam.

$$E_{l,m}(r) = E_0 \frac{\omega_0}{\omega(z)} H_l\left[\sqrt{2}\,\frac{x}{\omega(z)}\right] H_m\left[\sqrt{2}\,\frac{y}{\omega(z)}\right] \tag{5.15}$$

$$\times \exp\left[-\frac{ik(x^2+y^2)}{2q(z)} - ikz + i(l+m+1)\eta\right]$$

where x and y are the transverse coordinates and z is the coordinate along the axis of symmetry, $\omega(z)$, the spot size is the beam radius at its 1/e point, ω_0 is the spot size at the beam "waist" (z = 0), q is the all important complex beam parameter (not to be confused with the probe ratio)

$$\frac{1}{q(z)} = \frac{1}{R(z)} - i\,\frac{\lambda}{\pi n \omega^2(z)} \tag{5.16}$$

where R is the radius of curvature of the wavefronts, and η is given by

$$\eta = \tan^{-1}\left[\frac{\lambda z}{\pi n \omega_0^{\,2}}\right] \tag{5.17}$$

The effect of this factor η on the longitudinal modes of a PCR has been dealt with by AuYeung et al.[1]

The variation of the complex beam parameter as it passes through free space and other optical elements can be conveniently described in terms of the ABCD matrices of geometrical optics. The beam parameter q_{out} after passage through an optical element described by a particular ABCD matrix, given the input parameter q_{in} is[9]

$$q_{out} = \frac{Aq_{in} + B}{Cq_{in} + D} \tag{5.18}$$

After applying these mathematical tools to the PCR it turns out that the modes are underdetermined by the radius of curvature of the ordinary cavity mirror. Many more modes are available than in a conventional resonator, where the radii of curvature of the two mirrors introduce more stringent boundary conditions. A laser employing a phase conjugate mirror is able to use the extra

modes to extract more energy from the gain medium than is possible in a conventional laser. Also, the aberration correction feature of the phase conjugate mirror makes the laser very forgiving to internal optical aberrations, as was observed in the experiment described below.

The arrangement for the cw argon ion laser experiment is shown in Fig. 5.7. Lasing was initially induced at the high gain line, 488.0 nm, between mirror M_3 and beam splitter BS (Fig. 5.7a). Light transmitted through the beam splitter caused oscillation in the PPCM, the resonator consisting of a $BaTiO_3$ crystal and mirrors M_1 and M_2. Reflecting mirror M_4 was used to assist in the buildup of oscillation. With oscillation established between M_1 and M_2, the beam splitter and the retroreflecting mirror M_4 were removed, as shown in Fig. 5.7b. The starting procedure described above was required since the coherence of the fluorescence was insufficient to allow the formation of the required refractive index grating in the crystal. Once the grating was established, the configuration of Fig. 5.7b corresponded to an equilibrium state, and the grating in the crystal was continuously maintained by the very beams which it coupled together.

The theory indicates that there is a certain two beam coupling strength (5.13) in the crystal, above which it is possible to maintain oscillation between the crystal and M_2 even in the absence of mirror M_1. We were able to demonstrate such oscillation in our laser. Fig. 5.7c depicts the starting arrangement. Once oscillation involving mirror M_2 was established, the beam splitter and mirror M_4 were removed and the laser continued to oscillate, as shown in Fig. 5.7d.

To demonstrate the distortion correction capability of the laser with the PPCM, we operated it in the configuration of Fig. 5.7d with a severe distortion placed between the barium titanate crystal and the laser gain medium. Fig. 5.8b shows a photograph of the intensity pattern of the beam exiting through mirror

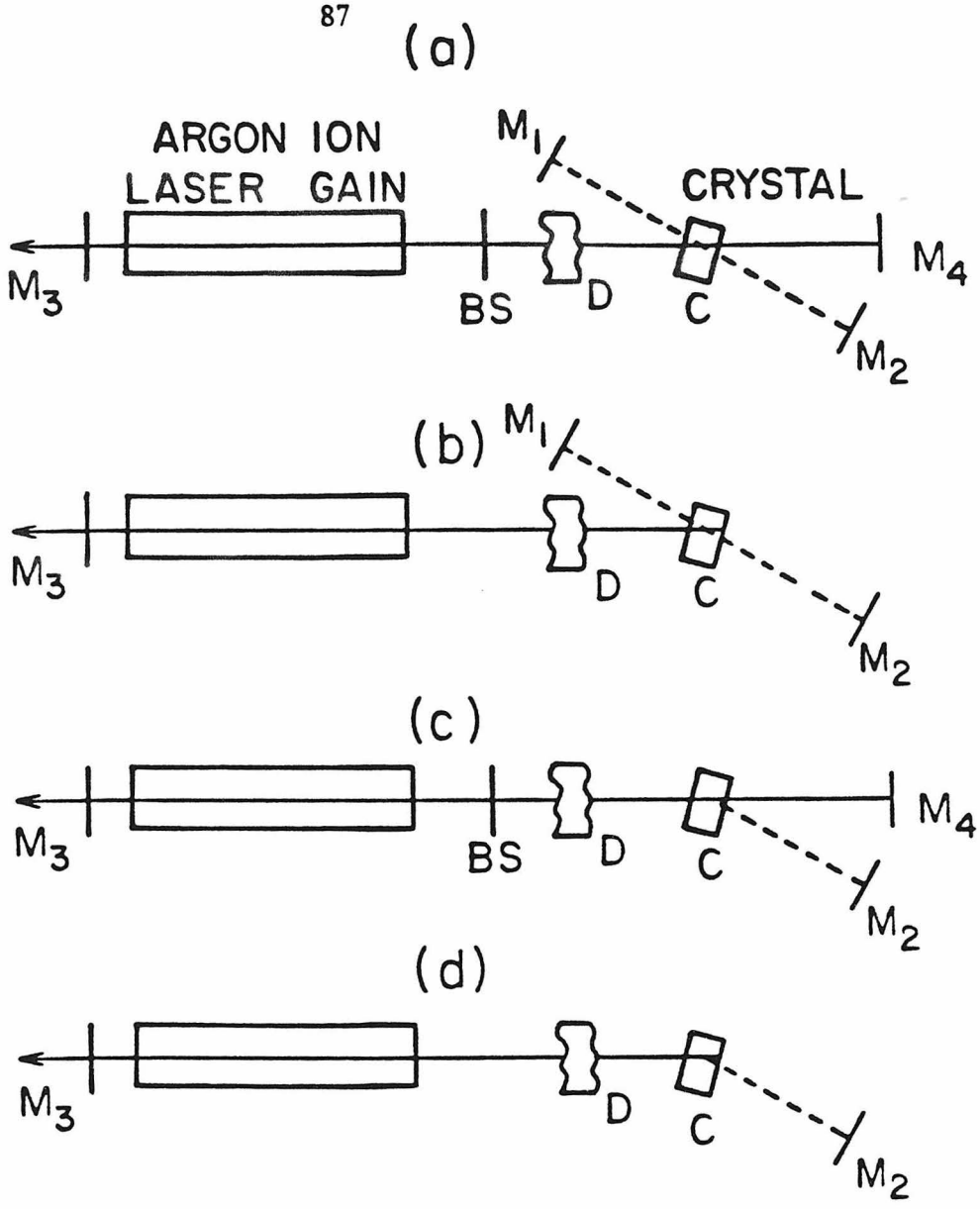

Figure 5.7 Passive phase conjugate resonator laser.
a) Starting configuration. Mirror M_3 was the standard high radius of curvature output mirror of the Spectra Physics argon ion laser. The distance from it to the barium titanate crystal C was 220cm. Mirror M_1 is flat and 50% reflecting, and mirror M_2 was concave 5cm radius of curvature and highly reflecting. The distances between mirror M_2 and the crystal, and mirror M_1 and the crystal were both 4.5cm. None of these parameters was critical to the operation of the laser; for example, M_2 could be replaced at the same location by a 50cm concave mirror. The position of the intracavity distortion D is indicated on the figure.
b) Operating configuration. The crystal is pumped as a phase conjugate mirror by the beams shown dashed in the M_2-M_1 cavity.
c) Starting configuration for laser without mirror M_1.
d) Operating configuration for laser without mirror M_1.

Figure 5.8 a) Photograph of the output of regular laser (i.e., crystal replaced by high reflectivity dielectric mirror) containing an intracavity distortion. The distance from the output mirror M_3 is one meter. The laser intensity is 1 mW, obtained at 38 amps laser tube current.
b)The output of the passive phase conjugate resonator laser containing the intracavity distortion. The distance from the output mirror M_3 is one meter. The laser intensity here is 3 mW, obtained at only 21 amps laser tube current. The power output at 38 amps is 500 mW.

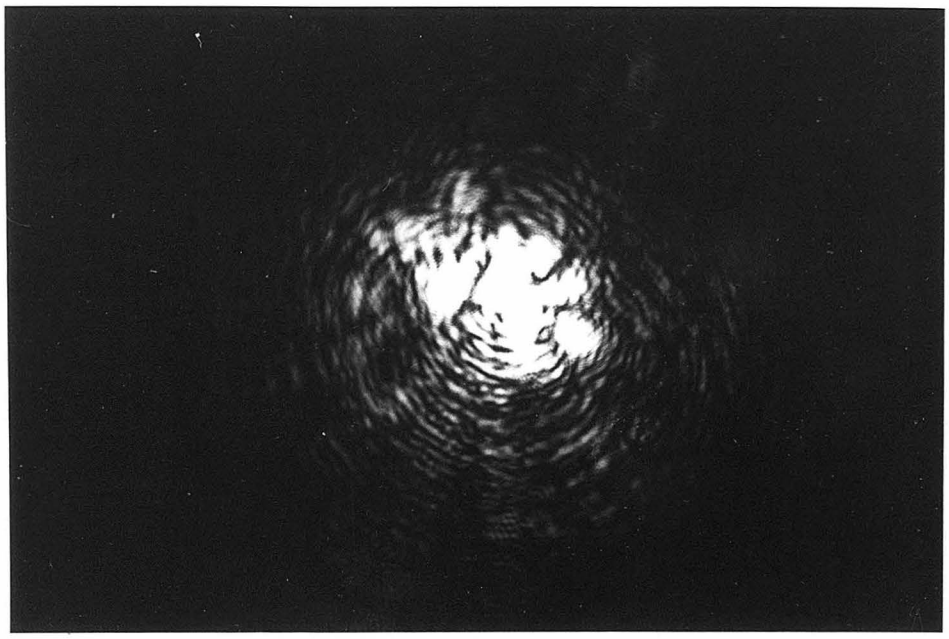

(a)

5mm

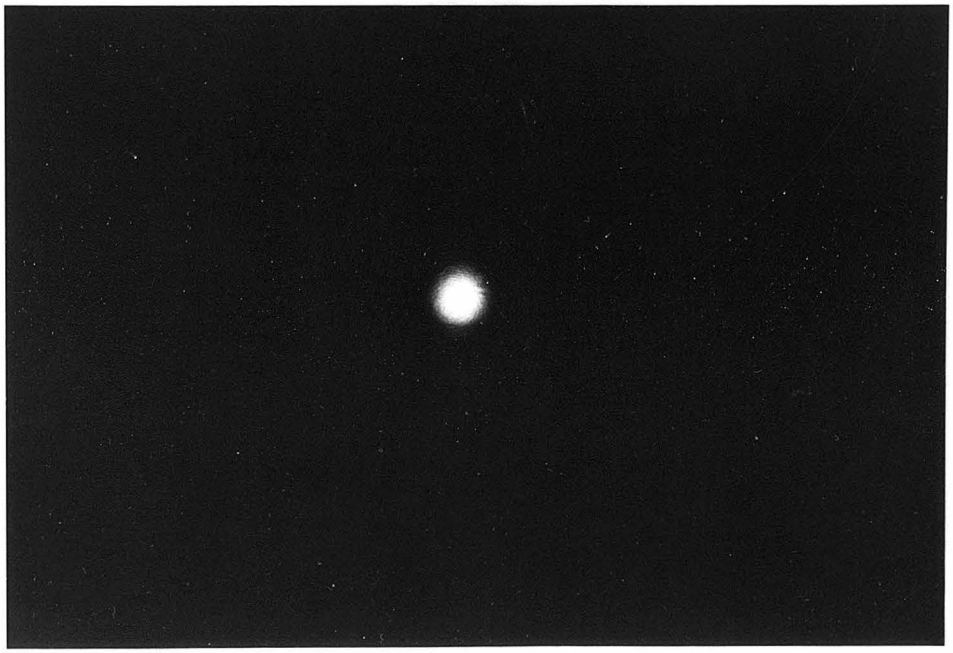

(b)

5mm

M_3. Operating the laser in a conventional fashion with the crystal replaced by a high reflectivity dielectric mirror and with the distortion in the beam path gave rise to the beam shown in Fig. 5.8a. The compensation effect of the PPCM is evident. The power output at 38 amps laser tube current in the conventional resonator with the distortion inside was about 1mW compared to about 500mW with the PPCM.

The loss of independence of the pump beams in the linear mirror results in one difference from a regular PCR. Longitudinal modes are present in the cavity, corresponding to the normal modes observed in a standing wave resonator and have been observed by using an optical spectrum analyzer to analyze the output of the laser. The correspondence between the modes of an ordinary laser and a PCR laser using a PPCM is not yet well understood and is the subject of ongoing investigations.

Intracavity distortion correction and double phase conjugation

In the preceding discussion, the laser with dynamic holographic intracavity distortion correction capability was interpreted as consisting of an ordinary end mirror, an argon ion laser gain medium, and a semilinear PPCM. We offer here two alternative interpretations. In the first, the laser (Fig 5.7d) is viewed as consisting of an ordinary end mirror M_1, an argon ion laser gain medium , the crystal as an *intracavity distortion correction device* and another ordinary mirror, M_3. The second interpretation comes from noting that the aberration compensation observed in the argon ion laser indicated that each of the oscillations - one in the M_1-crystal arm and the second in the M_3-crystal arm - was composed of two oppositely traveling waves which were phase conjugates of each other (Fig. 5.7d). The crystal thus acted simultaneously as a phase conjugate mirror to the two beams which were incident on it, coupling, in the process, the two arms

to each other. We can call a crystal operating in such a manner a *double phase conjugate mirror.*

Are the oscillation beams in a crystal with $I_1(0) = I_3(l) = 0$ always phase conjugates of each other? One possibility is that oscillation beams contribute most to the four-wave mixing process and experience maximum gain when the spatial overlap of counterpropagating beams is maximum, that is, when they are phase conjugates of each other. However, this explanation is inconsistent with the behaviour of another device (Fig 5.1b) which we built with the hope that it would be a phase conjugate mirror. A signal beam was incident on a beamsplitter and the transmitted beam was directed by mirror M_1 onto a barium titanate crystal as beam 2. The reflection from the beamsplitter was directed by mirror M_2 onto the crystal as beam 4. The theory developed below indicates that with sufficient coupling strength and $\pi/2$ phase shift between the interference fringes and refractive index fringes, oscillation beams 1 and 3 can be expected to build up via gratings written between beams 1 and 4 and beams 2 and 3. The wavevector of the beam 1 - beam 4 grating must be the same as that of the beam 2 - beam 3 grating so that both combine to form a single grating coupling all four beams. Thus we require

$$\mathbf{k}_1 - \mathbf{k}_4 = \mathbf{k}_3 - \mathbf{k}_2 \tag{5.19}$$

where $\mathbf{k}_j$ is the wavevector of beam j. In conventional applications of four-wave mixing $\mathbf{k}_1$, $\mathbf{k}_2$, and $\mathbf{k}_4$ are fixed so that (5.19) gives a unique value for $\mathbf{k}_3$, the wavevector of the phase conjugate beam. Since only $\mathbf{k}_2$ and $\mathbf{k}_4$ are fixed in the device of Fig. 5.1b, however, there is an extra degree of freedom manifested in the expected and observed appearance of beams 1 and 3 as cones of light with axis $\mathbf{k}_2 - \mathbf{k}_4$ and surfaces including both vectors $\mathbf{k}_2$ and $\mathbf{k}_4$. This means that self-induced oscillation by four-wave mixing does not always require that the coun-

terpropagating beams be phase conjugates of each other.

The full linear and semilinear mirrors involve feedback to the crystal of the oscillation beams while the beamsplitter device described above does not: in the linear and semilinear mirrors, beam 1 is reflected into beam 2 and vice versa by external mirrors while in the beamsplitter device, the oscillation beams are lost to the outside world. It is feedback that gives phase conjugate oscillations an advantage in gain over other kinds of oscillation. We will return to this point when we discuss the ring mirror in a later section.

When we come to design optical systems and circuits using a double phase conjugating PR crystal as a compensating element, it will be advantageous to have an expression for its transmissivity. From (5.2) and (5.8) we know that

$$|c|^2 = (a^2 - \Delta^2)/4 = [a^2(I_2(l) + I_4(0))^2 - (I_2(l) - I_4(0))^2]/4 \tag{5.20}$$

The transmissivities in each direction actually turn out to be identical

$$T \equiv \frac{I_1(l)}{I_4(0)} = \frac{I_3(0)}{I_2(l)} = \frac{|c|^2}{I_4(0)I_2(l)}$$

$$= \frac{a^2[q^{-1/2}+q^{1/2}]^2 - [q^{-1/2}-q^{1/2}]^2}{4} \tag{5.21}$$

where we have used the fact that the probe ratio q is simplified in this case to $I_4(0)/I_2(l)$. The device may then also be interpreted as an aberration correcting absorber, whose absorption depends on the intensity ratio of the two entering beams. The lowest possible threshold for this device obtained from the definition of a (5.9), is $\gamma l_t = -2$.

The simplest optical system involving the double phase conjugate mirror, apart from the folded cavity laser descibed above (Fig. 5.9a), is a ring laser with intracavity distortion correction capability (Fig. 5.9b). The optical feedback provided in the ring cavity should encourage phase conjugate operation. If the

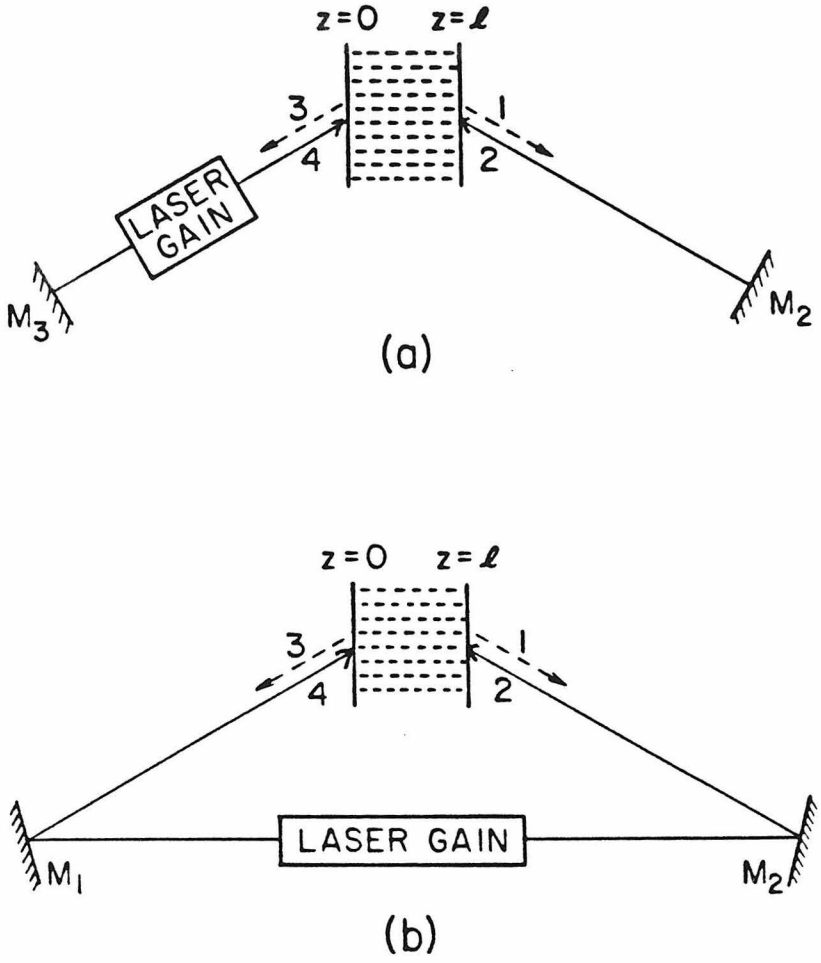

Figure 5.9 PR crystal acting as a double phase conjugate mirror in
a) The semilinear mirror,
b) A ring laser with dynamic intracavity distortion correction capability.

roundtrip gain is assumed to be G, so that $I_4(0) = GI_1(l)$ and $I_2(l) = GI_3(0)$, then after fitting these boundary conditions, we find that the equilibrium value of q is given by

$$q = 2\xi - 1 \pm 2[\xi(\xi - 1)]^{1/2} \tag{5.22}$$

where

$$\xi = (1 - G^{-1})/(1 - a^2) \tag{5.23}$$

Such a laser is therefore bistable: (5.22) offers two solutions, which are reciprocals of each other. This is can be understood on the basis of the symmetry of (5.21) in q and q^{-1}. The gain threshold for this ring laser as derived from the requirement $\xi \geq 1$ is simply $Ga^2 \geq 1$ (see 5.22). The two

The ring passive phase conjugate mirror

In this section we describe another kind of PPCM. Unlike the linear PPCM's it generates only one of its pumping beams via nonlinear optical interactions. The results of a theoretical analysis of this device are shown as well as experimental verification of its action as a phase conjugate mirror[13].

In the basic implementation of this device (Fig. 5.1c) the signal beam 2 passes through a photorefractive medium and returns to it as pumping beam 4 around an optical ring cavity, here represented by mirrors M_1 and M_2. It may be advantageous to use curved mirrors or intracavity lenses to minimize diffractive loss of any spatial information on the signal beam. The possibility then arises that the nonlinear optical coupling in the crystal may be such that both the second pumping beam 3 and the phase conjugate beam 1 build up as oscillation beams in the ring cavity. We now turn to a theoretical examination of this possibility. As in the case of the linear mirror use of the undepleted pumps approximation is inappropriate so here too we use the depleted pumps analysis of Chapter 4.

After fitting boundary conditions of this device, named the *ring mirror*, we find that buildup of oscillation in the ring is in fact possible when the spatial phase shift between the holographic refractive index grating and the light interference pattern is nonzero so that advantage is taken of unidirectional beam coupling effects typical of real time holography in PR crystals.

In previous calculations, beam 3 has been the phase conjugate beam. Here, however, we designate beam 1 as the phase conjugate, because we wish to retain the convention that $I_3(l) = 0$, so that previous results may be directly adapted to the solution required here. The phase conjugate reflectivity is then going to be $R = I_{12}(l)$. Let the product of the intensity reflectivities of the feedback mirrors M_1 and M_2 be M so that the appropriate boundary conditions for the ring mirror (Fig. 5.1c) are

$$I_4(0)/I_2(0) = M \tag{5.24a}$$

$$I_1(0)/I_3(0) = M \tag{5.24b}$$

(4.16) supplies the required intensities in terms of $I_{12}(0)$, $I_{34}(0)$, d_1 and d_2. Furthermore, from our analysis of the linear mirror, we have available expressions for $I_{12}(0)$ and $I_{34}(0)$ in terms of Δ and $I_{12}(l)$, these are (5.3) and (5.5) respectively. Thus, if we know d1, d2, and Δ we will be able to solve (5.24) for the reflectivity $I_{12}(l)$. Fortunately, these constants are immediately available to us:

$$\Delta = \frac{I_2(0) + I_3(0) - I_1(0) - I_4(0)}{I_2(0) + I_3(0) + I_1(0) + I_4(0)} = \frac{1 - M}{1 + M} \tag{5.25}$$

where we have made use of the boundary conditions (5.24). We observe that d_1 and d_2 may be found from the relations $d_2 - d_1 = \Delta$ and $d_1 + d_2 = 1$ so that

$$d_1 = M/(M + 1) \tag{5.26a}$$

and

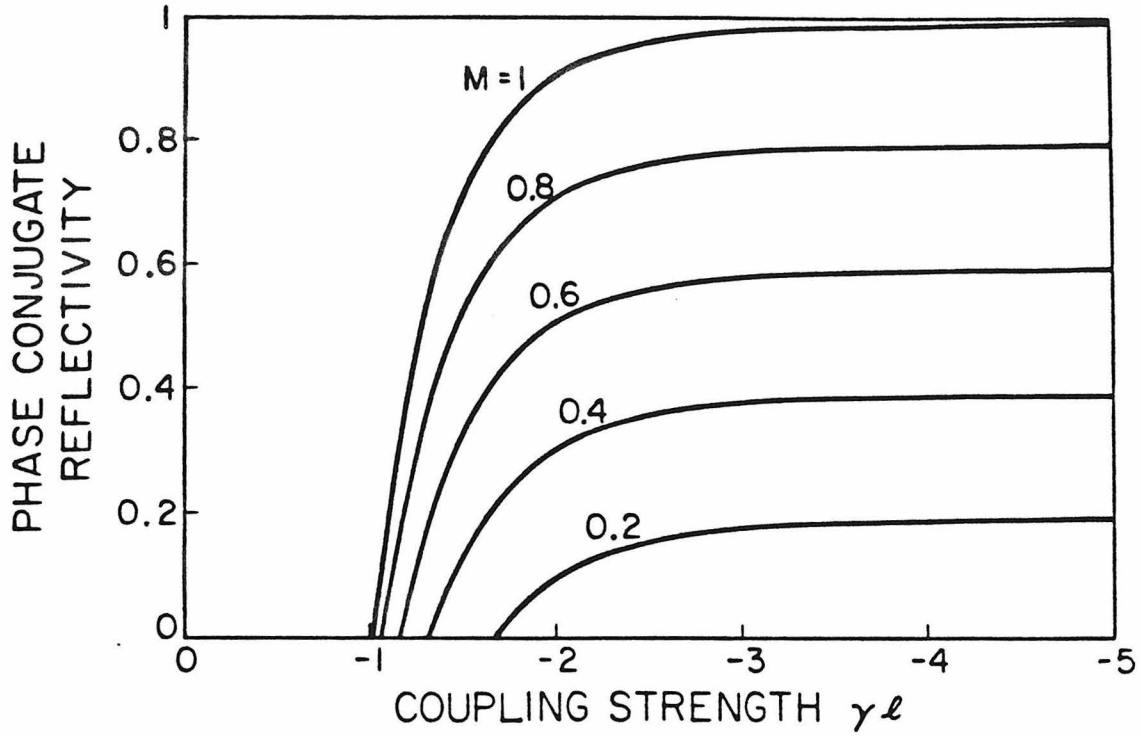

Figure 5.10 Reflectivity of the ring passive phase conjugate mirror as a function of coupling strength for several values of the product M of the intensity reflectivities of the feedback mirrors M_1 and M_2.

$$d_2 = 1/(M + 1) \tag{5.26b}$$

The reflectivity of the ring mirror is shown in Fig. 5.10 as a function of γl. It has been taken to be real so that it represents the $\pi/2$ phase shift characteristic of holographic recording in photorefractive crystals by diffusion of charge carriers. Curves for several values of the feedback parameter M are included. We see that at threshold, the reflectivity is zero: this threshold may be found by solving the boundary conditions in the limit of zero reflectivity, $I_{12}(l) = 0$. It is given by

$$\gamma l_t = \frac{(M+1)}{(M-1)} \ln\left[\frac{M+1}{2M}\right] \tag{5.27}$$

Concerning the faithfulness of phase conjugation in the ring mirror, it might be expected that since the self-induced pumping beams are not plane waves a certain amount of distortion would be introduced into the phase conjugate beam. In the case of the linear mirror, physical constraints imposed by the cavity mirrors may lead to filtering of the signal information from the pumping beams, but one of the pumps in the ring mirror is simply light transmitted through the crystal fed back to it by a passive optical system containing, at least in the experiment described below, very little spatial filtering. In the preceding discussion of the linear mirror, we proposed that feedback gives phase conjugate oscillations an advantage in gain over other kinds of oscillation. In the ring mirror we have $A_4 = M^{1/2}KA_2$ and $A_3^* = M^{-1/2}KA_1^*$ with **K** the lossless linear operator for propagation of beam 2 around the ring to beam 4. The relevant index grating is represented in the coupled wave equations by a term proportional to $A_1^*A_4 + A_2A_3^*$ which equals $M^{1/2}A_1^*KA_2 + M^{-1/2}A_2KA_1^*$ at the crystal face (z=0). Unless **K** is the identity or otherwise pathological, then both terms in the sum will add in phase at this crystal face if and only if A_1 is proportional to A_2^*.

The apparatus of Fig. 5.11 was used to demonstrate the phase conjugating

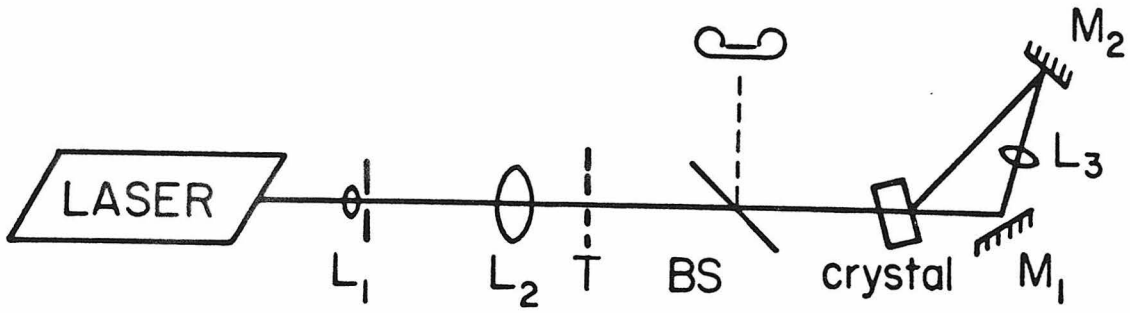

Figure 5.11 The experimental arrangement used to demonstrate phase conjugation in the ring passive phase conjugate mirror. An argon ion laser was used at 488nm in single longitudinal mode. Using a cartesian coordinate system with the abscissa coincident with the beam direction, the locations of the elements measured in centimeters were: 30x beam expander L_1 (61,0), transparency T (30,0), beam splitter for observing phase conjugate reflection BS (5,0), 14cm focal length 3cm dia. lens L_2 (41,0), barium titanate crystal (0,0), plane mirror M_1, (-9,0), plane mirror M_2 (-28,-20), 15cm focal length 3cm dia. lens L_3 (-18,-10) The c-axis of the crystal pointed in the direction of the vector (0.68,0.73). The crystal measured 5.1×4.8×5.1 mm and was poled into a single domain so that the c-axis was parallel to the 4.8 mm side.

nature of the ring mirror. The expanded and spatially filtered output of an argon ion laser in single longitudinal mode at 488.0nm passed through lens L_2 and illuminated an Air Force Resolution Chart. The beam then converged on the passive phase conjugate mirror, consisting of a single poled crystal of barium titanate in the M_1–M_2 ring cavity. Lens L_3 was provided to decrease diffractive loss in the ring. The reflected beam was picked off by a beam splitter BS and photographed at the location where a phase conjugate image would be expected. The result is shown in Fig. 5.12a. The phase conjugating behaviour of the passive phase conjugate mirror is evident although some lack of uniformity in the intensity of the image is apparent. This can be seen more clearly in Fig. 5.12b, which is the phase conjugate reflection of the uniformly expanded expanded laser beam vignetted by the aperture of lens L_2. We believe that the dark areas in the image at six and twelve o'clock are due to losses via the fanning effect[14] in which a single beam passing through a photorefractive crystal with a sufficiently large coupling constant loses intensity via holographic two beam coupling to a broad fan. Figs. 5.12c and 5.12d show the effect of fanning on the spatial distribution of intensity in such a signal beam. Mirrors M_1 and M_2 were removed from the ring mirror and holographic gratings in the crystal were allowed to decay by dark current leakage. The uniform signal beam was then allowed to pass through the crystal and a photograph (Fig. 5.12c) of this beam after passage through the crystal was immediately taken, before fanning could build up, the time scale of hologram writing being of the order of several seconds. Fig. 5.12d shows the same beam with intensity loss by fanning. A dark area developed, just as dark areas developed in the phase conjugate beam of Fig. 5.12b.

Figure 5.12 Experimental results for the ring mirror showing:
a) The phase conjugate image of an Air Force Resolution Chart.
b) The phase conjugate image of uniform expanded beam vignetted by lens L_2.
c) The effect of fanning on the signal beam with apparatus as in Figure 3, without transparency T and mirrors M_1 and M_2. Beam transmitted through crystal before build-up of fanning.

d) Beam transmitted through crystal after build-up of fanning.

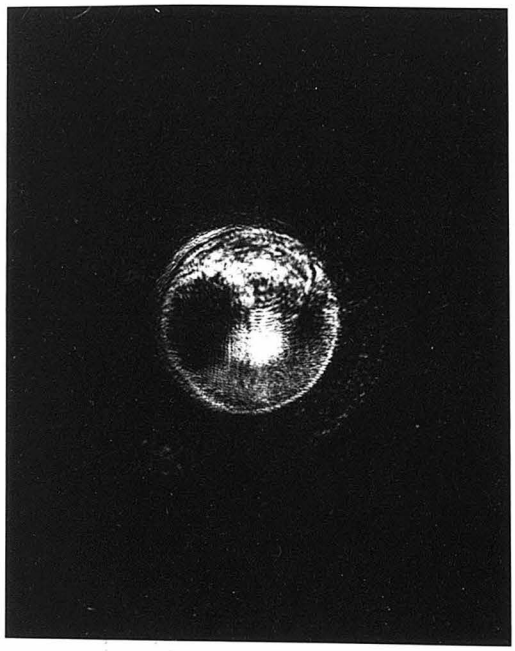

(b)

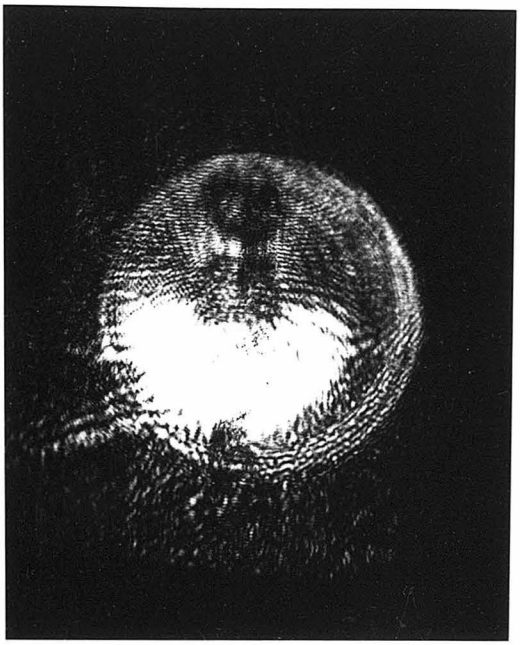

(d)

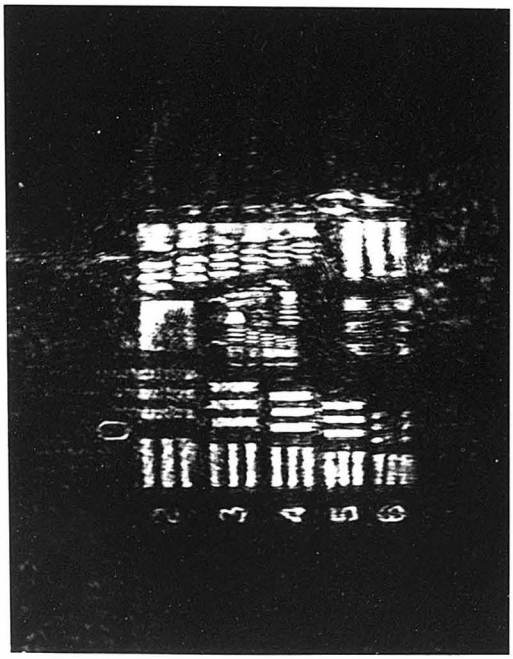

(a)

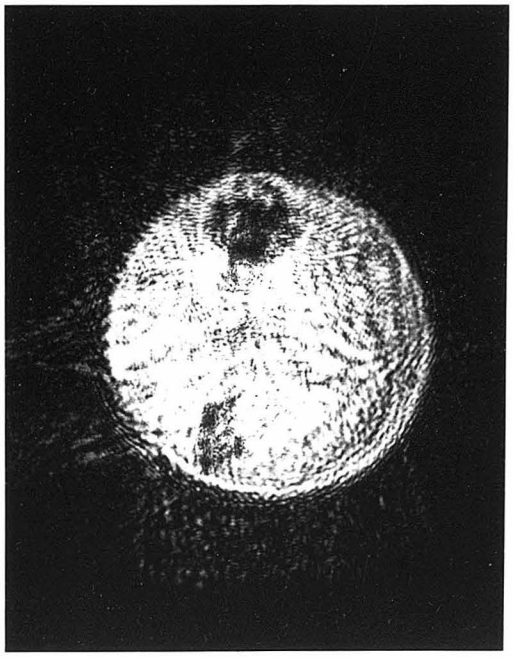

(c)

The two-interaction-region passive phase conjugate mirror

Recently, Feinberg has reported a passive phase conjugate mirror comprising a single crystal (Fig 5.1d) which makes use of totally internally reflecting surfaces of the crystal as feedback mirrors[15]. We identify this device as the *two-interaction-region (2IR) mirror*, since it uses two interaction regions linked inside the single crystal.

By interpreting this device as a ring mirror containing a double phase conjugate mirror in its feedback loop, we can present a simple theoretical analysis making direct use of our previous calculations. We saw above that the transmissivity of the double phase conjugate mirror is the same for both of the beams incident on it. Thus the 2IR mirror can be thought of as a ring mirror whose feedback M is multiplied by the effective transmission due to the double phase conjugate mirror (5.21). We can immediately write down appropriately modified versions of the ring mirror boundary conditions.

$$I_4(0)/I_2(0) = T(\Delta',a')M \tag{5.28a}$$

$$I_1(0)/I_3(0) = T(\Delta',a')M \tag{5.28b}$$

where primed quantities refer to the double phase conjugate mirror and the Δ used in the left hand side of these equations is given by

$$\Delta = \frac{1 - T(\Delta',a')M}{1 + T(\Delta',a')M} \tag{5.29}$$

These equations (5.28), (5.29) must then be solved numerically for Δ' and reflectivity $R = I_{12}(l)$.

Threshold versus reflectivity versus ease of alignment

Both the linear and ring mirrors have self starting thresholds ((5.6) and (5.27)): when they are exceeded, oscillation beams of infinitesimal intensity

experience gain. This self starting ability is not possessed by the semilinear or 2IR mirror since oscillation beams of these devices experience gain only when their intensities are above a certain nonzero threshold. Starting these devices thus requires seeding of their oscillation beams. The 2IR and linear mirrors have in fact been shown to be able to start without the aid of externally provided seeding but it is believed to be dependent on effective seeding by the fanning effect which is due to two beam coupling amplification of scattered light and not to the four-wave mixing process referred to here.

Equation (5.27) shows that the threshold coupling strength in the ring mirror for unity feedback, M = 1, is $\gamma l_t = -1$. The self-starting threshold for the linear mirror is $\gamma l_t = \frac{1}{2}\ln M$ (see (5.6)) where M is the product of the intensity reflectivities of the linear cavity mirrors, so that with ideal feedback (M = 1) the threshold coupling strength is zero. The threshold of the semilinear mirror with unity reflectivity for the external mirror is found from (5.13) to be $\gamma l_t = -2.49$, while the threshold for the 2IR mirror with ideal feedback is $\gamma l_t = -4.68$.

The linear mirror thus has the simultaneous advantages of having very low threshold and of self-starting by four-wave mixing. It does, however, require careful alignment. Of the remaining passive phase conjugate mirrors, all of them easily aligned, the ring mirror seems to be most attractive in that it has the lowest threshold and is self-starting. A major advantage of the 2IR mirror has been that it is completely self contained in a single crystal, using total internal reflection at the crystal faces for feedback. The ring mirror can also be implemented in this same manner using crystals whose surfaces are cut at appropriate angles.

Figure 5.13 gives a direct comparison of the reflectivities of each of the PPCM's for ideal feedback in each case. The zero threshold of the linear mirror

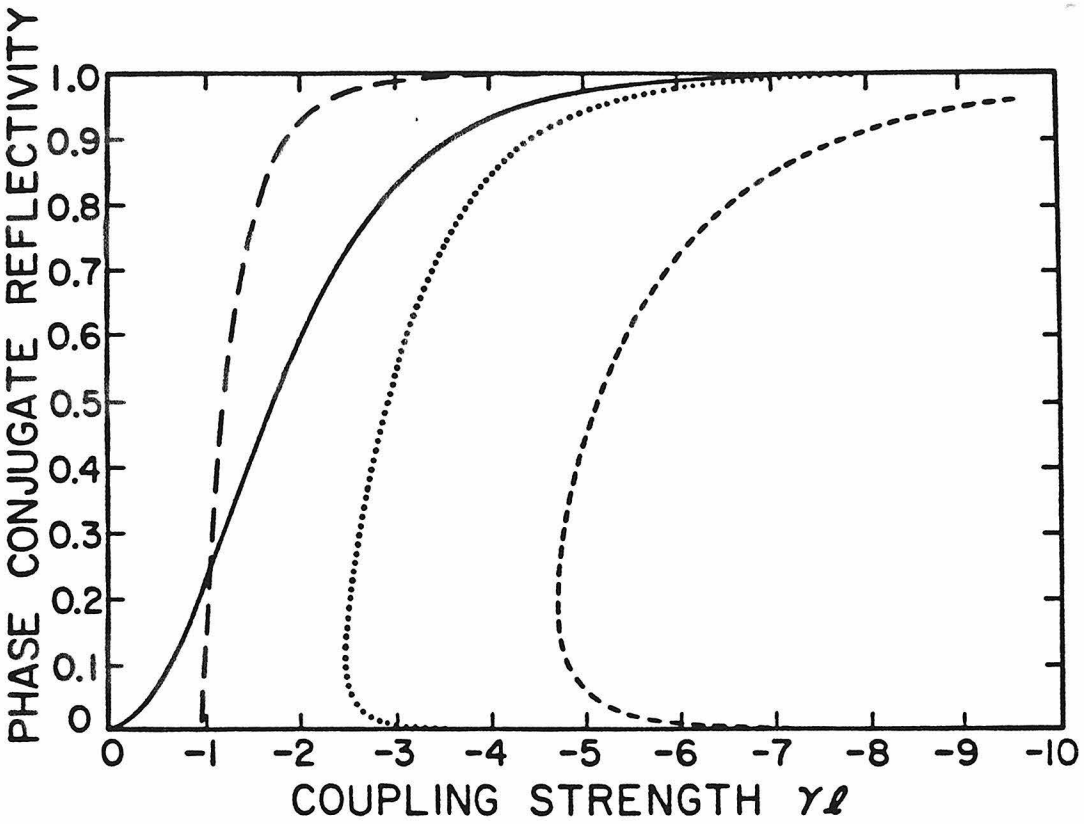

Figure 5.13 Graphs of phase conjugate reflectivities of the various passive phase conjugate mirrors with ideal feedback
a) The linear mirror with $M_1 = M_2 = 1$, (solid)
b) The semilinear mirror with $M_2 = 1$, (dots)
c) The ring mirror with $M = 1$ (long dashes)
d) The two interaction region mirror with $M = 1$ (dashes)

is shown and we see that the semilinear mirror reflectivity is always lower than that of the full linear mirror, as might be expected, since with one mirror removed, there is always going to be some extra loss. The ring mirror reflectivity, after taking off from its threshold, soon exceeds all of them.

Conclusion

The two vital elements in this work have been the solution of the coupled wave equations with pump depletion and the availability of PR crystals with large coupling strengths. The value of such concurrent theoretical and experimental work is undeniable: it has led to many new, useful devices such as passive and double phase conjugate mirrors and their demonstration in aberration correction in lasers and image processing. In the future we can expect similarly important developments, and as research proceeds into optimizing the photorefractive effect, the applications of these devices to problems in image processing and aberration correction are bound to multiply.

References for Chapter 5

1. J. Au Yeung, D. Fekete, D. Pepper and A. Yariv, IEEE J. of Quantum Electron. **QE-15**, 1180 (1979)

2. I.M. Bel'yugdin, M.G. Galushkin and E.M. Zemskov, Sov. J. Quantum Electron. **9**, 20 (1979)

3. I.M. Bel'yugdin and E.M. Zemskov, Sov. J. Quantum Electron. **9**, 1198 (1979)

4. P.A. Belanger, A. Hardy and A.E. Siegman, Appl. Opt. **19**, 602 (1980)

5. J.F. Lam and W.P. Brown, Opt. Lett. **5**, 61 (1980)

6. M.G. Reznikov and A.I. Khizhnyak, Sov. J. Quantum Electron. **10**, 633 (1980)

7. R.C. Lind and D.G. Steel, Opt. Lett. **6**, 554 (1981)

8. J. Feinberg, Opt. Lett. **5**, 519 (1980)

9. J.O. White, M. Cronin-Golomb, B. Fischer and A. Yariv, Appl. Phys. Lett. **40**, 450 (1982)

10. M. Cronin-Golomb, B. Fischer, J. Nilsen, J.O. White and A. Yariv, Appl. Phys. Lett. **41**, 219 (1982)

11. M. Cronin-Golomb, B. Fischer, J.O. White and A. Yariv, Appl. Phys. Lett. **41**, 689 (1982)

12. A. Yariv, "Quantum Electronics", (Wiley, New York, 1975)

13. M. Cronin-Golomb, B. Fischer, J.O. White and A. Yariv, to be published, Appl. Phys. Lett, June 1 (1983)

14. V.V. Voronov, I.R. Dorosh, Yu. S. Kuz'minov and N.V. Tkachenko, Sov. J. Quant. Electron. **10**, 1346 (1980)

15. J. Feinberg, Opt. Lett. **7**, 486 (1982)